Photonic Crystal Fibres as the Transmission Medium for Future Optical Communication Systems

Zsigri, Beata

Publication date:
2006

Document Version
Publisher's PDF, also known as Version of record

Photonic Crystal Fibres as the Transmission Medium for Future Optical Communication Systems

Beáta Zsigri

February 10, 2006

Department of Communication, Optics & Materials
Technical University of Denmark
Building 345V
2800 Kgs. Lyngby
DENMARK

Resumé

I løbet af dette Ph.d. projekt er luft-silica fotoniske krystalfibre (PCF) blevet undersøgt med henblik på anvendelser indenfor telekommunikation. PCF har en kompliceret cladding-struktur, hvor luft-huller på langs af hele fiberlængden sikrer ledning af lyset. Fotoniske krystalfibre kan klassificeres i to overordnede grupper: indeksguidende PCFer og fotoniske båndgabsfibre (PBGF). Indeksguidende PCF har mange ligheder med konventionelle fibre. Derimod er PBGFer en fundamentalt anderledes type fiber, og deres egenskaber er betydeligt anderledes, end dem man ser for konventionelle fibre og indeksguidende PCFer. Begge PCF typer udviser adskillige nye egenskaber, der ikke kan opnås med standard fiber teknologi, og som er meget attraktive for optiske kommunikationssystemer. Til trods for, at PCFer har eksisteret i et årti, er deres udnyttelse indenfor telekommunikation først startet for nylig. Denne afhandling følger udviklingen af PCFer som transmissionsmedium fra begyndelsen og frem til i dag, og præsenterer state-of-the-art resultater for forskellige systemanvendelser.

Indeksguidende PCFer er blevet undersøgt til transmissionsformål. I denne afhandling præsenteres nogen af de tidligste transmissionseksperimenter med PCF. Blandt andet beskrives en af de første rapporterede 10 Gbit/s transmissioner over 5.6 km PCF. Den totale transmissions længde over indeksguidende PCF er efterfølgende blevet øget til 57.6 km, hvilket langt overstiger de længder, der hidtil var opnået. Den totale kapacitet ved en enkeltbølgelængde er øget til 80 Gbit/s. Dette er den højeste kapacitet opnået ved en enkelt bølgelængde over PCF ved hjælp af polarisations multiplexning og differential phase-shift-keying signal transmission.

Indeksguidende PCFer er også blevet undersøgt med henblik på an-

vendelser indenfor optisk signalbehandling, og de er blevet benyttet til at bygge fuldt funktionelle - og fuldstændigt PCF baserede - optiske transmissionslinier og netværk. Den første 40 Gbit/s transmission er demonstreret med spektral inversion på halvvejen til kompensering af dispersion i en stærkt ulineær fotonisk krystalfiber. Det første optiske netværk med broadcast, transmissions og bølgelængde konverterings egenskaber - alle opnået i PCF - er præsenteret.

Herudover er indeksguidende PCFer blevet udnyttet til dispersionskompensering. Et nyt design for dispersionskompenserende fotonisk krystalfiber (DC-PCF), der udviser en stor dispersions koefficient på -1353 ps/(nm·km) ved 1550 nm og samtidig har en relativ dispersionshældning tilpasset til standard single mode fiber, er blevet præsenteret. Det foreslåede design sammenlignes med andre rapporterede DC-PCF designs. Fordelene og begrænsningerne for det præsenterede design diskuteres. Således er potentialet for indeksguidende PCFer, som transmissionsmedium, som ulineært medium til signalbehandling, eller som dispersionskompenserende fiber til fremtidige langdistance transmissions systemer, demonstreret.

Endelig er fotonisk båndgabsfiber blevet undersøgt til telekommunikationsanvendelser. Dette arbejde fokuserer på luft-ledende fotoniske båndgabsfibre (AG-PBGFer) og deres systemanvendelser. Den første og på nuværende tidspunkt eneste rapporterede data transmission over AG-PBGF er beskrevet. Potentialer og aktuelle begrænsninger ved AG-PBGF diskuteres. Et polarisation delay interferometer, der udnytter den store dobbeltbrydning i AG-PBGF, er blevet realiseret i en 2.4 m AG-PBGF til demodulering af 9.95 og 39.8 Gbit/s differential phase-shift-keying modulerede signaler. Således demonstreres anvendelsen af AG-PBGF til at realisere stabile og kompakte fiberdobbeltbrydningsbaserede optiske komponenter.

Abstract

During this Ph.D. work, air-silica photonic crystal fibres (PCFs) have been investigated for telecommunication applications. PCFs have a complicated cladding structure, where air holes, running along the entire fibre length, ensure light guidance. Photonic crystal fibres can be classified into two major groups: index guiding PCFs and photonic bandgap fibres (PBGFs). Several aspects of index guiding PCFs are similar to conventional fibres. On the contrary, PBGFs form a fundamentally new class of fibres and their properties differ considerably from those observed for both conventional fibres and index guiding PCFs. Nevertheless, both PCF types exhibit numerous novel properties – not obtainable by standard fibre technology – that are very attractive for optical communication systems. Even though PCFs have now existed already for a decade, their exploitation for telecommunication applications has begun only recently. This thesis follows the evolution of PCFs as transmission media from the beginning up to now and presents state-of-the-art results of their various possible system applications.

Index guiding PCFs have been investigated for transmission purposes. In this thesis, some of the initial transmission experiments comprising PCFs are presented. Among others, the first reported 10 Gbit/s transmission over 5.6 km PCF is described. The total transmission distance over index guiding PCF is increased to 57.6 km, more than four times longer than the achievable lengths of the date. The total capacity carried on a single wavelength is increased to 80 Gbit/s, the highest capacity transmitted on a single wavelength over PCF today, by polarisation multiplexed differential phase shift keying signal transmission.

Index guiding PCFs have also been studied for signal processing applications as well, and exploited for building fully functional, entirely

PCF based optical transmission links and networks. The first 40 Gbit/s transmission over 5.6 km PCF with mid-span spectral inversion dispersion compensation realised in a highly nonlinear photonic crystal fibre is demonstrated. The first optical network with broadcast, transmission and wavelength conversion functionalities, all realised in PCFs is presented.

Furthermore, index guiding PCFs have been investigated for dispersion compensation. A novel dispersion compensating photonic crystal fibre (DC-PCF) design, which exhibits a large dispersion coefficient of -1353 ps/(nm·km) at 1550 nm, while relative dispersion slope matching with standard single mode fibre is ensured, has been presented. The proposed design is compared with other reported DC-PCF designs. Advantages and limitations of the presented design are discussed.

Thereby, the great potential of index guiding PCFs as transmission media, as nonlinear media for signal processing or as dispersion compensating fibre for future high capacity long-haul transmission systems is demonstrated.

Finally, the telecommunication applications of photonic bandgap fibres are investigated. This work focusses on air-guiding photonic bandgap fibres (AG-PBGFs) and their system applications. The first and currently only reported data transmission over AG-PBGF is described. The potentials and current limitations of AG-PBGFs as transmission fibres are discussed. A polarisation delay interferometer, exploiting the large birefringence of AG-PBGFs, realised in only 2.4 m AG-PBGF for demodulation of 9.95 and 39.8 Gbit/s differential phase shift keying modulated signals is demonstrated, thereby demonstrating the feasibility of AG-PBGF for realising stable and compact fibre-birefringence based optical devices.

Acknowledgements

First of all I would like to express my gratitude to my supervisors Prof. Palle Jeppesen, Dr. Christophe Peucheret and Dr. Martin D. Nielsen for their support, advice and helpful discussions over the years. Additionally, I would like to thank Dr. Jesper Lægsgaard, who officially has not been my supervisor, however he provided great help and guided my way in the investigations of dispersion compensating fibres.

Crystal Fibre A/S is acknowledged for making the experimental investigations of photonic crystal fibres possible by providing all the photonic crystal fibre spools used in this work.

I would like to thank Hans-Jürgen Deyerl, Henrik R. Sørensen, Theis P. Hansen, Thomas T. Alkeskjold, Rune S. Jacobsen, Mikael Svalgaard and many others for their great collaborative work.

I owe a great thanks to Christophe, for all the knowledge he gave me and for the great and fruitful time we spent in the laboratory. I am grateful for Torger and Jorge for always being there when I needed some help with my computer, simulations or with anything. I would like to thank Pablo, Jesper, Torger, Jorge, Jesper and Theis for their useful comments to my thesis.

Special thanks goes to past and present colleges of the Systems Competence Area for the lots of fun we shared and for the inspiring working environment. I will always remember our long lasting lunches. Thanks Yan–my office mate–for the great chats and lots of chinese candies.

And last but not least, I would like to thank my family, Csilla, András, Lotti, Anikó and Morten, for all the great time we spent together. I am grateful for the support and encouragement you gave me during the years. Ulrik, thanks for the good time, running and skiing trips, and for the marvelous food. Thanks to all of you for being patient.

Ph.D. Publications

The following publications have resulted from this Ph.D. project.

Journal papers:

[A1] B. Zsigri, C. Peucheret, M. D. Nielsen, and P. Jeppesen. "Demonstration of broadcast, transmission, and wavelength conversion functionalities using photonic crystal fibers", accepted to *IEEE Photonics Technology Letters*

[A2] C. Peucheret, Y. Geng, B. Zsigri, T. T. Alkeskjold, T. P. Hansen, and P. Jeppesen. "Demodulation of DPSK signals up to 40 Gb/s using a highly birefringent photonic bandgap fiber", *IEEE Photonics Technology Letters*, vol. 18, no. 12, pp. 1392–1394, June 2006

[A3] R. S. Jacobsen, K. N. Andersen, P. I. Borel, J. Fage-Pedersen, L. H. Frandsen, O. Hansen, M. Kristensen, A. V. Lavrinenko, G. Moulin, H. Ou, C. Peucheret, B. Zsigri, and A. Bjarklev. "Strained silicon as a new electro-optic material", *Nature*, vol. 441, no. 7090, pp. 199–202, May 2006

[A4] H.-J. Deyerl, C. Peucheret, B. Zsigri, F. Floreani, N. Plougmann, S. J. Hewlett, M. Kristensen, and P. Jeppesen. "A compact low dispersion fiber Bragg grating with high detuning tolerance for advanced modulation formats", *Optics Communications*, vol. 247, no. 1-3, pp. 93–100, March 2005

[A5] R. S. Jacobsen, A. V. Lavrinenko, L. H. Frandsen, C. Peucheret, B. Zsigri, G. Moulin, J. Fage-Pedersen, and P. I. Borel. "Direct experimental and numerical determination of extremely high group indices in photonic crystal waveguides", *Optics Express*, vol. 13, no. 20, pp. 7861–7871, October 2005

[A6] C. Peucheret, Y. Geng, M. Svalgaard, B. Zsigri, H. R. Sørensen, N. Chi, H.-J. Deyerl, M. Kristensen, and P. Jeppesen. "Direct UV written Michelson interferometer for RZ signal generation using phase-to-intensity modulation conversion", *IEEE Photonics Technology Letters*, vol. 17, no. 8, pp. 1674–1676, August 2005

[A7] B. Zsigri, C. Peucheret, M. D. Nielsen, and P. Jeppesen. "Recirculating loop transmission experiment over 57.6-km photonic crystal fiber", *Optics Engineering*, vol. 44, no. 7, pp. 070504–1–2, July 2005

[A8] T. Tokle, B. Zsigri, C. Peucheret, and P. Jeppesen. "Generation and transmission of a 160 Gbit/s polarisation multiplexed RZ-DBPSK-ASK signal", *Electronics Letters*, vol. 41, no. 7, pp. 433–434, March 2005

[A9] C. Peucheret, B. Zsigri, T. P. Hansen, and P. Jeppesen. "10 Gbit/s transmission over air-guiding photonic bandgap fibre at 1550 nm", *Electronics Letters*, vol. 41, no. 1, pp. 27–29, January 2005

[A10] C. Peucheret, B. Zsigri, K. P. Hansen, M. D. Nielsen, and P. Jeppesen. "Photonic crystal fibers for transmission and optical signal processing", *IEEE LEOS, Lasers & Electro-Optics Society Newsletter*, vol. 18, no. 4, pp. 7–8, August 2004

[A11] B. Zsigri, J. Lægsgaard, and A. Bjarklev. "A novel photonic crystal fibre design for dispersion compensation", *Journal of Optics A: Pure and Applied Optics*, vol. 6, no. 7, pp. 717–720, July 2004

[A12] C. Peucheret, B. Zsigri, P. A. Andersen, K. S. Berg, A. Tersigni, P. Jeppesen, K. P. Hansen, and M. D. Nielsen. "40 Gbit/s transmission over photonic crystal fibre using mid-span spectral inversion in highly nonlinear photonic crystal fibre", *Electronics Letters*, vol. 39, no. 12, pp. 919–921, June 2003

[A13] B. Zsigri, C. Peucheret, M. D. Nielsen, and P. Jeppesen. "Transmission over 5.6 km large effective area and low loss (1.7 dB/km) photonic crystal fibre", *Electronics Letters*, vol. 39, no. 10, pp. 796–798, May 2003

Conference papers:

[B1] A. V. Lavrinenko, R. S. Jacobsen, J. Fage-Pedersen, L. H. Frandsen, B. Zsigri, C. Peucheret, and P. I. Borel. "Extreme group index measured and calculated in 2D SOI-based photonic crystal waveguides", in *Technical Digest IEEE Lasers and Electro-Optics Society Annual Meeting, LEOS'05,* Sydney, Australia, pp. 320–321, October 2005, paper TuR4

[B2] A. V. Lavrinenko, R. S. Jacobsen, J. Fage-Pedersen, B. Zsigri, C. Peucheret, L. Frandsen, M. Kristensen, and P. Borel. "Direct numerical and experimental determination of group index dispersion in photonic crystall waveguides", in *Proc. SPIE, vol. 5950 (presented at SPIE International Congress on Optics and Optoelectronics, Warsaw, Poland),* August 2005, paper 5950-15

[B3] B. Zsigri, C. Peucheret, M. D. Nielsen, and P. Jeppesen. "Implementation of broadcast, transmission and wavelength conversion functionalities using photonic crystal fibers", in *Proceedings OptoElectronics and Communications Conference, OECC'05,* Seoul, Korea, pp. 790–791, July 2005, paper 8B3-1

[B4] T. Tokle, B. Zsigri, C. Peucheret, and P. Jeppesen. "Transmission of 160 Gbit/s simultaneous phase and amplitude modulated signal over 50 km fibre span", in *Proceedings OptoElectronics and Communications Conference, OECC'05,* pp. 776–777, Paper 8B1-3, July 2005

[B5] B. Zsigri, T. Tokle, C. Peucheret, M. D. Nielsen, and P. Jeppesen. "80 Gbit/s polarization multiplexed DPSK signal transmission over photonic crystal fiber", in *Proceedings OptoElectronics and Communications Conference, OECC'05,* Seoul, Korea, pp. 402–403, July 2005, paper 7B3-3

[B6] C. Peucheret, Y. Geng, B. Zsigri, T. T. Alkeskjold, T. P. Hansen, and P. Jeppesen. "Demodulation of DPSK signals up to 40 Gb/s using a highly birefringent photonic bandgap fibre", in *Proceedings OptoElectronics and Communications Conference, OECC'05,* Seoul, Korea, pp. 50–51, July 2005, paper 5D1-2

[B7] T. Tokle, P. A. Andersen, Y. Geng, B. Zsigri, C. Peucheret, and P. Jeppesen. "Generation, transmission and wavelength conversion an 80 Gbit/s RZ-DBPSK-ASK signal", in *Technical Digest Conference on Lasers and Electro-Optics, CLEO'05,* Baltimore, Maryland, U.S.A., Paper CMQ4, May 2005

[B8] C. Peucheret, B. Zsigri, H. R. Sørensen, M. Svalgaard, N. Chi, H.-J. Deyerl, M. Kristensen, and P. Jeppesen. "Direct UV written Michelson interferometer for RZ signal generation using phase-to-intensity modulation conversion", in *Proceedings European Conference on Optical Communication, ECOC'04,* Stockholm, Sweden, vol. 2, pp. 288–289, September 2004, paper Tu4.7.5

[B9] B. Zsigri, C. Peucheret, M. D. Nielsen, and P. Jeppesen. "Transmission over 57.6 km of photonic crystal fiber", in *Proceedings OptoElectronics and Communications Conference, OECC'04,* Yokohama, Japan, pp. 482–483, July 2004, paper 14D1-2

[B10] C. Peucheret, B. Zsigri, T. P. Hansen, and P. Jeppesen. "Transmission of information over air-guiding photonic bandgap fiber at 1550 nm", in *Proceedings OptoElectronics and Communications Conference, OECC'04,* Yokohama, Japan, pp. 480–481, July 2004, paper 14D1-1

[B11] P. A. Andersen, B. Zsigri, C. Peucheret, P. Jeppesen, K. P. Hansen, and M. D. Nielsen. "Photonic crystal fibers used in a multi-wavelength source and as transmission fiber in a WDM system", in *Technical Digest Conference on Lasers and Electro-Optics, CLEO'04,* San Francisco, California, U.S.A., May 2004, paper CThG4

[B12] B. Zsigri, C. Peucheret, A. Buxens, and P. Jeppesen. "Performance comparison of optical single side band generation techniques", in *Proceedings European Conference on Optical Communication, ECOC'03,* Rimini, Italy, vol. 3, pp. 524–525, September 2003, paper We3.5.3

[B13] C. Peucheret, B. Zsigri, H.-J. Deyerl, S. J. Hewlett, M. Kristensen, and P. Jeppesen. "Low dispersion fibre Bragg grating with high detuning tolerance for advanced modulation formats", in *Proceedings European Conference on Optical Communication, ECOC'03,* Rimini, Italy, vol. 1, pp. 8–9, September 2003, paper Mo3.2.4

[B14] C. Peucheret, B. Zsigri, P. A. Andersen, K. S. Berg, A. Tersigni, P. Jeppesen, K. P. Hansen, and M. D. Nielsen. "Transmission over photonic crystal fiber at 40 Gbit/s using mid-span spectral inversion in a highly nonlinear photonic crystal fiber", in *Technical Digest Conference on Lasers and Electro-Optics, CLEO'03,* Baltimore, Maryland, U.S.A., June 2003, post-deadline paper CThPDB4

Other publications:

[C1] B. Zsigri, C. Peucheret, T. P. Hansen, T. T. Alkeskjold, and P. Jeppesen. "Photonic bandgap fibres in optical communication systems: challenges and early demonstrations", in *European Conference on Optical Communication, ECOC'06,* Cannes, France, September 2006, workshop on Photonic Crystal Fibres versus Classical Fibres for Telecommunications

[C2] A. V. Lavrinenko, R. S. Jacobsen, J. Fage-Pedersen, L. H. Frandsen, B. Zsigri, C. Peucheret, and P. I. Borel. "Slow light in photonic crystal waveguides", in *Danish Optical Society (DOPS) Annual Meeting 2005,* Risø National Laboratory, Denmark, p. 13, November 2005

[C3] B. Zsigri, C. Peucheret, H.-J. Deyerl, M. Fujita, and M. Kristensen. "Filtering tolerance of optical single-side band modulation for narrow channel spacing wavelength division multiplexing systems", in *Danish Optical Society (DOPS) Annual Meeting 2002,* Risø National Laboratory, Denmark, November 2002

Contents

Chapter 1

Introduction

Optical fibres are an essential part of optical telecommunication systems. Today all implemented systems use conventional[1] fibres. Large variety of conventional fibres exists, optimised for instance for transmission, nonlinear signal processing or Raman amplification [1, 2]. These fibres have solid core and homogenous, solid cladding. To confine light in the core, their core must have higher refractive index than the surrounding cladding [3]. In silica fibres, the refractive index difference between core and cladding is achieved by doping pure silica with germanium or fluorine to rise or lower the refractive index, respectively. The practical refractive index difference between core and cladding is limited typically to around 10^{-3} by the obtainable doping levels and by material stress [3]. This in turn sets a limitation on the obtainable optical properties.

In 1996 a new single material optical fiber, photonic crystal fibre (PCF), was proposed [4]. The fibre is composed of a single material, where an air hole arrangement, running along the entire fibre length, forms the cladding region. In this thesis only silica-air photonic crystal fibres are considered. Contrary to conventional fibres where doping is indispensable, in PCFs light guidance is ensured by the presence of holes in the cladding, thus doping is not necessary. The attraction of PCFs comes from the promise that these fibers may eliminate the limitations

[1] Fibres, with solid core and cladding, achieving the refractive index difference between core and cladding by doping, will be referred to as conventional fibre throughout this thesis, in order to make a clear distinction from photonic crystal fibres having microstructured cladding.

set by the materials and designs of conventional fibres. PCFs were expected to change many of the aspects that were an established fact in optical communications.

When PCFs are mentioned, most people associate them with fibres that guide light by the photonic bandgap (PBG) effect [5, 6]. This, however, does not entirely cover the reality. PCFs can be divided into two main groups: index guiding PCFs and photonic bandgap fibres (PBGFs). Index guiding PCFs guide light by modified total internal reflection (M-TIR), and are in many sense analogous to conventional fibres. Despite the analogy, the microstructured cladding structure of index guiding PCFs results in various unique guiding properties. Due to the microstructured cladding the refractive index difference between core and cladding is strongly wavelength dependent - contrary to conventional fibres where it can be assumed nearly wavelength independent. Additionally the large refractive index difference between air and silica and their geometrical flexibility allows large design freedom. Their optical properties, such as dispersion, nonlinearity, effective area, single mode bandwidth can be tailored to extremes, to values and profiles that are not obtainable with conventional fibres.

On the other hand, PBGFs form a fundamentally different class of fibres. These fibres guide light by the PBG effect. PBGFs posses radically new optical properties that are not by any means analogous to the corresponding properties of conventional fibres. The PBG effect allows light guidance in fibres whose core has lower refractive index than the surrounding cladding. This allows light guidance in air, which may feature ultra low loss and linear signal propagation.

Index guiding PCFs and PBGFs have found their application in several different areas, a few examples are metrology [17], optical coherence tomography [18], spectroscopy [19], high power delivery [20] or sensors [21, 22].

PCFs attracted great attention in the telecommunication market as well. However, for most of the telecommunication applications, low loss fibres are essential. The loss of both index guiding PCFs and PBGFs at the early development stage was very high, 50 dB/km [11] and 50 dB/m [7], respectively. The fibre lengths were also limited to a couple of kilometres for index guiding PCFs and only to a few metres for PBGFs. The combination of the initial large losses and short fibre

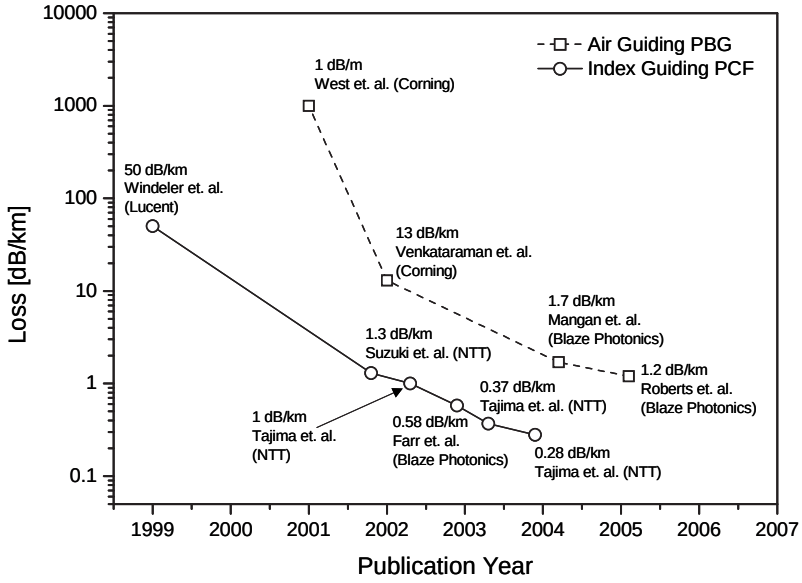

Figure 1.1: The loss reduction of both index guiding PCFs (circles-solid line) and PBG fibres (squares-dashed line) plotted as a function of the publication year [7–16]. The fibre loss, the first author of the paper and his affiliation are indicated.

lengths limited their practical use in telecommunication applications.

In recent years, improvements in the fabrication process have resulted in a dramatical decrease of the attenuation level of both PCF types as it is illustrated in Figure 1.1. These improvements resulted in the currently lowest loss of 0.28 dB/km [16] and the longest drawn length of 100 km [23] for index guiding PCFs and the corresponding 1.2 dB/km loss [10] and 800 m length [9] for PBGFs. The reported record losses did not yet reached the promised ultra low loss, and are still higher than the loss of standard single mode fibres (SSMFs). Nevertheless, the reported, rapid loss reduction, stimulated the research activities on their telecommunication applications.

This thesis covers the telecommunication applications of both index guiding PCFs and PBGFs. The initial goal of the presented work was to introduce PCFs as transmission media. The purpose of the subsequent experiments was to increase the total transmission distance and total capacity carried over PCF, and to investigate some of the unique properties of these fibres. The final goal was to realise a fully functional, entirely PCF based all optical network by exploiting PCFs for both transmission and signal processing purposes.

In spite of the fact that PCFs have existed already for ten years, they are still considered as a new technology for optical communications. Therefore in Chapter 2, the basic classification of PCFs is presented, introducing the different fibre types covered in this work. Based on the results of current literature, the properties of index guiding PCFs, that are important for system applications, will be briefly discussed, emphasising the major differences between conventional fibres and index guiding PCFs.

In Chapter 3, the application of index guiding PCFs as transmission fibres is discussed. This chapter follows the evolution of index guiding PCFs as transmission fibres from the beginning up to now. Some of the first experimental investigations of index guiding PCFs for transmission are described. A transmission experiment increasing the per wavelength capacity to the currently highest reported bit rate of 80 Gbit/s by means of polarisation multiplexing is presented. Furthermore, successful transmission over a total PCF length of 57.6 km, which constitutes a four-fold increase compared to the longest previously reported transmission distance over PCF, is presented.

In Chapter 4, signal processing applications of index guiding highly nonlinear photonic crystal fibres (HNL-PCFs) is addressed. Optical systems realising both signal processing and transmission using index guiding PCFs are presented. The first entirely PCF based, dispersion compensated 40 Gbit/s PCF transmission system is described, realising mid-span spectral inversion in HNL-PCF as dispersion compensation. Furthermore, an entirely PCF based optical network, with broadcasting, transmission and wavelength conversion functionalities is presented.

In Chapter 5 the potentials of index guiding PCFs as dispersion compensating fibres are investigated. First, the different dispersion compensating photonic crystal fibre (DC-PCF) designs proposed up to now, are discussed. Subsequently, a novel doped core, honeycomb DC-PCF design is proposed and its dispersion properties are numerically investigated. The dispersion properties and effective area of the proposed fibre are compared to other DC-PCF designs. The advantages and disadvantages of DC-PCFs are discussed.

In Chapter 6, system applications of air-guiding photonic bandgap fibres (AG-PBGFs) are explored. First a brief introduction to the properties of AG-PBGFs is given. Afterwards, the world first report on the application of AG-PBGF as transmission medium is presented and the current limitations of this fibre type are discussed. The first reported system application of AG-PBGFs, the demonstration of a polarisation delay interferometer, realised in only 2.4 m of AG-PBGF, used for the demodulation of 9.95 and 39.8 Gbit/s differential phase shift keying (DPSK) modulated signal, is presented.

The thesis is concluded in Chapter 7.

References to Chapter 1

[1] D. J. DiGiovanni, S. K. Das, L. L. Blyler, W. White, R. K. Boncek, and S. E. Golowich. *Design of Optical Fibers for Communications Systems*, In I. Kaminow and T. Li, editors, *Optical Fiber Telecommunications IVB Components,* Chapter 2, Academic Press, March 2002. ISBN 0-12-395173-9.

[2] Q. N. T. Le. *Fibres for 160 Gbit/s transmission and above.* Ph.D. thesis, Research Center COM, Technical University of Denmark,

Kgs. Lyngby, Denmark, October 2003. ISBN 87-90974-44-1.

[3] G. P. Agrawal. *Fiber-Optic Communication Systems.* John Wiley & Sons, Inc., Second edition, 1997. ISBN 0-471-17540-4.

[4] J. C. Knight, T. A. Birks, P. St. J. Russell, and D. M. Atkin. "All-silica single-mode optical fiber with photonic crystal cladding", *Optics Letters*, vol. 21, no. 19, pp. 1547–1549, October 1996.

[5] J. C. Knight, J. Broeng, T. A. Birks, and P. St. J. Russell. "Photonic band gap guidance in optical fibers", *Science*, vol. 282, no. 5393, pp. 1476–1477, November 1998.

[6] P. Russell. "Photonic crystal fibers", *Science*, vol. 299, no. 5605, pp. 358–362, January 2003.

[7] J. A. West, N. Venkataramam, C. M. Smith, and M. T. Gallagher. "Photonic crystal fibers", in *Proceedings European Conference on Optical Communication, ECOC'01,* Amsterdam, The Netherlands, pp. 582–585, September 2001, paper Th.A.2.

[8] N. Venkataramam, M. T. Gallagher, C. M. Smith, D. Müller, J. A. West, K. W. Koch, and J. C. Fajardo. "Low loss (13 dB/km) air core photonic band-gap fibre", in *Proceedings European Conference on Optical Communication, ECOC'02,* September 2002, post-deadline paper PD1.1.

[9] B. J. Mangan, L. Farr, A. Langford, P. J. Roberts, D. P. Williams, F. Couny, M. Lawman, M. W. Mason, S. Coupland, R. Flea, H. Sabert, T. A. Birks, J. C. Knight, and P. St. J. Russell. "Low loss (1.7 dB/km) hollow core photonic bandgap fiber", in *Technical Digest Optical Fiber Communication Conference, OFC'04,* Los Angeles, California, U.S.A., February 2004, post-deadline paper PDP24.

[10] P. J. Roberts, F. Couny, H. Sabert, B. J. Mangan, D. P. Williams, L. Farr, M. W. Mason, A. Tomlinson, T. A. Birks, J. C. Knight, and P. St. J. Russell. "Ultimate low loss of hollow-core photonic crystal fibres", *Optics Express*, vol. 13, no. 1, pp. 236–244, January 2005.

[11] R. S. Windeler, J. L. Wagener, and D. J. DiGiovanni. "Silica-air microstructured fibers: Properties and applications", in *Technical Digest Optical Fiber Communication Conference, OFC'99,* San Diego, California, U.S.A., pp. 106–107, February 1999, paper FG1.

[12] K. Suzuki, H. Kubota, S. Kawanishi, M. Tanaka, and M. Fujita. "High-speed bi-directional polarisation division multiplexed optical transmission in ultra low-loss (1.3 dB/km) polarisation maintaining photonic crystal fibre", *Electronics Letters*, vol. 37, no. 23, pp. 1399–1401, November 2001.

[13] K. Tajima, K. Nakajima, K. Kurokawa, N. Yoshizawa, and M. Ohashi. "Low-loss photonic crystal fibers", in *Technical Digest Optical Fiber Communication Conference, OFC'02,* Anaheim, California, U.S.A., pp. 523–524, March 2002, thS3.

[14] L. Farr, J. C. Knight, B. J. Mangan, and P. J. Roberts. "Low loss photonic crystal fibre", in *Proceedings European Conference on Optical Communication, ECOC'02,* Copenhagen, Denmark, September 2002, post-deadline paper PD 1.3.

[15] K. Tajima, J. Zhou, K. Nakajima, and K. Sato. "Ultra low loss and long length photonic crystal fiber", in *Technical Digest Optical Fiber Communication Conference, OFC'03,* Atlanta, Georgia, U.S.A., March 2003, post-deadline paper PD1.

[16] K. Tajima, J. Zhou, K. Kurokawa, and K. Nakajima. "Low water peak photonic crystal fibres", in *Proceedings European Conference on Optical Communication, ECOC'03,* Rimini, Italy, pp. 42–43, September 2003, post-deadline paper Th4.1.6.

[17] R. Holzwarth, M. Zimmermann, Th. Udem, T. W. Hänsch, P. Russbüldt, K. Gäbel, R. Poprawe, J. C. Knight, W. J. Wadsworth, and P. St. J. Russell. "White-light frequency comb generation with a diode-pumped Cr:LiSAF laser", *Optics Letters*, vol. 26, no. 17, pp. 1376–1378, September 2001.

[18] Y. Wang, Y. Zhao, J. S. Nelson, Z. Chen, and R. S. Windeler. "Ultrahigh-resolution optical coherence tomography by broadband

continuum generation from a photonic crystal fiber", *Optics Letters*, vol. 28, no. 3, pp. 182–184, February 2003.

[19] B. von Vacano, W. Wohlleben, and M. Motzkus. "Actively shaped supercontinuum from a photonic crystal fiber for nonlinear coherent microspectroscopy", *Optics Letters*, vol. 31, no. 3, pp. 413–415, February 2006.

[20] J. D. Shephard, J. D. C. Jones, D. P. Hand, G. Bouwmans, J. C. Knight, P. St. J. Russell, and B. J. Mangan. "High energy nanosecond laser pulses delivered single-mode through hollow-core PBG fibers", *Optics Express*, vol. 12, no. 4, pp. 717–723, February 2004.

[21] J. B. Jensen, L. H. Pedersen, P. E. Hoiby, L. B. Nielsen, T. P. Hansen, J. Riishede, D. Noordegraaf, K. Nielsen, A. Carlsen, and A. Bjarklev. "Photonic crystal fiber based evanescent-wave sensor for detection of biomolecules in aqueous solutions", *Optics Letters*, vol. 29, no. 17, pp. 1974–1976, September 2004.

[22] J. B. Jensen, J. Riishede, J. Broeng, J. Laegsgaard, T. T. Larsen, T. Sorensen, K. Hougaard, E. Knudsen, S. B. Libori, and B. A. "Photonic crystal fibers: fundamental properties and applications within sensors", in *Proceedings of IEEE Sensors 2003,* vol. 1, pp. 269–278, October 2003.

[23] K. Kurokawa, K. Tajima, J. Zhou, K. Nakajima, T. Matsui, and I. Sankawa. "Penalty-free dispersion-managed soliton transmission over 100 km low loss PCF", in *Technical Digest Optical Fiber Communication Conference, OFC'05,* Anaheim, California, U.S.A., March 2005, post-deadline paper PDP21.

Chapter 2

Introduction to photonic crystal fibres

This chapter introduces the definitions and terminologies used throughout this thesis in connection with photonic crystal fibres (PCFs). The aim is to briefly introduce the most important unique properties, which make PCFs attractive for optical communication. In Section 2.1 classification of the different PCFs types are presented. In Section 2.2 the basic properties of air-silica PCFs are discussed, emphasising the major differences between PCFs and conventional fibres.

2.1 Classification of photonic crystal fibres

In PCFs the optical waveguiding is ensured by an arrangement of air holes in the cladding running along the entire fibre length. Inspired by the cladding structure, these fibres are generally referred to as photonic crystal fibres, microstuctured or holey fibres, although, many other names exist and are used for specific PCF designs. In this work only fibres constructed from air-silica material will be considered. The schematic drawing of the cross section of a typical PCF is shown in Figure 2.1. The fibre is constructed from air holes arranged, in principle in any arbitrary, although usually periodic, pattern in silica, forming the cladding. The three most commonly used cladding structures are the triangular or closely packed, the honeycomb and the Kagomé structures [1], all three

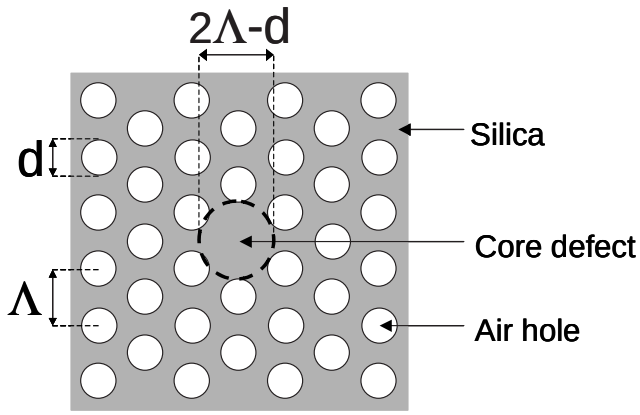

Figure 2.1: Cross section of a single material, silica photonic crystal fibre. The cladding is a periodic arrangement of air holes while the core is formed by omitting a central air hole. Design parameters, hole size (d) and hole-to-hole spacing (Λ) are also illustrated. The core region assumed to have a diameter of $2\Lambda - d$ is encircled by a dashed line.

depicted in Figure 2.2. These structures are also referred to as hexagonal structures. The core is formed by inducing a defect in the structure either by omitting an air hole or by adding extra air holes. Thus PCFs exist both with solid or hollow cores. A PCF can be described by its cladding structure, the air hole size (diameter), d, and the distance between neighbouring air holes, called the pitch or hole-to-hole spacing, Λ, as illustrated in Figure 2.1. The relative hole size, (d/Λ) defined as the ratio of the air hole size and the hole-to-hole spacing is also a commonly used parameter. Another measure often used to describe PCFs is the air filling fraction, defined as the fraction of the area of the air holes to the area of the silica in the cladding. To define the core diameter in PCFs is not as clear as that for standard fibres with a circular core. Nonetheless the core diameter of hexagonal PCFs with one air hole defect is often counted for as $2\Lambda - d$, also indicated in Figure 2.1. Depending on the design, PCFs can be classified into two major groups: index guiding PCFs and photonic bandgap fibres (PBGFs), as illustrated in Figure 2.3.

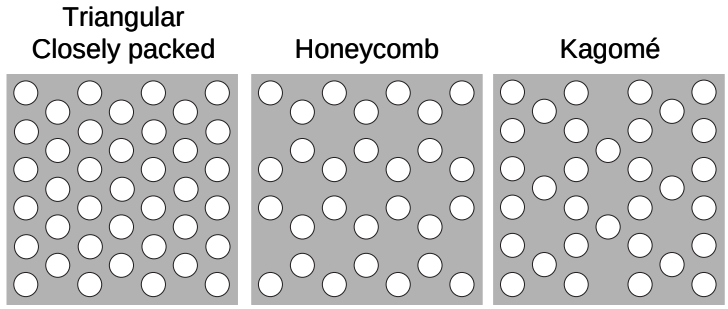

Figure 2.2: Periodic air hole arrangements. Triangular or closely packed (left), honeycomb (middle) and Kagomé (right) structures.

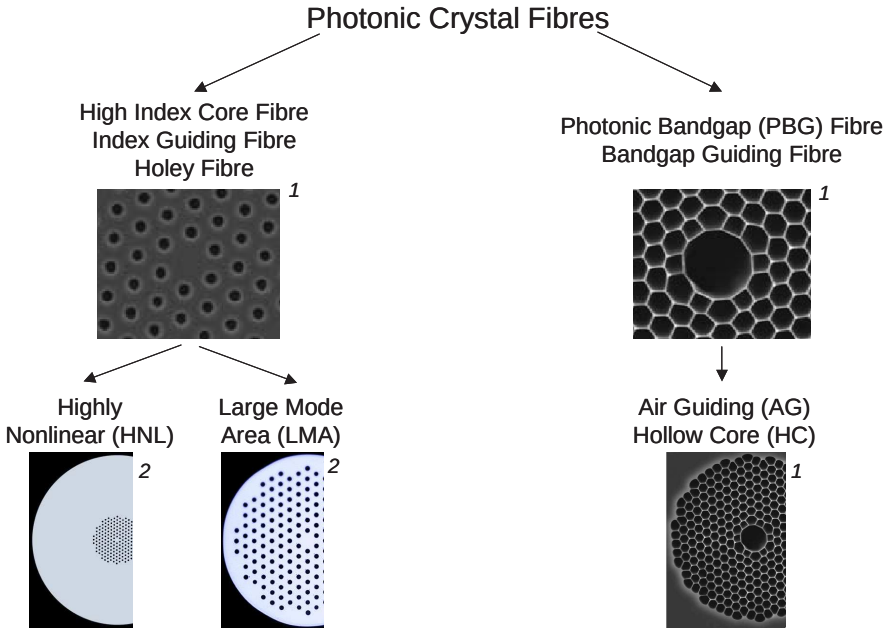

Figure 2.3: Classification of the PCFs considered in this thesis. The microscope images noted by (1) are the property of Blaze Photonics and the ones noted by (2) are the property of Photonic Crystal Fibre A/S.

Index guiding photonic crystal fibres

Index guiding PCFs possess a high refractive index core surrounded by a lower effective refractive index cladding. Thus these fibres guide light by a guiding mechanism similar to conventional fibres, referred to as modified total internal reflection (M-TIR). Typically index guiding fibres have solid core, may it be doped or un-doped. In index guiding PCFs the periodicity of the cladding is not critical for light confinement [2]. The role of the cladding air holes is to reduce the effective refractive index of the cladding to a required level. Nevertheless these fibres are designed with a periodic cladding structure in order to obtain a good control over the optical properties and to ensure reproducibility.

High index core PCFs can be further classified into smaller subgroups such as highly nonlinear photonic crystal fibres (HNL-PCFs), high numerical aperture fibres (HNAFs) and large mode area photonic crystal fibres (LMA-PCFs). This thesis focuses on transmission, signal processing and dispersion compensation applications of LMA-PCF and HNL-PCF for future optical transmission systems. For details on HNAFs the reader is referred to [3–5].

LMA-PCFs are usually single material fibres, meaning that the core-cladding index contrast is controlled purely by the effect of the cladding air holes; the core is un-doped. Most commonly the cladding has a closely packed [6–8] or sometimes honeycomb structure [9, 10]. The core is formed by omitting one or more central holes. LMA-PCFs are designed with a small refractive index difference between core and cladding [6, 10]. This is achieved by small relative hole size and simultaneously a large hole-to-hole spacing, roughly ten times the transmitted signal wavelength ($\Lambda = 10\lambda$) or even larger. Typically the relative hole size (d/Λ) is between 0.4 and 0.6 [11]. LMA-PCFs possess various unique properties that are very attractive for optical communication systems, such as the endlessly single mode property [12], single mode operation for extreme large effective area fibres [6, 10], potentially low loss and nonlinearity [8, 13] and a weakly wavelength dependent effective mode area [14]. These properties are addressed in Section 2.2. The application of LMA-PCFs as transmission media in optical communication systems is presented in Chapter 3.

For HNL-PCFs the effective nonlinearity per unit length is of great interest in order to reduce the device lengths and to relax the optical

power requirements of nonlinearity based devices. A commonly used measure of the fibre nonlinearity is the nonlinear coefficient, γ, given by [15].

$$\gamma = \frac{2\,\pi}{\lambda}\frac{n_2}{A_{\text{eff}}} \tag{2.1}$$

where λ is the signal wavelength, n_2 is the nonlinear-index and A_{eff} is the effective mode area.

Due to the very large refractive index difference of air and silica, HNL-PCFs can be designed to achieve strong light confinement, and thereby very small effective areas, and hence large nonlinear coefficients. In contrast to LMA-PCFs, HNL-PCFs are designed with large relative hole size such that their cladding can have a high content of air [16]. Hole sizes in the range of $0.5\Lambda - 0.9\Lambda$ are practical. The pitch can vary on a broad scale depending on the operational wavelength of the fibre. Pitches in the range of $0.8 - 2$ μm are typical [17–19]. The theoretical lower bound of the obtainable effective area, calculated for an isolated silica rod in air, is $\sim$1.45 μm^2 [20]. In practice, the smallest effective area presented for a pure silica PCF is $\sim$1.5 μm^2 at 1550 nm resulting in $\gamma = 60$ W^{-1}·km^{-1} (using 2.2×10^{-20} m^2/W for the nonlinear-index of pure silica in equation 2.1) [21]. As a comparison with standard fibre technology the smallest effective mode area presented is 11 μm^2 [22]. Additionally HNL-PCFs can have a doped core which further increase the mode confinement and the nonlinear-index. In this case, the core of HNL-PCF is formed by replacing the central air hole of the structure by a doped silica rod [18, 23]. HNL-PCFs are very attractive for signal processing applications due to their widely tailorable dispersion profile [18] and their high effective nonlinearity [21]. Signal processing applications of HNL-PCFs are presented in Chapter 4. Furthermore, PCFs with small cores can be exploited for dispersion compensation as described in Chapter 5.

Photonic bandgap fibres

The other main group of PCFs is referred to as photonic bandgap fibres (PBGFs) or bandgap guiding fibres. Contrary to index guiding PCFs and conventional fibres, the core of PBGFs has a lower refractive index than the effective refractive index of the surrounding microstructured

cladding. PBGFs guide light based on the photonic bandgap (PBG) effect which can be interpreted in a simple way as follows: the cladding structure is a two-dimensional periodic dielectric structure in the cross section of the fibre, while it is invariant along the fibre length. The scale of the periodicity is on the order of the light wavelength. Similarly to electronic bandgaps of semiconductors, the cladding exhibits some forbidden wavelength bands. Light incident on the cladding structure with wavelengths within the bandgap of the structure will be reflected since they are not allowed to propagate in the cladding. Therefore all wavelengths within the bandgap will be trapped in the low index core. Typically, PBGFs are fabricated with uniform periodic cladding structures. Perturbations of the uniformity result in the closing of the bandgaps [24].

PBGFs can be divided into three subgroups: low index core (LIC), Bragg fibres and air guiding or hollow core fibres. LIC [25–28] and Bragg fibres [29–32] have mostly historical significance. The mode field of these fibres can not be approximated by Gaussian distribution. Both LIC and Bragg fibres exhibit a ring shaped mode profile with a minimum intensity point at the center of the fibre core. Due to mode mismatch between ring shaped and Gaussian mode profile, coupling to other fibres or components results in high loss. Therefore these fibres are not practical for system applications. In this thesis the system applications of air guiding fibres are addressed. Their properties and applications are discussed in Chapter 6.

2.2 Properties of index guiding photonic crystal fibres

Until now, a part of the large variety of PCF designs has been described. They have been classified based on their guiding mechanism and their applications. In the following, the unique properties, which have a great importance for telecommunication applications, of index guiding PCFs will be reviewed. Properties such as mode profile, symmetry, V-parameter, endlessly single mode property, loss and polarisation mode dispersion (PMD) will be discussed.

2.2.1 Mode profile, core size

The unique cladding structure of PCFs results most commonly in hexagonal shape, six fold symmetric core (see e.g. Figure 2.1 for a triangular cladding structure with one missing hole as the core). The fundamental mode of PCFs also exhibits the sixfold symmetry of the triangular cladding structure rather than being rotationally symmetric. The shape of the fundamental mode strongly depends on the wavelength relative to the size of the cladding structure. For incident light having a wavelength much larger than the pitch, the cladding structure will act as a homogenous material with lowered refractive index compared to silica, rather than a periodic structure. Light with wavelength in this regime will penetrate into the holes located around the core which results in a hexagonal mode shape (see e.g. Figure 4 in [33]). On the other hand, when the incident light wavelength is comparable or smaller than the structure itself, the field is strongly modulated by the structure. The light will avoid the cladding air holes and will be guided in the intersecting silica bridges. This results in a flower like mode profile [12]. Nevertheless the fundamental mode can be very well approximated by a Gaussian distribution in the case where the field does not penetrate too deeply in the cladding region [14, 34, 35]. The mode field diameter (MFD) of PCFs can be expressed analogously to standard fibres [14].

2.2.2 V-parameter and the endlessly single mode property

In contrast to conventional single mode fibres where the fibre is single mode only above a wavelength, the cut-off wavelength, index guiding PCFs can be designed to be single mode for all wavelengths for which silica glass is transparent. This is one of the most interesting unique properties of PCFs arising from their microstructured cladding structure and it is referred to as the endlessly single mode (ESM) property [36].

The ESM property was both confirmed by experimental observation of the far field pattern [12] and later also explained theoretically [37,38]. In contrast to conventional fibres whose core and cladding refractive index difference can be assumed to be wavelength independent, the refractive index difference between the core and cladding of PCFs is strongly wavelength dependent [39]. The wavelength dependent refractive index

difference permits single mode operation at all wavelengths.

The ESM behaviour can be qualitatively described by analysing the normalised frequency or V-parameter. The V-parameter of standard fibres can be expressed as [40]:

$$V(\lambda) = \frac{2\,\pi\,a}{\lambda}\sqrt{n_{\text{core}}^2 - n_{\text{clad}}^2} \tag{2.2}$$

where a is the core radius, λ is the light wavelength in vacuum and n_{core}, n_{clad} are the refractive indices of the core and cladding, respectively. The second-order cut-off of standard fibres can be determined using the V-parameter. For wavelengths for which the V-parameter value is larger than 2.405, the fibre becomes multimode [40].

The length scale of the V-parameter in equation (2.2) is the core radius, a. However, it is not obvious to apply equation (2.2) directly to PCFs as they do not have a well defined core radius. Mortensen et al. showed that the V-parameter can be unambiguously defined for PCFs by choosing as a natural length scale the pitch (Λ) and suggested the generalised equation [37]:

$$V_{\text{PCF}}(\lambda) = \frac{2\,\pi\,\Lambda}{\lambda}\sqrt{n_{\text{co}}^2(\lambda) - n_{\text{cl}}^2(\lambda)} \tag{2.3}$$

where n_{co} is the effective index of the fundamental mode and n_{cl} is the effective index of the fundamental space-filling mode in the triangular lattice. The fundamental space-filling mode is the fundamental mode of the infinite extent cladding in the absence of the core thus this is the maximum propagation constant allowed in the cladding [36]. This equation can be also expressed in a form in which the V-parameter depends only on the structural parameters d/Λ [38]. The single mode cut-off of PCFs has been determined by using equation (2.3) to be $V_{\text{PCF}} < \pi$.

From equation (2.2) it is obvious that the V-parameter of conventional fibres is inversely proportional to the wavelength (assuming wavelength independent refractive index difference between core and cladding). On the contrary, the refractive index difference of PCFs is strongly wavelength dependent. With decreasing wavelengths, the refractive index of the cladding converges to the refractive index of the core. In [39] Birks et al. shows that indeed the two product terms in equation (2.3) entirely cancel each other. Therefore the V-parameter of PCFs converges to an

upper bound value that is determined by the cladding structure of the fibre.

Fibres designed such that the upper bound of V_{PCF} is equal to π are endlessly single mode. The endlessly single mode criterion for a closely packed structure PCF with core formed by omitting one air hole is $d/\Lambda < 0.44$ [37,38], although this value can differ for other PCF structures [41]. An endlessly single mode photonic crystal fibre (ESM-PCF) design can be scaled to arbitrary sizes by changing the pitch and will still be single mode. This suggests that theoretically extreme large effective area single mode fibres with ultra wide bandwidth and single mode operation are obtainable. Single mode PCFs with large effective area (600, 680 $\mu\mathrm{m}^2$ [6, 9,10]) and very broad single mode wavelength region [42,43] are available and are very attractive for optical communication.

2.2.3 Bending loss

As any other fibres, PCFs suffer from bending loss. However, due to their complex cladding structure, they exhibit bending loss both at short and at long wavelengths, unlike conventional fibres where only the long wavelength bend edge exists [10,44–49]. This additional bend edge is the result of the wavelength dependent refractive index difference. Thereby, similarly to long wavelengths, the mode confinement is weak for short wavelengths. The two band edges determine an operational wavelength window whose width and position is strongly dependent on the structural parameters d and Λ. The hole size determines the width while Λ determines the centre of the operational window. The minimum bend loss occurs at the centre of the operational window which is located at $\lambda \sim \Lambda/2$ [44]. As a consequence, due to the large Λ value of LMA-PCFs the long wavelength edge falls in the region where silica is non transparent. Nevertheless the finite width of the operational window limits the usable wavelength range of endlessly single mode fibres.

In [49] an equation for the macro bending loss of PCFs is given, which only depends on the wavelength and the structural parameters d and Λ. The dependence of the critical radius, $\mathrm{R_{cr}}$ (defined as the radius at which the loss is 3 dB for one fibre loop), on the wavelength and Λ is shown to be [36, 47, 49]:

$$R_{\mathrm{cr}} \propto \frac{\Lambda^3}{\lambda^2} \tag{2.4}$$

The cubic dependence on Λ results in the critical bend radius increasing rapidly with increasing mode areas, while the inverse square wavelength dependence explains the lower wavelength bend edge. Investigation shows that the bending loss can be reduced by increasing the number of cladding air hole rings [46].

Even though, in principle, ESM-PCF designs can be scaled to form arbitrarily large mode areas, in practice the bending loss sets a limitation on the maximum achievable effective area. The usable wavelength range of endlessly single mode photonic crystal fibres is also limited by the bending loss.

2.2.4 Confinement loss

Theoretically, fibres with an infinite cladding structure would be leakage-free. Confinement or leakage loss originates from the finite width of the cladding structure. In LMA-PCFs, by choosing the parameters d and Λ properly, the confinement loss can be negligible [50]. Nevertheless, for small core fibres where the core size is comparable or smaller in dimension than the carried light wavelength, confinement loss gives a significant contribution to the total loss of the fibre [20, 51]. Confinement loss is especially dominating in the wavelength region interesting for telecommunication applications, as usually significant negative waveguide dispersion is realised due to dispersion engineering. The large negative waveguide dispersion around 1550 nm can be achieved by letting the field penetrate into the cladding region, which in turn gives rise to increased confinement loss [52]. Low confinement loss can be achieved for small core PCFs by designing the fibre with at least 6 rings of air holes for a closely packed structure [51]. Increasing the number of air hole rings results in a further reduced confinement loss. Confinement loss can be also reduced by doping the core thus reaching a stronger mode confinement [23].

2.2.5 Fibre loss

The loss spectrum of index guiding PCFs is similar to that of conventional fibers, mostly determined by the silica base material. Therefore, it can be described analogously to conventional fibre. The optical loss of index guiding PCFs (α [dB/km]) was described by Kurokawa et al. as follows [53]:

$$\alpha[\mathrm{dB/km}] = \frac{A}{\lambda^4} + B + \alpha_{\mathrm{OH}} + \alpha_{\mathrm{IR}} \tag{2.5}$$

where A is the Rayleigh scattering coefficient, B is the loss caused by scattering due to imperfections, α_{OH} is the OH absorption loss, α_{IR} is the infrared absorption loss.

Rayleigh scattering and infrared absorption losses are intrinsic losses of the fibre. Rayleigh scattering in pure silica core fibres can be smaller than in germanium doped fibres, as it increases with the Ge concentration. The currently lowest Rayleigh coefficient obtained in a pure silica core PCF is 0.85 dB/(km·μm^4) [54] which compares to the about 1 dB/(km·μm^4) value common for Ge doped standard single mode fibre (SSMF) and to the ∼0.75 dB/(km·μm^4) value measured at 1570 nm of conventional pure silica core fibres [55, 56].

The IR absorption loss is slightly dependent on doping and therefore values comparable to those of SSMFs are typical also for PCFs.

Today, the loss of PCFs is mostly dominated by imperfection and OH absorption losses. Imperfection loss in PCF originates predominantly from hole surface roughness. The two major contributions are scratches and deposited contaminations arising during the stacking process, and fluctuations in the fibre diameter due to non-uniformities in the hole diameter or hole spacing. These roughnesses when comparable in size with the incident light wavelength can increase scattering losses. [53].

The other major contribution to the loss of PCFs is due to OH contamination. OH contamination can be either in the silica glass itself or can penetrate the fibre core during fabrication. By using high-purity silica glass and improved dehydration processes, PCFs with minimised OH absorption have been presented [7].

A comparison of the currently lowest loss PCF and SSMF shows that further improvement in the hole surface roughness and lowering the Rayleigh scattering is possible [8]. LMA-PCFs possess pure silica

cores, therefore the Rayleigh contribution of the loss is expected to be lower than that of Ge doped SSMF. It is believed that the loss of LMA-PCFs will be similar to that of conventional pure silica core fibres which is around 0.15 dB/km at 1550 nm [56].

On the other hand, the loss of HNL-PCFs is much higher than the currently lowest losses reported for index guiding PCFs [7]. HNL-PCFs designed for telecommunication applications with losses of about 9 dB/km have been demonstrated [18]. The main origin of the increased loss is the small structure and strong mode confinement, thus the field propagating in the fibre is more effected by the structural imperfections and the impurities on the air-silica boundaries. Furthermore HNL-PCFs often have doped cores, which increase scattering losses. Additionally these fibres suffer from higher confinement losses than LMA-PCFs. Nevertheless, given that for nonlinear applications short fiber lengths are required, the higher loss of this type of fibers can be tolerated.

2.2.6 Dispersion

In analogy to conventional fibers, the dispersion of index guiding PCFs is dominated by two terms, the material and waveguide dispersions.

Dispersion of large mode area photonic crystal fibres

As the core of LMA-PCFs is usually un-doped silica, the material dispersion coincides with pure silica dispersion. The waveguide dispersion always gives a positive contribution, although with increasing MFDs the significance of waveguide dispersion is decreased. Therefore, the dispersion converges to the level of the pure silica material dispersion for increasing MFDs [11]. The dispersion curve of a LMA-PCF with 600 μm^2 effective area is shown in Figure 2.4 [6].

Nielsen et al. point out that the dispersion of fibres with MFD larger than $\sim$5 μm is determined purely by their MFD and independent of the d/Λ parameter [11]. Due to the anomalous waveguide dispersion of PCFs, positive dispersion values are obtainable even below the zero dispersion wavelength of pure silica. This is not possible in conventional fibres where the obtainable index difference sets a limitation on the achievable waveguide dispersion. The dispersion of LMA-PCF always tends to be higher than that of conventional fibres with corresponding

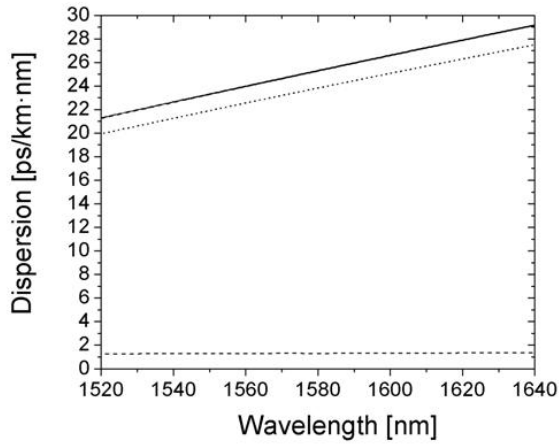

Figure 2.4: Dispersion as a function of wavelength for a large mode area photonic crystal fibre with a 600 μm^2 effective area [6]. The material dispersion (dotted), the waveguide dispersion (dashed line) and the total dispersion (solid) are shown. The graph is the courtesy of Crystal Fibre A/S.

MFD [11]. This high dispersion can be beneficial in wavelength division multiplexing (WDM) systems as it reduces the nonlinear interactions between channels [57].

Dispersion of highly nonlinear photonic crystal fibres

Accurate regulation of the dispersion profile is in many cases the key to obtain good performance in nonlinearity based devices. Currently for telecommunication applications the dispersion profile around 1550 nm is the main concern. As opposed to LMA-PCFs the dispersion of small core HNL-PCFs is dominated by waveguide dispersion. Therefore by modifying the cladding structure or the relative hole size the dispersion of HNL-PCFs can be purposefully changed.

Unlike conventional fibres, HNL-PCFs may posses two zero dispersion wavelengths and a negative dispersion slope at 1550 nm [52]. A nonlinear PCF with zero dispersion wavelength at 1550 nm has been demonstrated. However this fibre had large dispersion slope at this wavelength [23]. Nonlinear PCFs with very broad near zero flattened

dispersion profiles are also obtainable [18, 19, 58–60]. The simultaneous control of the zero dispersion wavelength and the dispersion slope has also been achieved by using a three-fold symmetric hybrid core region HNL-PCF [61]. Another important feature of HNL-PCFs is that their zero dispersion wavelength can be shifted all the way down to the visible region [17, 62]. These unique dispersion properties, not obtainable by conventional fibre technology, make HNL-PCF very attractive for telecommunications for various signal processing applications.

2.2.7 PMD

One of the most severe degradation mechanisms in ultra long haul, high speed transmission systems can be PMD. The polarisation properties of the highly nonlinear fibres (HNLFs) are also important in order to maximise the nonlinear interactions in the fibre.

While conventional fibres ideally have perfect circular cores, PCFs possess mostly hexagonal or other non-circular shaped cores. As birefringence - a part of PMD - originates from fibre asymmetry or mechanical stress, the question about the polarisation properties of PCFs naturally rises.

In any fibre the total birefringence can be expressed as the sum of the geometrical birefringence and the stress-induced birefringence. The geometrical birefringence is caused by a non-circular waveguide, whereas stress-induced birefringence is generated by forces set by the non-circular core.

Ideally, the birefringence of a perfect hexagonal PCF, due to the sixfold rotational symmetry is zero [63]. However, in reality small imperfections break this symmetry giving rise to local birefringence which leads to differential group delay (DGD) between the polarisation modes. It has been shown that local birefringence is likely to increase for small core fibres compared to fibres with larger structures [64].

Stress-induced birefringence can be created intentionally such as in the case of polarisation maintaining fibres [65]. In conventional fibres the different thermal expansion coefficients associated with the different types of materials and doping can cause unintentional stress induced birefringence. In PCFs, as they often are single material fibres, this term is eliminated. Unintentional stress-induced birefringence can also

be generated by cabling, bending or twisting the fibre.

The wavelength and temperature dependences of the birefringence for both LMA-PCFs and HNL-PCFs have been experimentally investigated [64, 66]. The results showed that the intrinsic birefringence of LMA-PCFs is a nearly 100 times less temperature sensitive than for conventional fibres, although it exhibits a very strong wavelength dependence, which suggests that the guiding characteristics change with wavelength [67, 68].

For LMA-PCFs, very low PMD values, comparable to state-of-the-art conventional fibres have been presented [8, 66, 69], which indicates that PCFs can be produced with nearly perfect symmetrical structures. On the contrary, HNL-PCFs having very small structures and often doped core thus usually possess very high PMD values [64, 67, 68].

2.2.8 Splicing of photonic crystal fibres

The possibility of splicing PCFs to conventional fibres or alternatively to another PCF is essential for transmission or signal processing applications. PCFs can be spliced to other fibres using splicers used for conventional fibre technology. Optimising the heat temperature and the heating time in order to avoid the collapse of the cladding holes, splicing loss values of 0.3 to 0.5 dB for both LMA-PCF and HNL-PCF are obtainable [5, 23, 70].

2.3 Summary

In this chapter PCF was introduced. The cladding of these fibres is formed by an air hole arrangement in silica, running along the fibre length. The core is formed by omitting some of the air holes or by including additional air holes. PCFs can guide light by two different mechanisms. Based on the guiding mechanism, fibres can be divided into two major groups. Index guiding PCFs rely on M-TIR, whereas PBGFs guide light by utilising the PBG effect. The design of either type of PCFs can be optimised for various applications. Index guiding PCFs can be further divided into three subgroups, based on their design: LMA-PCFs, HNL-PCFs and HNAFs. PBGFs can be classified into the subgroups of air-guiding PBGFs, LIC fibres and Bragg fibres.

Optical properties, important for telecommunication applications, of LMA-PCFs and HNL-PCFs have been discussed. Properties such as mode profile, V-parameter, endlessly single mode property, bending loss, confinement loss, fibre loss, dispersion and PMD have been discussed. A range of unique optical properties, not obtainable by conventional fibres, originate from the microstructured cladding, thus the strongly wavelength dependent refractive index difference between the core and cladding of PCFs. The effective refractive index of the cladding is close to the refractive index of silica for long relative wavelengths while it is close to the refractive index of air for short relative wavelengths (relative wavelength here means the wavelength relative to pitch).

The core of PCFs has generally a hexagonal shape. The mode profile exhibits the same hexagonal shape as the core and thereby a sixfold rotational symmetry. PCFs can be designed to possess weakly wavelength dependent MFDs. Single mode operation for all practical wavelengths is possible for PCFs with parameters $d/\Lambda < 0.44$, referred to as the endlessly single mode property. In principle, ESM-PCFs can be scaled to obtain arbitrary large effective area fibres with a wide wavelength region where single mode operation is ensured, although bending loss sets a practical limitation on both the useful single mode regime and on the achievable effective areas. As a result of the strongly wavelength dependent refractive index difference, the useful single mode regime of PCFs is limited by bending losses both at the short and long wavelength region. This is in contrast with conventional fibres for which the single mode regime on the short wavelength side is restricted by the second-order cut-off [36].

Confinement loss occurs due to the finite width of the microstructured cladding. Confinement loss can be significantly reduced by increasing the number of air hole rings in the cladding. Negligible confinement loss can be obtained for LMA-PCFs. However for small core PCFs, it contributes significantly to the total fibre loss. The loss of LMA-PCFs is expected to be lower than the loss of SSMF and be on the level of pure silica core fibres. Nevertheless, today the loss of LMA-PCFs is still higher than the loss of SSMF, which can be mostly attributed to scattering due to hole surface roughness.

The dispersion of LMA-PCFs is dominated by the silica material dispersion. The waveguide dispersion of these type of PCFs is always

positive. However with increasing core sizes the waveguide dispersion becomes negligible. On the other hand, for HNL-PCFs the waveguide dispersion dominates. Therefore, by changing the structural parameters (d and Λ) and the hole arrangement in the cladding, the dispersion of HNL-PCFs can be tailored on a wide scale to meet the needs of the applications. In addition, very low PMD values, comparable to state-of-the-art conventional fibres, are obtainable for LMA-PCFs. On the contrary, small core HNL-PCFs may exhibit very large PMD.

The unique properties such as weakly wavelength independent mode field diameter, endlessly single mode property, extreme large effective area fibre with single mode operation, the potentially very low loss and nonlinearity and the low PMD values, make LMA-PCFs an attractive candidate as a transmission fibre in long-haul, high bit rate transmission systems. The very high nonlinearity and widely tailorable dispersion profile of HNL-PCFs make these fibres very promising for signal processing applications.

References to Chapter 2

[1] S. E. B. Libori. *Photonic Crystal Fibers - From Theory to Practice.* Ph.D. thesis, Research Center COM, Technical University of Denmark, Kgs. Lyngby, Denmark, February 2002. ISBN 87-90974-29-8.

[2] T. M. Monro, P. J. Bennett, N. G. R. Broderick, and D. J. Richardson. "Holey fibers with random cladding distributions", *Optics Letters*, vol. 25, no. 4, pp. 206–208, February 2000.

[3] J. Lægsgaard, K. P. Hansen, M. D. Nielsen, T. P. Hansen, J. Riishede, K. Hougaard, T. Sørensen, T. T. Larsen, N. A. Mortensen, J. Broeng, J. B. Jensen, and A. Bjarklev. in *Proceedings International Microwave and Optoelectronics Conference, IMOC'2003,* Iguaza Falls, Brazil, vol. 1, pp. 259–264, September 2003.

[4] J. Limpert, T. Schreiber, S. Nolte, H. Zellmer, A. Tünnermann, R. Iliew, F. Lederer, J. Broeng, G. Vienne, A. Petersson, and C. Jakobsen. "High-power air-clad large-mode-area photonic crystal fiber laser", *Optics Express*, vol. 11, no. 7, pp. 818–823, April 2003.

[5] A. Bjarklev, J. Broeng, and A. S. Bjarklev. *Photonic crystal fibres.* Kluwer academic publishers, First edition, 2003.

[6] M. D. Nielsen, J. R. Folkenberg, and N. A. Mortensen. "Single-mode photonic crystal fibre with effective area of 600 μm^2 and low bending loss", *Electronics Letters*, vol. 39, no. 25, pp. 1802–1803, December 2003.

[7] K. Tajima, J. Zhou, K. Kurokawa, and K. Nakajima. "Low water peak photonic crystal fibres", in *Proceedings European Conference on Optical Communication, ECOC'03,* Rimini, Italy, pp. 42–43, September 2003, post-deadline paper Th4.1.6.

[8] K. Tajima and J. Zhou. "Ultra low loss and long length photonic crystal fiber", in *IEICE Transactions on Electronics,* vol. E88-C, pp. 870–875, May 2005.

[9] J. C. Knight, T. A. Birks, R. Cregan, P. St. J. Russell, and J. P. de Sandro. "Large mode area photonic crystal fibre", *Electronics Letters*, vol. 34, no. 13, pp. 1347–1348, June 1998.

[10] J. C. Baggett, T. M. Monro, K. Furusawa, and D. J. Richardson. "Comparative study of large-mode holey and conventional fibers", *Optics Letters*, vol. 26, no. 14, pp. 1045–1047, July 2001.

[11] M. D. Nielsen, C. Jacobsen, N. A. Mortensen, J. R. Folkenberg, and H. R. Simonsen. "Low-loss photonic crystal fibers for transmission systems and their dispersion properties", *Optics Express*, vol. 12, no. 7, pp. 1372–1376, April 2004.

[12] J. C. Knight, T. A. Birks, P. St. J. Russell, and J. P. de Sandro. "Properties of photonic crystal fiber and the effective index model", *Journal of the Optical Society of America A*, vol. 15, no. 3, pp. 748–752, March 1998.

[13] T. Kato, M. Hirano, M. Onishi, and M. Nishimura. "Ultra-low non-linearity low-loss pure silica core fibre for long-haul WDM transmission", *Electronics Letters*, vol. 35, no. 19, pp. 1615–1617, September 1999.

[14] M. D. Nielsen, N. A. Mortensen, J. R. Folkenberg, and A. Bjarklev. "Modal cutoff and the V parameter in photonic crystal fibers", *Optics Letters*, vol. 28, no. 23, pp. 2309–2311, December 2003.

[15] G. P. Agrawal. *Nonlinear Fiber Optics.* Academic Press, Inc., Second edition, 1995. ISBN 0-12-045142-5.

[16] T. M. Monro and D. J. Richardson. "Holey optical fibres: Fundamental properties and device applications", *Optical Telecommunications*, vol. 4, no. 1, pp. 175–186, 2003.

[17] J. C. Knight, J. Arriaga, T. A. Birks, A. Ortigosa-Blanch, W. J. Wadsworth, P. St. J. Russell, and D. M. Atkin. "Anomalous dispersion in photonic crystal fiber", *IEEE Photonics Technology Letters*, vol. 12, no. 7, pp. 807–809, July 2000.

[18] K. P. Hansen. "Dispersion flattened hybrid-core nonlinear photonic crystal fiber", *Optics Express*, vol. 11, no. 13, pp. 1503–1509, June 2003.

[19] A. Ferrando, E. Silvestre, P. Andrés, J. J. Miret, and M. V. Andrés. "Designing the properties of dispersion-flattened photonic crystal fibers", *Optics Express*, vol. 9, no. 13, pp. 687–697, December 2001.

[20] V. Finazzi, T. M. Monro, and D. J. Richardson. "Small-core silica holey fibers: nonlinearity and confinement loss trade-offs", *Journal of the Optical Society of America B*, vol. 20, no. 7, pp. 1427–1436, July 2003.

[21] W. Belardi, J. H. Lee, K. Furusawa, Z. Yusoff, P. Petropoulos, M. Ibsen, T. M. Monro, and D. J. Richardson. "A 10 Gbit/s tuneable wavelength converter based on four-wave mixing in highly nonlinear holey fibre", in *Proceedings European Conference on Optical Communication, ECOC'02,* Copenhagen, Denmark, September 2002, post-deadline paper PD1.2.

[22] T. Okuno, M. Onishi, T. Kashiwada, S. Ishikawa, and M. Nishimura. "Silica-based functional fibers with enhanced nonlinearity and their applications", *IEEE Journal of Selected Topics in Quantum Electronics*, vol. 5, no. 5, pp. 1385–1391, September/October 1999.

[23] K. P. Hansen, J. R. Jensen, C. Jacobsen, H. R. Simonsen, J. Broeng, P. M. W. Skovgaard, A. Petersson, and A. Bjarklev. "Highly nonlinear photonic crystal fiber with zero-dispersion at 1.55 μm", in *Technical Digest Optical Fiber Communication Conference, OFC'02,* Anaheim, California, U.S.A., March 2002, post-deadline paper FA9.

[24] J. A. West and D. C. Allan. "Effect of disorder on photonic bandgap fibers", in *Proceedings European Conference on Optical Communication, ECOC'02,* Copenhagen, Denmark, pp. 1–2, September 2002, paper S1.4.

[25] J. C. Knight, J. Broeng, T. A. Birks, and P. St. J. Russell. "Photonic band gap guidance in optical fibers", *Science*, vol. 282, no. 5393, pp. 1476–1477, November 1998.

[26] J. Broeng, S. E. Barkou, A. Bjarklev, J. C. Knight, T. A. Birks, and P. St. J. Russell. "Highly increased photonic band gaps in silica/air structures", *Optics Communications*, vol. 156, no. 4-6, pp. 240–244, November 1998.

[27] J. B. Nielsen, T. Søndergaard, S. E. Barkou, A. Bjarklev, J. Broeng, and M. B. Nielsen. "Two-dimensional Kagomé structure, fundamental hexagonal photonic crystal configuration", *Electronics Letters*, vol. 35, no. 20, pp. 1736–1737, September 1999.

[28] J. Broeng, T. Søndergaard, S. E. Barkou, P. M. Barbeito, and A. Bjarklev. "Waveguidance by the photonic bandgap effect in optical fibres", *Journal of Optics A: Pure and Applied Optics*, vol. 1, no. 4, pp. 477–482, July 1999.

[29] G. Vienne, Y. Xu, C. Jakobsen, H. J. Deyerl, T. P. Hansen, B. H. Larsen, J. B. Jensen, T. Sørensen, M. Terrel, Y. Huang, R. Lee, N. A. Mortensen, J. Broeng, H. Simonsen, A. Bjarklev, and A. Yariv. "First demonstration of air-silica Bragg fiber", in *Technical Digest Optical Fiber Communication Conference, OFC'04,* Los Angeles, California, U.S.A., February 2004, post-deadline paper PDP25.

[30] G. Vienne, Y. Xu, C. Jakobsen, H.-J. Deyerl, J. B. Jensen, T. Sørensen, T. P. Hansen, Y. Huang, M. Terrel, R. K. Lee, N. A.

Mortensen, J. Broeng, H. Simonsen, A. Bjarklev, and A. Yariv. "Ultra-large bandwidth hollow-core guiding in all-silica Bragg fibers with nano-supports", *Optics Express*, vol. 12, no. 15, pp. 3500–3508, July 2004.

[31] S. Février, R. Jamier, J.-M. Blondy, S. L. Semjonov, M. E. Likhachev, M. M. Bubnov, E. M. Dianov, V. F. Khopin, M. Y. Salganskii, and A. N. Guryanov. "Low loss large mode area Bragg fibre", in *Proceedings European Conference on Optical Communication, ECOC'05,* Glasgow, Scotland, September 2005, post-deadline paper 4.4.3.

[32] S. Février, P. Viale, F. Gérôme, P. Leproux, P. Roy, J.-M. Blondy, B. Dussardier, and G. Monnom. "Very large effective area single-mode photonic bandgap fibre", *Electronics Letters*, vol. 39, no. 17, pp. 1240–1242, August 2003. doi:10.1049/el:20030841.

[33] K. G. Hougaard, A. Bjarklev, E. Knudsen, S. B. Libori, and J. Riishede. "Coupling to photonic crystal fibers", in *Technical Digest Optical Fiber Communication Conference, OFC'02,* Anaheim, California, U.S.A., pp. 627–628, March 2002, paper ThGG11.

[34] N. A. Mortensen and J. R. Folkenberg. "Near-field to far-field transition of photonic crystal fibers: symmetries and interference phenomena", *Optics Express*, vol. 10, no. 11, pp. 475–481, June 2002.

[35] N. A. Mortensen, J. R. Folken, P. M. W. Skovgaard, and J. Broeng. "Numerical aperture of single-mode photonic crystal fibers", *IEEE Photonics Technology Letters*, vol. 14, no. 8, pp. 1094–1096, August 2002.

[36] T. A. Birks, J. C. Knight, and P. St. J. Russell. "Endlessly single-mode photonic crystal fiber", *Optics Letters*, vol. 22, no. 13, pp. 961–963, July 1997.

[37] N. A. Mortensen, J. R. Folkenberg, M. D. Nielsen, and K. P. Hansen. "Modal cutoff and the V parameter in photonic crystal fibers", *Optics Letters*, vol. 28, no. 20, pp. 1879–1881, 2003.

[38] M. D. Nielsen and N. A. Mortensen. "Photonic crystal fiber design based on the V-parameter", *Optics Express*, vol. 11, no. 21, pp. 2762–2768, October 2003.

[39] T. A. Birks, J. C. Knight, B. J. Mangan, and P. St. J. Russell. "Photonic crystal fibres: an endless variety", *IEICE Transactions on Electronics*, vol. E84-C, no. 5, pp. 585–592, May 2001.

[40] G. P. Agrawal. *Fiber-Optic Communication Systems.* John Wiley & Sons, Inc., Second edition, 1997. ISBN 0-471-17540-4.

[41] M. D. Nielsen, N. Mortensen, J. R. Folkenberg, A. Petersson, and A. Bjarklev. "Improved all-silica endlessly single-mode photonic crystal fiber", in *Technical Digest Optical Fiber Communication Conference, OFC'03,* Atlanta, Georgia, U.S.A., vol. 2, pp. 701–702, March 2003, paper FI7.

[42] J. C. Knight, T. A. Birks, P. St. J. Russell, and D. M. Atkin. "All-silica single-mode optical fiber with photonic crystal cladding", *Optics Letters*, vol. 21, no. 19, pp. 1547–1549, October 1996.

[43] K. Nakajima, J. Zhou, K. Tajima, K. Kurokawa, C. Fukai, and I. Sankawa. "Ultrawide-band single-mode transmission performance in a low-loss PCF", *Journal of Lightwave Technology*, vol. 23, no. 1, pp. 7–11, January 2005.

[44] T. Sørensen, J. Broeng, A. Bjarklev, E. Knudsen, and S. E. B. Libori. "Macro-bending loss properties of photonic crystal fibre", *Electronics Letters*, vol. 37, no. 5, pp. 287–289, March 2001.

[45] T. Sørensen, J. Broeng, A. Bjarklev, T. P. Hansen, E. Knudsen, S. E. B. Libori, H. R. Simonsen, and J. R. Jensen. "Spectral macro-bending loss considerations for photonic crystal fibres", *IEE Proceedings-Optoelectronics*, vol. 149, pp. 206–210, October 2002.

[46] J. C. Baggett, T. M. Monro, K. Furusawa, V. Finazzi, and D. J. Richardson. "Understanding bending losses in holey optical fibers", *Optics Communications*, vol. 227, pp. 317–335, September 2003.

[47] N. A. Mortensen and J. R. Folkenberg. "Low-loss criterion and effective area considerations for photonic crystal fibres", *Journal*

of Optics A: Pure and Applied Optics, vol. 5, pp. 163–167, March 2003.

[48] M. D. Nielsen, J. R. Folkenberg, N. A. Mortensen, and A. Bjarklev. "Bandwidth comparison of photonic crystal fibers and conventional single-mode fibers", *Optics Express*, vol. 12, no. 3, pp. 430–435, February 2004.

[49] M. D. Nielsen, N. A. Mortensen, M. Albertsen, J. R. Folkenberg, A. Bjarklev, and D. Bonacinni. "Predicting macrobending loss for large-mode area photonic crystal fibers", *Optics Express*, vol. 12, no. 8, pp. 1775–1779, April 2004.

[50] T. P. White, R. C. McPhedran, C. M. de Sterke, L. C. Botten, and M. J. Steel. "Confinement losses in microstructured optical fibers", *Optics Letters*, vol. 26, no. 21, pp. 1660–1662, November 2001.

[51] V. Finazzi, T. M. Monro, and D. J. Richardson. "Confinement loss in highly nonlinear holey optical fibres", in *Technical Digest Optical Fiber Communication Conference, OFC'02,* Anaheim, California, U.S.A., pp. 524–525, March 2002.

[52] K. Hansen, J. Folkenberg, A. Petersson, and A. Bjarklev. "Properties of nonlinear photonic crystal fibers for telecommunication applications", in *Technical Digest Optical Fiber Communication Conference, OFC'03,* Atlanta, Georgia, U.S.A., pp. 694–696, March 2003, post-deadline paper PD02.

[53] K. Kurokawa, K. Tajima, K. Tsujikawa, and K. Nakajima. "Reducing the loss in photonic crystal fibres", in *Proceedings European Conference on Optical Communication, ECOC'05,* Glasgow, Scotland, vol. 2, pp. 279–282, September 2005, paper Tu4.4.1.

[54] K. Kurokawa, K. Tajima, J. Zhou, K. Nakajima, T. Matsui, and I. Sankawa. "Penalty-free dispersion-managed soliton transmission over 100 km low loss PCF", in *Technical Digest Optical Fiber Communication Conference, OFC'05,* Anaheim, California, U.S.A., March 2005, post-deadline paper PDP21.

[55] M. Ohashi, K. Shiraki, and K. Tajima. "Optical loss property of silica-based single-mode fibers", *Journal of Lightwave Technology*, vol. 10, no. 5, pp. 539–543, May 1992.

[56] K. Nagayama, M. Kakui, M. Matsui, T. Saitoh, and Y. Chigusa. "Ultra-low-loss (0.1484 dB/km) pure silica core fibre and extension of transmission distance", *Electronics Letters*, vol. 38, no. 20, pp. 1168–1169, September 2002.

[57] P. Bayvel and R. Killey. *Nonlinear Optical Effects in WDM Transmission*, In I. Kaminow and T. Li, editors, *Optical Fiber Telecommunications IVB Components,* Chapter 13, Academic Press, March 2002. ISBN 0-12-395173-9.

[58] W. H. Reeves, J. C. Knight, P. St. J. Russell, and P. J. Roberts. "Demonstration of ultra-flattened dispersion in photonic crystal fibers", *Optics Express*, vol. 10, no. 14, pp. 609–613, July 2002.

[59] F. Poli, A. Cucinotta, S. Selleri, and A. H. Bouk. "Tailoring of flattened dispersion in highly nonlinear photonic crystal fibers", *IEEE Photonics Technology Letters*, vol. 16, no. 4, pp. 1065–1067, April 2004.

[60] K. Saitoh, M. Koshiba, T. Hasegawa, and E. Sasaoka. "Chromatic dispersion control in photonic crystal fibers: application to ultra-flattened dispersion", *Optics Express*, vol. 11, no. 8, pp. 843–852, April 2003.

[61] K. P. Hansen, J. R. Folkenberg, C. Peucheret, and A. Bjarklev. "Fully dispersion controlled triangular-core nonlinear photonic crystal fiber", in *Technical Digest Optical Fiber Communication Conference, OFC'03,* Atlanta, Georgia, U.S.A., pp. 806–808, March 2003, post-deadline paper PD02.

[62] D. Mogilevtsev, T. A. Birks, and P. St. J. Russell. "Group-velocity dispersion in photonic crystal fibers", *Optics Letters*, vol. 23, no. 21, pp. 1662–1664, November 1998.

[63] M. J. Steel, T. P. White, C. M. de Sterke, R. C. McPhedran, and L. C. Botten. "Symmetry and degeneracy in microstructured optical fibers", *Optics Letters*, vol. 26, no. 8, pp. 488–490, April 2001.

[64] T. Ritari, H. Ludvigsen, M. Wegmüller, M. Legeré, N. Gisin, J. R. Folkenberg, and M. D. Nielsen. "Experimental study of polarization properties of highly birefringent photonic crystal fibers", *Optics Express*, vol. 12, no. 24, pp. 5931–5939, November 2004.

[65] J. R. Folkenberg, M. D. Nielsen, N. A. Mortensen, C. Jakobsen, and H. R. Simonsen. "Polarization maintaining large mode area photonic crystal fiber", *Optics Express*, vol. 12, no. 5, pp. 956–960, March 2004.

[66] T. Ritari, T. Niemi, H. Ludvigsen, M. Wegmüller, N. Gisin, J. R. Folkenberg, and A. Petersson. "Polarization-mode dispersion of large mode-area photonic crystal fibers", *Optics Communications*, vol. 226, no. 1-6, pp. 233–239, September 2003.

[67] M. Wegmüller, M. Legeré, N. Gisin, T. Ritari, H. Ludvigsen, J. R. Folkenberg, and K. P. Hansen. "Experimental investigation of wavelength and temperature dependence of phase and group birefringence in photonic crystal fibers", in *Proceedings International Conference on Transparent Optical Networks,* Wroclaw, Poland, pp. 111–114, July 2004, paper We.A2.7.

[68] M. Wegmüller, F. Scholder, A. Fougères, N. Gisin, T. Niemi, G. Genty, H. Ludvigsen, O. Deparis, and M. Wicks. "Evaluation of measurement techniques for characterization of photonic crystal fibers", in *Technical Digest Conference on Lasers and Electro-Optics, CLEO'02,* Long Beach, California, U.S.A., p. 617, May 2002, paper JThA4.

[69] T. Larsen, A. Bjarklev, A. Peterson, J. Folkenberg, and P. Pehrson. "Second-order polarization-mode dispersion in photonic crystal fibers", in *Technical Digest Optical Fiber Communication Conference, OFC'03,* Atlanta, Georgia, U.S.A., vol. 86, pp. 372–373, March 2003, paper WJ6.

[70] J. Lægsgaard and A. Bjarklev. "Reduction of coupling loss to photonic crystal fibers by controlled hole collapse: a numerical study", *Optics Communications*, vol. 237, no. 4-6, pp. 431–435, July 2004.

Chapter 3

Transmission over index guiding photonic crystal fibres

From the time, index guiding photonic crystal fibres (PCFs) have been first demonstrated [1], they draw much attention, and their properties have been intensively investigated. Index guiding large mode area photonic crystal fibres (LMA-PCFs) exhibit several qualities that make them attractive candidates as transmission fibres, as it has been discussed in the previous chapter. Advantages arising from their pure silica core are the potentially reduced loss and nonlinearity, compared to standard single mode fibres (SSMFs) [2, 3]. Furthermore numerous properties, not obtainable by conventional fibres, originate from their microstructured cladding such as the endlessly single mode property [4].

The first proposal of using index guiding PCFs as transmission fibres was already published at the end of year 2001 by Suzuki et al. [5]. They demonstrated a 10 Gbit/s return-to-zero (RZ) bi-directional signal transmission at 1550 nm over 1.5 km of polarisation maintaining PCF. This experiment also reported the lowest loss (1.3 dB/km) and longest drawn fibre piece at that time.

Further demonstrations of the advantages of index guiding PCFs as transmission fibres, however, have been delayed due to the immature fabrication technique. After the first demonstration of PCF transmission, it took less than a year before the loss of index guiding PCFs could

be reduced below 1 dB/km [6, 7]. At this moment, when the loss has been decreased to the same order of magnitude as the loss of conventional fibres, activities considering index guiding PCFs for data transmission have started. Already today, there have been several system experiments demonstrating the potential of LMA-PCFs as transmission fibres. Transmission experiments with increasing capacities over various lengths of PCFs, and experiments exploiting the endlessly single mode property have been conducted.

In this chapter, several experiments considered as milestones in using PCFs as transmission fibres are described. The first three presented experiments are 10, 20 and 40 Gbit/s data transmission over 5.6 km index guiding PCF. These initial experiments are among the first in the world investigating PCFs as transmission fibres. An experiment increasing the total capacity transmitted on a single wavelength to 80 Gbit/s by using a polarisation multiplexing technique is also introduced. This experiment verifies that the polarisation properties of LMA-PCFs may make them suitable for high speed, polarisation multiplexed applications. Furthermore, a recirculating loop experiment is described which increased the total transmission distance over index guiding PCFs by more than four times of any other PCF transmission presented earlier. Afterwards, other demonstrations of index guiding PCFs as transmission fibres are discussed. Finally the chapter is summarised.

3.1 Fibre characteristics

All photonic crystal fibres used in the experiments presented in this chapter were made from pure silica. All PCFs were provided by Crystal Fibre A/S. The cladding region consisted of numerous air holes placed in a closed packed arrangement around a solid region formed by omitting one single central hole, comprising the fibre core. The fibres were designed to be endlessly single mode and their cladding diameter of 125 μm and coated diameter of 240 μm were compatible to those of conventional SSMFs. Furthermore, the fibres were equipped with FC/PC connectorised SSMF pigtails spliced to the PCF.

The first generation 5.6 km transmission span consisted of two spools with lengths of 2.6 and 3.0 km. The hole-to-hole spacing was 7.5 μm and the diameter of the air holes relative to the pitch was 0.43. An

Fibre spool	L [km]	α $\left[\frac{\text{dB}}{\text{km}}\right]$	D $\left[\frac{\text{ps}}{(\text{nm}\cdot\text{km})}\right]$	PMD $\left[\frac{\text{ps}}{\sqrt{\text{km}}}\right]$	A_{eff} [μm^2]	MFD [μm]	d/Λ	Λ [μm]
PCF1	2.6	1.7	32	0.1	72	9.6	0.43	7.5
PCF2	3.0	1.7	32	0.1	72	9.6	0.43	7.5
PCF3	8.8	<1	34.5	–	44	7.5	0.49	7.5
PCF4	10.4	<1	31.5	–	64	9	0.49	6.3

Table 3.1: Properties of the transmission PCFs used in the system experiments. L refers to the total length of the spool, α gives the fiber loss and not the span loss. Fibres PCF3 and PCF4 were spliced from 2 and 3 pieces with lengths 2.6+6.2 km and 3.0+3.2+4.2 km, respectively. All other parameters (except the d/Λ and Λ) are given at 1550 nm.

effective area of 72 μm^2 at 1550 nm was calculated from the estimated mode field diameter (MFD) [8], assuming Gaussian distribution of the field. The loss was measured as 2.7 dB/km at 1310 nm and 1.7 dB/km at 1550 nm for both fibres. A nonlinear coefficient of 1.2 W^{-1}km^{-1} was measured using the continuous wave - self phase modulation (CW-SPM) method [9]. The polarisation mode dispersion (PMD) was measured to be 0.1 ps/$\sqrt{\text{km}}$ using the Jones eigenmatrix analysis method [10,11]. At 1550 nm, the chromatic dispersion for both spools was 32 ps/(nm·km).

By improving the production technology fibres with lower loss and longer length were drawn. All the second generation transmission PCF pieces had less than 1 dB/km loss at 1550 nm. Two spools with lengths of 8.8 and 10.4 km were spliced together from five pieces of fibre with an average length of 4 km, where the longest piece was 6.4 km long. The hole-to-hole spacing was 7.5 and 6.3 μm for the 8.8 and 10.4 km spools, respectively, and the relative air hole size was 0.49 in both cases. The 8.8 km fibre had a MFD of 7.5 μm and a dispersion of 34.5 ps/(nm·km) at 1550 nm, while the MFD and the dispersion of the 10.4 km fibre were 9 μm and 31.5 ps/(nm·km) at 1550 nm, respectively. These MFD values, assuming Gaussian distribution of the field, translate into effective areas of 44 and 64 μm^2 for the 8.8 and 10.4 km spools, respectively.

The parameters of all four fibre spools have been provided by Crystal Fibre A/S, apart from the nonlinear coefficient and the PMD parameters. The parameters are summarised in Table 3.1. These fibres will be

referred to as large mode area photonic crystal fibre in the experiment descriptions.

3.2 Transmissions at 10, 20 and 40 Gbit/s over photonic crystal fibre

Some of the earliest experiments, introducing transmission over PCF, are discussed in this section. The presented experiments are among the firsts demonstrating the potential of LMA-PCF for high speed data transmission.

These experiments are performed using the first generation transmission PCFs, PCF1 and PCF2. The bit rate is increased from 10 to 20 and 40 Gbit/s. Due to the high dispersion of LMA-PCFs (roughly double as much as for SSMF at 1550 nm), significant signal distortion is observable already at 20 Gbit/s over 5.6 km PCF. Dispersion compensation using chirped fibre Bragg gratings (FBG) [12] or conventional dispersion compensating fibre (DCF) [13] have been considered.

The system performance is evaluated by measuring the bit error rate (BER) as a function of average received power. The receiver sensitivity is calculated at a BER of 1.0×10^{-9}. The signal degradation caused by the investigated system is quantified by using the power penalty, defined as the difference between the sensitivity measured after and before the investigated system and expressed in dB.

3.2.1 10 Gbit/s transmission

One of the first reports on the potential of index guiding PCFs as transmission fibre demonstrated a 10 Gbit/s non return-to-zero (NRZ) signal transmission at 1550 nm over 5.6 km PCF [14].

Experimental setup

The experimental setup is shown in Figure 3.1. Continuous wave (CW) light at 1550 nm is externally modulated by a chirp-free $LiNbO_3$ Mach-Zehnder (MZ) modulator to generate an NRZ encoded optical signal. The length of the pseudo random bit sequence (PRBS) used as modulating signal is 2^{31}-1 bits. The generated 10 Gbit/s NRZ signal is am-

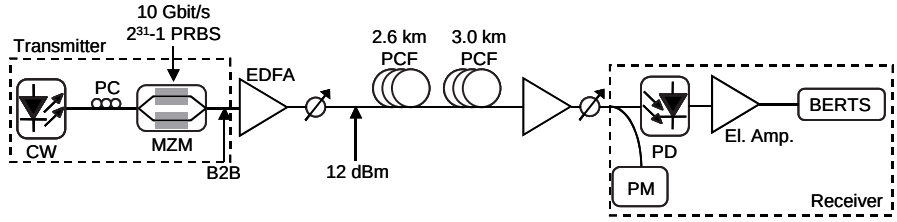

Figure 3.1: Experimental setup for 10 Gbit/s NRZ signal transmission over 5.6 km PCF. PM - power meter.

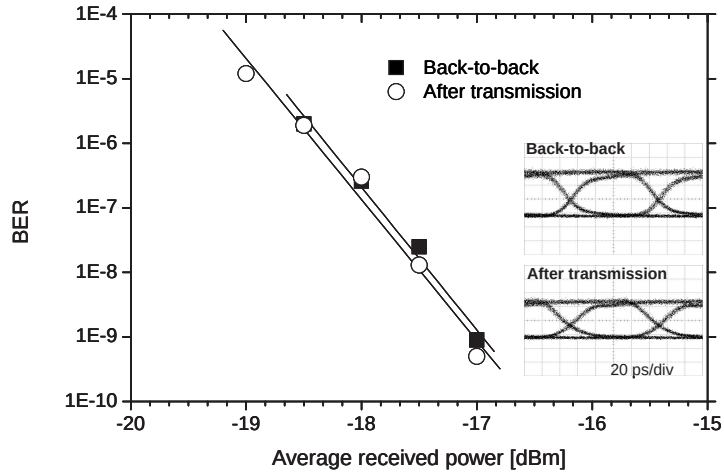

Figure 3.2: Bit error rate curves measured in the back-to-back case and after transmission over 5.6 km PCF for 10 Gbit/s NRZ signal. Corresponding eye-diagrams are shown as insets. Horizontal scale of the inset: 20 ps/div.

plified by an erbium doped fibre amplifier (EDFA) to an average power of 12 dBm before it is coupled into the PCF transmission span. The transmission span consists of two index guiding PCF spools with 2.6 and 3.0 km lengths (PCF1 and PCF2 as described in Table 3.1). Each of the two fibre spools was approximately twice as long as the longest PCF previously used for transmission. An EDFA at the output of the fibre compensated for the span loss. The signal degradation is quantified by measuring the BER at the receiver. The BER is measured after direct detection.

Results

The back-to-back eye-diagram (recorded at the output of the transmitter) and the eye-diagram after transmission over 5.6 km PCF are shown as insets in Figure 3.2. The eye-diagrams show that there was no significant distortion induced on the signal during propagation. The bit error rate curves measured in the back-to-back case and after transmission, plotted in Figure 3.2, are almost indistinguishable, showing that there was no sensitivity degradation measured after transmission.

3.2.2 20/40 Gbit/s transmission using chirped fibre Bragg gratings dispersion compensation

Dispersion and polarisation effects such as PMD or birefringence have a significant deleterious impact for high bit rate systems [15, 16]. For 10 Gbit/s transmission over 5.6 km of LMA-PCF none of these distortions were observable. In the following experiment, the bit rate is increased to 20 and 40 Gbit/s. At these bit rates, already significant dispersion induced signal distortion is observable. To compensate for the accumulated dispersion of the fibre, a chirped FBG is used. For details on dispersion compensation using chirped FBG please refer to [17, 18].

Experimental setup

The experimental setup is shown in Figure 3.3. CW light at 1553.5 nm is externally modulated into the NRZ format by a chirp-free $LiNbO_3$ MZ modulator, capable of up to 40 Gbit/s operation. The PRBS was 2^{31}-1 bits long. NRZ modulated signals at 20 or 40 Gbit/s are generated.

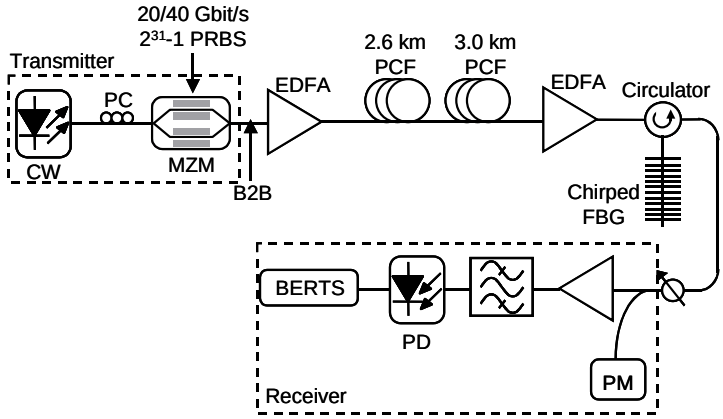

Figure 3.3: Experimental setup for 20/40 Gbit/s PCF transmission. Dispersion compensation is achieved by a chirped FBG connected via a circulator. PM - power meter.

The signal is amplified by an EDFA to an average power of 12 dBm before it is coupled into the PCF transmission span. The transmission span is composed of two index guiding PCF spools with 2.6 and 3.0 km lengths (PCF1 and PCF2 from Table 3.1), as in the case of 10 Gbit/s transmission. At the output of the fibres, an EDFA compensated for the span loss. A chirped FBG[1], inserted via a circulator, compensated for the chromatic dispersion of the transmission fibres. The 3 dB bandwidth of the FBG is ∼0.3 nm and its centre wavelength is 1553.5 nm. The dispersion of the FBG at 1550 nm is ∼−200 ps/nm. The signal is received by a pre-amplified receiver consisting of an EDFA followed by an optical bandpass filter (OBPF) with 3.5 nm 3 dB bandwidth centred at 1553.5 nm, and a photodetector (PD) with a 3 dB bandwidth of 50 GHz.

Results

The eye diagrams recorded for the back-to-back case (at the output of the transmitter), after transmission through 5.6 km of PCF and after the entire transmission span, including the transmission fibre and the

[1]The chirped FBG was fabricated by Hans-Jürgen Deyerl, former employee of COM-Glass Competence Area.

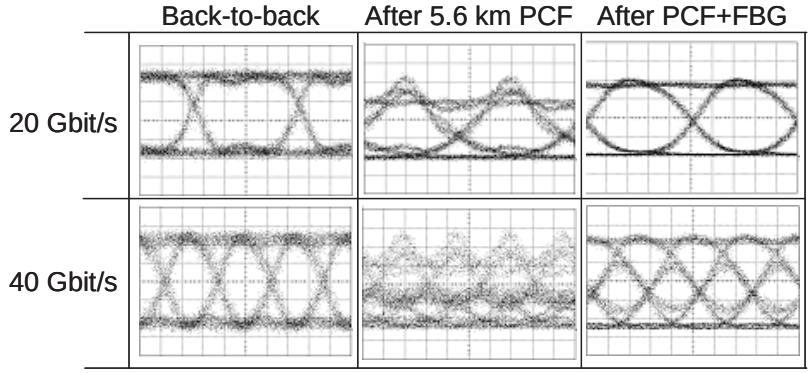

Figure 3.4: Eye-diagrams for both 20 and 40 Gbit/s operation in the back-to-back case, after transmission over 5.6 km PCF and at the output of the chirped FBG. Horizontal scale: 10 ps/div.

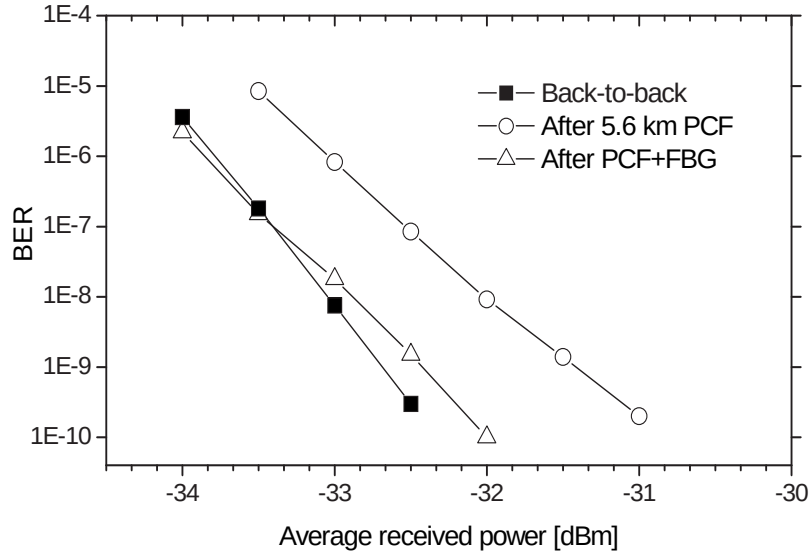

Figure 3.5: BER curves measured in the back-to-back case, after transmission over 5.6 km PCF and at the output of the chirped FBG for 20 Gbit/s operation.

chirped FBG, are shown in Figure 3.4 for both 20 and 40 Gbit/s signals. The eye diagrams recorded at the output of the 5.6 km fibre are significantly distorted due to dispersion as it is expected at these bit rates for accumulated dispersion of ∼181 ps/nm. The eye diagram of the 20 Gbit/s signal is still open, but the 40 Gbit/s eye diagram is severely distorted. The 20 Gbit/s eye diagram recorded after dispersion compensation using the FBG is wide open. On the contrary, the 40 Gbit/s signal remained distorted, due to the insufficient bandwidth of the FBG.

The BER curves measured for the 20 Gbit/s signal in the back-to-back case, after transmission, and at the output of the FBG are plotted in Figure 3.5. A back-to-back sensitivity of −32.7 dBm was obtained. The dispersion induced penalty measured at the output of the PCF was 1.3 dB and it was reduced to only 0.3 dB by using FBG dispersion compensation.

3.2.3 40 Gbit/s transmission with dispersion compensation using conventional dispersion compensating fibre

Due to the limited bandwidth of the FBG, the dispersion compensation of the 40 Gbit/s signal is achieved by conventional DCF. For details on dispersion compensation using DCF please refer to [13, 18]. At this point it should be noted that dispersion compensation could have been obtained by dispersion compensating photonic crystal fibres (DC-PCFs) also. Several DC-PCF designs have already been proposed, exhibiting orders of magnitude higher dispersion coefficients than conventional DCF. However, it is only recently that the first DC-PCF fibre has been fabricated with a dispersion coefficient of −1211 ps/(nm·km) at 1550 nm [19]. DC-PCFs are discussed in details in Chapter 5.

Experimental setup

The experimental setup is shown in Figure 3.6. A CW laser source emitting at 1550 nm is externally modulated into the NRZ format by a chirped $LiNbO_3$ MZ modulator. The PRBS is 2^{31}-1 bits long. The generated 40 Gbit/s chirped NRZ modulated signal is amplified to an average power of 12 dBm before it is launched into the transmission span. The transmission span consisted of 1 km DCF followed by 5.6 km

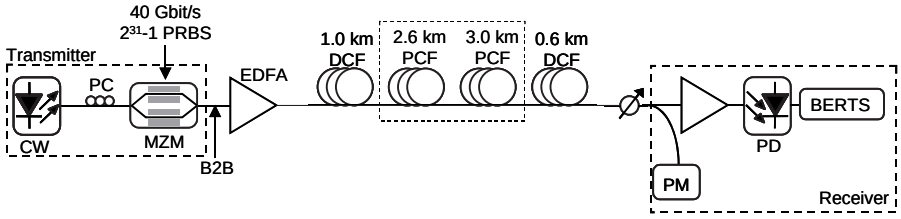

Figure 3.6: Experimental setup for 40 Gbit/s dispersion compensated PCF transmission. The dispersion compensation is achieved by conventional DCF. PM - power meter.

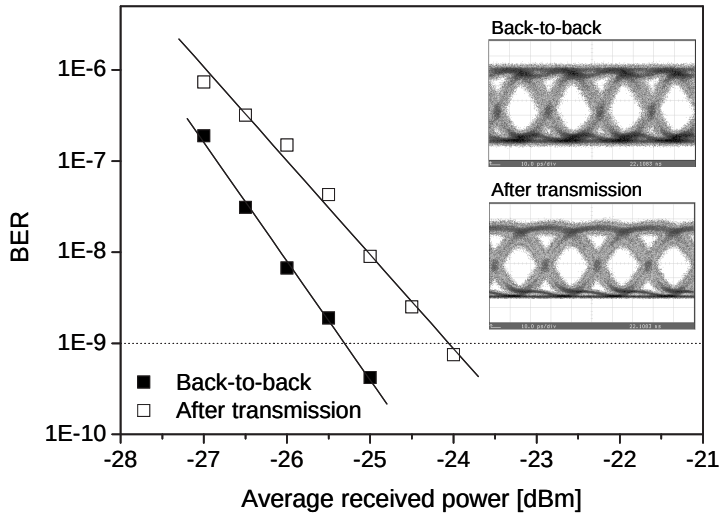

Figure 3.7: BER curves as a function of average received power measured for the 40 Gbit/s signal transmission in the back-to-back case and after transmission over 5.6 km dispersion compensated PCF line. Corresponding eye-diagrams are shown as insets. Horizontal scale: 10 ps/div.

PCF and 0.6 km DCF, with dispersion at 1550 nm of −101.5, 179.2 and −62.1 ps/nm, respectively. The DCFs are conventional fibres. A preamplified receiver, consisting of an EDFA followed by a PD (50 GHz 3 dB bandwidth), is used to receive the signal.

Results

The BER curves measured in the back-to-back case and after the transmission link, including dispersion compensation, are plotted in Figure 3.7. The corresponding eye-diagrams are shown as insets. The back-to-back sensitivity was −25.3 dBm and the penalty induced by the transmission link was 1.2 dB. The performance degradation is attributed to the interplay of signal chirp and self phase modulation (SPM) induced chirp, due to the high input power coupled into the DCF.

In the previously described experiments, the major deteriorating effect was dispersion which could be compensated either by chirped FBG or conventional DCF. However on such a short transmission length at bit rates below 40 Gbit/s other important deteriorating effects of high speed, long haul systems such as PMD can not be investigated. Therefore, either the capacity of the system or the transmission length or both has to be increased for further investigations. In the following sections experiments increasing the total system capacity by polarisation multiplexing technique, or increasing the total transmission distance by using a recirculating loop are described.

3.3 80 Gbit/s polarisation multiplexed DPSK signal transmission

To further increase the total capacity of a system, the polarisation dimension of the light can be exploited. Polarisation multiplexing has already been introduced for conventional unidirectional transmission over non polarisation maintaining fibres [20]. However, PMD is believed to constitute a limitation for high speed and polarisation multiplexed transmission systems [21]. Therefore, it is a basic requirement for fibres used for future transmission links that they should possess low PMD. As the first and second order PMD values measured for transmission PCFs are comparable with state-of-the-art SSMF, PCFs may be suitable for high speed, polarisation multiplexed systems [22, 23].

Lately, the differential phase shift keying (DPSK) format has been shown to excel among the proposed novel modulation formats due to its superior performance in long haul transmission systems [24–26]. Due to its deterministic envelope and narrow spectrum, it exhibits better

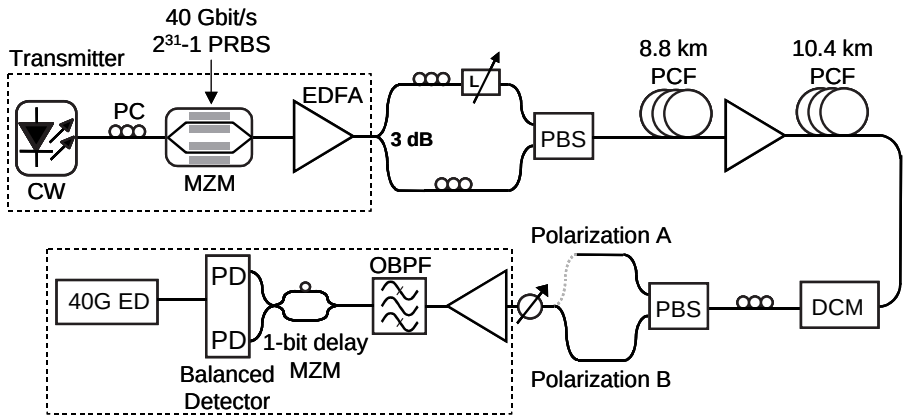

Figure 3.8: Experimental setup for 80 Gbit/s polarisation multiplexed DPSK transmission over PCF.

tolerance to nonlinearities and dispersion [27]. DPSK signals can also be detected by a balanced receiver, resulting in 3 dB improved receiver sensitivity compared to on-off keying [28].

In this experiment, two 40 Gbit/s DPSK signals have been polarisation multiplexed to form an 80 Gbit/s signal that was transmitted over 19.2 km PCF [29].

3.3.1 Experimental setup

The experimental setup is shown in Figure 3.8. A CW laser was modulated by a dual drive MZ modulator into the DPSK format [24]. After amplification, the signal was split into two parts with equal power and the signals on the two paths were delayed compared to each other. The states of polarisation of the two signals were set to match the two orthogonal polarisation axes of the polarisation beam splitter (PBS) used to combine the two signals before they were input to the transmission span. The transmission span consisted of two spools of transmission PCF (PCF3 and PCF4) with lengths of 8.8 and 10.4 km, resulting in an accumulated dispersion of 631.2 ps/nm at 1550 nm, followed by a dispersion compensating module (DCM). The DCM was composed of conventional DCF, SSMF and an EDFA resulting in about −625 ps/nm total dispersion around 1550 nm. At the receiver, the signals carried

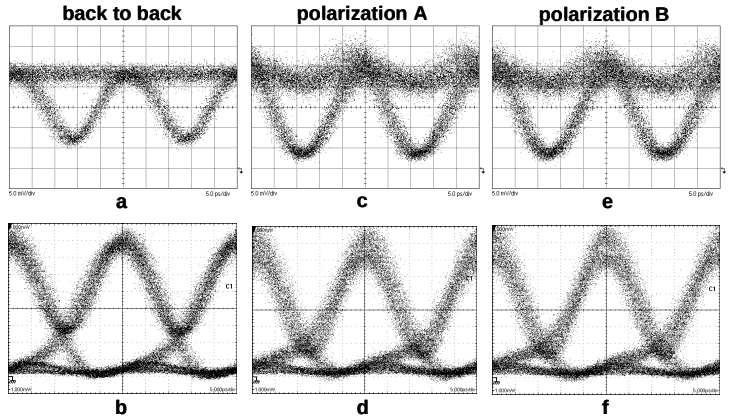

Figure 3.9: Intensity patterns and single ended detected eye-diagrams for the 40 Gbit/s DPSK back-to-back signal (a, b) and for the signal after transmission (c-f). Horizontal scale: 5 ps/div.

on the two orthogonal polarisation states were separated using a polarisation controller followed by a PBS before they were detected with a pre-amplified receiver consisting of an EDFA, a one bit delay fibre interferometer and a balanced receiver with a 3 dB bandwidth of 45 GHz.

3.3.2 Results

Figure 3.9-a shows the intensity pattern in the back-to-back case (measured at the output of the booster EDFA placed after the MZ modulator). The corresponding demodulated back-to-back eye diagram (represented here for single ended detection) is shown in Figure 3.9-b. The intensity patterns obtained after transmission for the two orthogonal polarisations, referred as polarisation A and B, are visible in Figure 3.9-c, e, respectively. The corresponding demodulated eye diagrams (also represented for single ended detection) are shown in Figure 3.9-d, f. The two states of polarisation exhibit nearly identical quality after transmission. A slight overshoot appears in the middle of the bit slots, which can be attributed to residual dispersion. The BER curves measured in the back-to-back configuration and for the two 40 Gbit/s DPSK tributaries after transmission are plotted in Figure 3.10. The calculated average of the two BERs measured for the two orthogonal tributaries after trans-

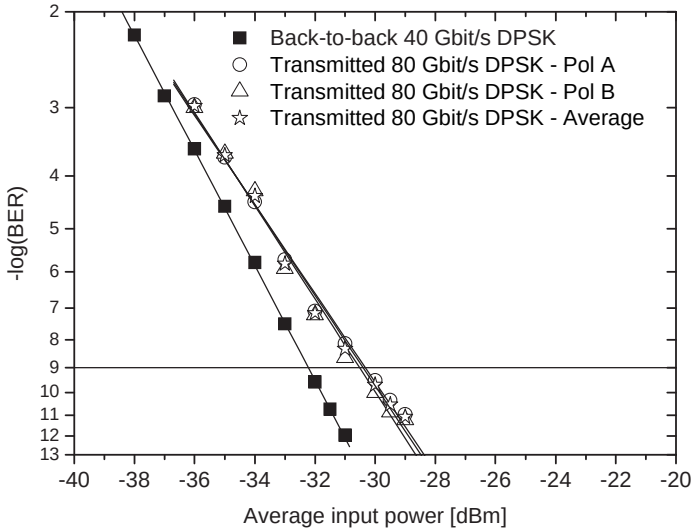

Figure 3.10: BER curves as a function of average received power for 80 Gbit/s polarisation multiplexed DPSK transmission. The BER curves were measured for the 40 Gbit/s DPSK back-to-back signal and for the transmitted 80 Gbit/s signal for both states of polarisations. The calculated average BER of the two transmitted 40 Gbit/s DPSK tributaries is also shown.

mission is also shown. A back-to-back sensitivity of −32.2 dBm was obtained. The performance of the two 40 Gbit/s DPSK tributaries was almost identical with transmission power penalties of 1.9 and 1.7 dB, resulting in an average power penalty of 1.8 dB for the 80 Gbit/s DPSK polarisation multiplexed signal.

This experiment demonstrates, to the author's best knowledge, the highest data rate up to now carried on a single wavelength over PCF.

3.4 Transmission over 57.6 km index guiding photonic crystal fibre

At the beginning of the PCF transmission era, the longest fibre length, drawn in one piece was limited to first 1.5 km, then 6 km afterwards 10 to 12.7 km. Thereby PCF transmission experiments were also limited to the corresponding transmission distances. The total transmission dis-

tance can be increased by recirculating loop experiments. Recirculating loop experiments are a powerful tool, commonly used in laboratories to emulate the performance of long haul terrestrial or undersea systems [30, 31]. A typical setup consists of a transmitter, a number of transmission spans inserted in a loop and a receiver. The loop configuration allows the signal to propagate several round trips through the transmission spans inserted in the loop. Thus the total transmission distance can be increased to a multiple number of the length of the transmission spans in the loop. Using recirculating loop, transmission experiments over transoceanic distances with large capacities have been already demonstrated in the laboratory without using huge amounts of fibres and amplifiers [32–34].

In the experiment described below, a recirculating loop is used to extend the transmission lengths over PCF beyond the fabrication limits at that time. The recirculating loop consisted of 19.2 km index guiding, transmission PCF, and the total transmission distance over PCF was extended to 57.6 km by achieving three round trips.

3.4.1 Experimental setup

The setup used for the recirculating loop experiment is shown in Figure 3.11. The transmitter consisted of a CW laser source emitting at 1550 nm followed by a polarisation controller and a chirp-free $LiNbO_3$ MZ modulator. A PRBS with a length of 2^{31}-1 bits was applied to the MZ modulator to generate a 10 Gbit/s NRZ modulated signal. In order to increase the transmission distance, a transmission loop was used. The modulated signal was boosted by an EDFA before it was coupled into the loop-switch via a variable attenuator and a polarisation controller. In the loop-switch, acousto-optic switches (AOS) were employed to block either the fill or loop signal. For details on the transmission loop please refer to [30]. In the loop, the signal was first boosted by an EDFA before being launched in the transmission line. The transmission line consisted of two spools of index guiding PCF, (PCF3 and PCF4 see table 3.1) with a total length of 19.2 km. The average input power into the PCF was 15.8 dBm. At the output of the second PCF, an EDFA was used to compensate for the span loss before the signal was reinjected into the loop switch. A 10 dB power splitter enabled the signal to be coupled

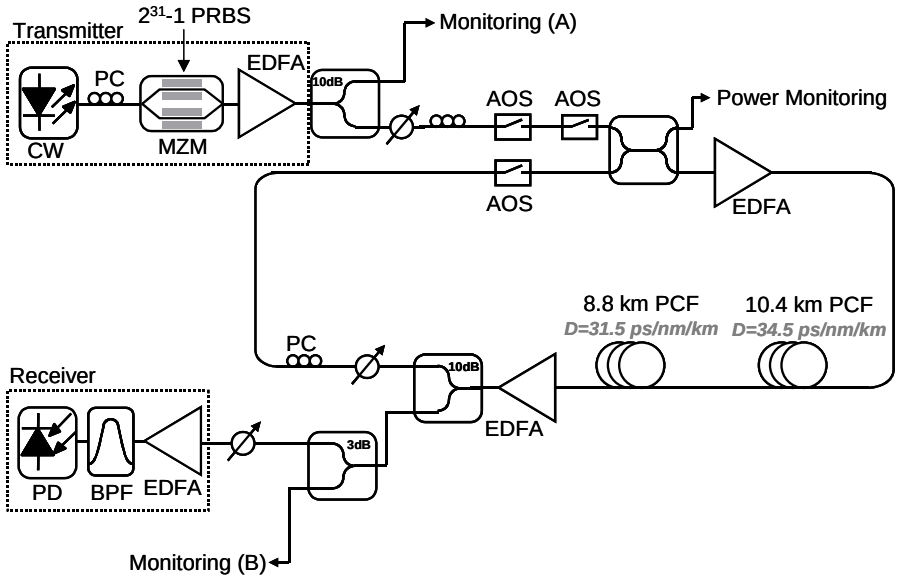

Figure 3.11: Experimental setup for the recirculating loop experiment through 19.2 km PCF.

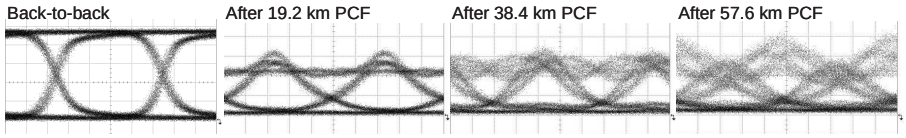

Figure 3.12: Eye-diagrams recorded in the back-to-back case, after 19.2, 38.4 and 57.6 km propagation over PCF. Horizontal scale: 20 ps/div.

into an optically pre-amplified receiver.

3.4.2 Results

The back-to-back eye-diagram (recorded at monitoring port A in Figure 3.11) corresponding to an extinction ratio of 14.8 dB is shown in Figure 3.12. The eye-diagrams after 19.2, 38.4 and 57.6 km transmission over PCF (recorded at monitoring port B in Figure 3.11) are shown in Figure 3.12. All eye diagrams were monitored in a 26 GHz bandwidth. The eye-diagrams distortion is mainly attributed to dispersion.

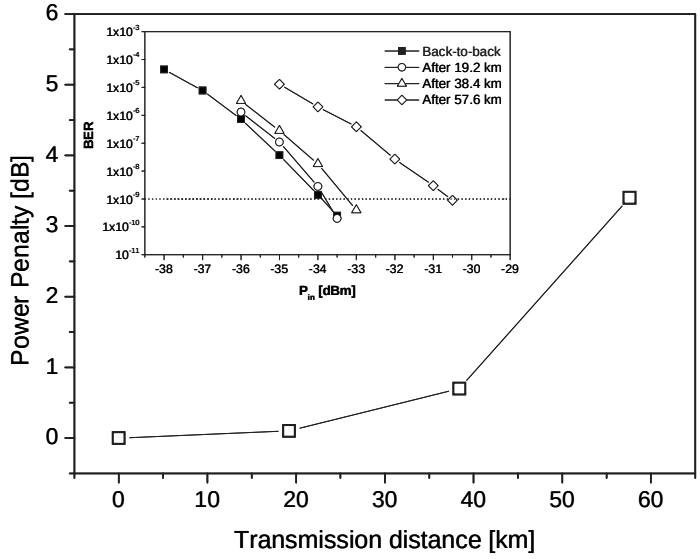

Figure 3.13: Power penalty as a function of transmission distance for the recirculating loop experiment. BER curves measured in the back-to-back case, after 19.2, 38.4 and 57.6 km propagation over PCF are shown in the inset.

Due to the high fibre input power, some pulse reshaping due to SPM in the anomalous dispersion regime can also be observed in the eyes. The BER curves measured in the back-to-back case and after transmission are shown in Figure 3.13 as an inset. A back-to-back sensitivity of −33.9 dBm has been obtained. The power penalty measured after 19.2, 38.4 and 57.6 km (corresponding to 631.2, 1262.4 and 1893.6 ps/nm accumulated dispersion, respectively) was 0.1, 0.7 and 3.4 dB, respectively. As a comparison, in case of linear propagation, 1 dB power penalty is expected in standard single mode fibre based transmission links for around 1000 ps/nm accumulated dispersion [18]. The measured lower power penalty values confirm the interaction of SPM with anomalous dispersion.

The presented experiment increased the longest transmission distance over index guiding PCF by mean of a recirculating loop to 57.6 km, that was more than four times longer than any other reported PCF transmission at the time. In 2005, this result was surpassed by increasing the

longest transmission distance over a dispersion compensated PCF link to 100 km [35]. As the transmission distance of the recirculating loop experiment was mainly limited by dispersion, the transmission distance could have been increased even further by using DCF.

3.5 Other system demonstrations

The rapid decrease of the loss of index guiding PCFs stimulated the research on using these fibres as transmission fibres. In the last three years, beside the previously described experiments, several other demonstrations of the potential of PCFs as transmission fibres have been reported. All PCF transmission experiments, published until now are summarised in Figure 3.14 indicating the publication year, transmission length and the total capacity.

One of the early experiments using index guiding PCF as transmission fibre realised a wavelength division multiplexing (WDM) system. Through 10 km index guiding PCF have been transmitted 8×10 Gbit/s channels. The fibre used in this experiment had the lowest loss of 0.37 dB/km and longest length drawn in one piece, at that time [41]. This experiment was a significant step towards low loss, long length transmission PCF.

Another WDM system demonstrated an entirely index guiding PCF based system. A 5×10 Gbit/s WDM source was realised by spectral slicing of a supercontinuum, generated in a short highly nonlinear photonic crystal fibre (HNL-PCF). The signals were then transmitted over 5.6 km of transmission PCF [48].

The superior performance of the endlessly single mode (ESM) design has been demonstrated in an ultra-wide band WDM transmission system [46,47]. A total of 190 Gbit/s data of 10 Gbit/s channels was transmitted in the 850, 1310 and 1550 nm wavelength regions over 5.2 km endlessly single mode photonic crystal fibre (ESM-PCF).

The applicability of low loss transmission PCFs as media for distributed Raman amplification for both dense-WDM system and for short-wavelength amplification has been also demonstrated [51, 54].

Index guiding PCFs offer an advantage over conventional fibres, for both broadband WDM systems and Raman amplification, since they can be designed with very weakly wavelength dependent MFD, due to

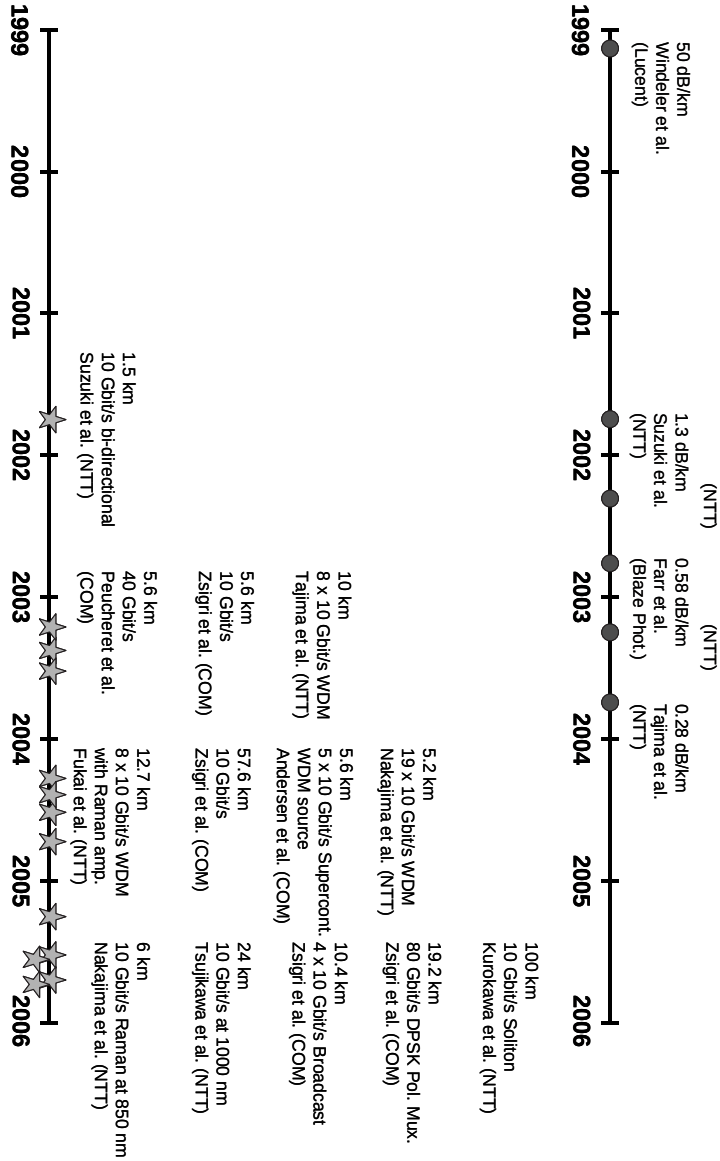

Figure 3.14: Chronological order of the PCF transmission experiments published until now. The time line above indicates the published record losses as a comparison. The length of the transmission experiments, the total capacity together with the first author and the shortened affiliation are shown in the figure. References for the record loss are [5–7, 36–42]. References of the transmission experiments are [5, 14, 29, 35, 41, 43–54]

their wavelength dependent refractive index difference [55]. In WDM systems, the weakly wavelength dependent MFD ensures similar propagation conditions, with regards to nonlinearity or coupling loss at the connection of two components, for all the wavelength channels. In Raman amplified systems, the weakly wavelength dependent MFD ensures good mode field overlap between pump and signal.

Dispersion managed soliton propagation over 100 km of index guiding PCF has been also demonstrated [35]. This paper reports the currently longest index guiding PCF (100 km), which increases by an order of magnitude the fibre length drawn in one piece.

Recently, a transmission experiment at 1000 nm demonstrated the feasibility of LMA-PCFs to be used as transmission fibre in local area networks [53].

3.6 Summary

Applications of index guiding photonic crystal fibres (PCFs) as transmission fibres have been introduced in this chapter. Transmission experiments increasing the total transmission capacity and transmission distance have been described.

One of the world's first experiment demonstrating the potential of index guiding PCF as transmission fibre has been described. Penalty free transmission of a 10 Gbit/s NRZ modulated signal at 1550 nm through 5.6 km of photonic crystal fibre has been successfully demonstrated. We have also performed 20 and 40 Gbit/s transmission over 5.6 km using either a FBG or DCF for dispersion compensation.

The bit rate carried on a single wavelength has been increased to 80 Gbit/s by polarisation multiplexing two 40 Gbit/s DPSK tributaries. The 80 Gbit/s signal has been then transmitted over 19.2 km low PMD PCF. Not only this experiment demonstrates the highest data rate carried on a single wavelength over PCF today, but it also confirms the low PMD of the fibre. By exploiting the very low PMD of the tested PCF, which is the result of its very high symmetry, it is demonstrated that the polarisation properties of index guiding PCFs may make those fibres suitable for high speed, polarisation multiplexed systems.

The transmission distance has been increased by means of a recirculating loop experiment. A 10 Gbit/s NRZ signal was transmitted in a

recirculating loop consisting of a 19.2 km transmission PCF increasing the total transmission length over PCF to 57.6 km.

So far, the relatively high loss and short length available for index guiding PCFs set a limitation on their practical use in transmission systems. Recently, however, PCF technology has reached the point when longer lengths and loss, comparable to standard transmission fibres have been demonstrated for large mode area photonic crystal fibres. The presented experiments have shown the potential of index guiding PCFs as transmission fibres for high speed systems. These experiments add to the exploitation of a range of unique properties, not obtainable by conventional fibres, that have been demonstrated recently. A combination of all these experiments shows the strong potential of index guiding PCFs to serve as transmission media in future broad band optical communication systems.

References to Chapter 3

[1] J. C. Knight, T. A. Birks, P. St. J. Russell, and D. M. Atkin. "All-silica single-mode optical fiber with photonic crystal cladding", *Optics Letters*, vol. 21, no. 19, pp. 1547–1549, October 1996.

[2] T. Kato, M. Hirano, M. Onishi, and M. Nishimura. "Ultra-low nonlinearity low-loss pure silica core fibre for long-haul WDM transmission", *Electronics Letters*, vol. 35, no. 19, pp. 1615–1617, September 1999.

[3] M. D. Nielsen, J. R. Folkenberg, and N. A. Mortensen. "Single-mode photonic crystal fibre with effective area of 600 μm^2 and low bending loss", *Electronics Letters*, vol. 39, no. 25, pp. 1802–1803, December 2003.

[4] T. A. Birks, J. C. Knight, and P. St. J. Russell. "Endlessly single-mode photonic crystal fiber", *Optics Letters*, vol. 22, no. 13, pp. 961–963, July 1997.

[5] K. Suzuki, H. Kubota, S. Kawanishi, M. Tanaka, and M. Fujita. "High-speed bi-directional polarisation division multiplexed optical transmission in ultra low-loss (1.3 dB/km) polarisation main-

taining photonic crystal fibre", *Electronics Letters*, vol. 37, no. 23, pp. 1399–1401, November 2001.

[6] K. Tajima, K. Nakajima, K. Kurokawa, N. Yoshizawa, and M. Ohashi. "Low-loss photonic crystal fibers", in *Technical Digest Optical Fiber Communication Conference, OFC'02,* Anaheim, California, U.S.A., pp. 523–524, March 2002, thS3.

[7] L. Farr, J. C. Knight, B. J. Mangan, and P. J. Roberts. "Low loss photonic crystal fibre", in *Proceedings European Conference on Optical Communication, ECOC'02,* Copenhagen, Denmark, September 2002, post-deadline paper PD 1.3.

[8] M. D. Nielsen and N. A. Mortensen. "Photonic crystal fiber design based on the V-parameter", *Optics Express*, vol. 11, no. 21, pp. 2762–2768, October 2003.

[9] A. Boskovic, S. V. Chernikov, J. R. Taylor, L. Grüner-Nielsen, and O. A. Levring. "Direct continuous-wave measurement of n_2 in various types of telecommunication fiber at 1.55 μm", *Optics Letters*, vol. 21, no. 24, pp. 1966–1968, December 1996.

[10] B. L. Heffner. "Automated measurement of polarization mode dispersion using Jones matrix eigenanalysis", *IEEE Photonics Technology Letters*, vol. 4, no. 9, pp. 1066–1069, September 1992.

[11] B. L. Heffner. "Accurate, automated measurement of differential group delay dispersion and principal state variation using Jones matrix eigenanalysis", *IEEE Photonics Technology Letters*, vol. 5, no. 7, pp. 814–817, July 1993.

[12] M. Sumetsky and B. J. Eggleton. "Fiber Bragg gratings for dispersion compensation in optical communication systems", *Journal of Optical and Fiber Communications Reports*, vol. 2, no. 3, pp. 256–278, July 2005.

[13] L. Grüner-Nielsen, S. N. Knudsen, B. Edvold, T. Veng, D. Magnussen, C. C. Larsen, and H. Damsgaard. "Dispersion compensating fibers", *Optical Fiber Technology*, vol. 6, no. 2, pp. 164–180, April 2000.

[14] B. Zsigri, C. Peucheret, M. D. Nielsen, and P. Jeppesen. "Transmission over 5.6 km large effective area and low loss (1.7 dB/km) photonic crystal fibre", *Electronics Letters*, vol. 39, no. 10, pp. 796–798, May 2003.

[15] G. P. Agrawal. *Nonlinear Fiber Optics.* Academic Press, Inc., Second edition, 1995. ISBN 0-12-045142-5.

[16] G. P. Agrawal. *Fiber-Optic Communication Systems.* John Wiley & Sons, Inc., Second edition, 1997. ISBN 0-471-17540-4.

[17] T. A. Strasser and T. Erdogan. *Fiber Grating Devices in High-Performance Optical Communications Systems*, In I. Kaminow and T. Li, editors, *Optical Fiber Telecommunications IVB Components,* Chapter 2, Academic Press, March 2002. ISBN 0-12-395173-9.

[18] A. E. Willner and B. Hoanca. *Fixed and tunable management of fiber chromatic disperison*, In I. Kaminow and T. Li, editors, *Optical Fiber Telecommunications IVB Components,* Chapter 14, Academic Press, March 2002. ISBN 0-12-395173-9.

[19] B. J. Mangan, F. Couny, L. Farr, A. Langford, P. J. Roberts, D. P. Williams, M. Banham, M. W. Mason, D. F. Murphy, E. A. M. Brown, H. Sabert, T. A. Birks, J. C. Knight, and P. St. J. Russell. "Slope-matched dispersion-compensating photonic crystal fibre", in *Technical Digest Conference on Lasers and Electro-Optics, CLEO'04,* San Francisco, California, U.S.A., May 2004, post-deadline paper CPDD3.

[20] C. Wree, N. Hecker-Denschlag, E. Gottwald, P. Krummrich, J. Leibrich, E.-D. Schmidt, B. Lankl, and W. Rosenkranz. "High spectral efficiency 1.6-b/s/Hz transmission (8×40 Gb/s with a 25 GHz grid) over 200-km SSMF using RZ-DQPSK and polarization multiplexing", *IEEE Photonics Technology Letters*, vol. 15, no. 9, pp. 1303–1305, September 2003.

[21] D. van den Borne, N. E. Hecker-Denschlag, G.-D. Khoe, and H. de Waardt. "PMD and nonlinearity-induced penalties on polarization-multiplexed transmission", *IEEE Photonics Technology Letters*, vol. 16, no. 9, pp. 2174–2176, September 2004.

[22] T. Ritari, T. Niemi, H. Ludvigsen, M. Wegmüller, N. Gisin, J. R. Folkenberg, and A. Petersson. "Polarization-mode dispersion of large mode-area photonic crystal fibers", *Optics Communications*, vol. 226, no. 1-6, pp. 233–239, September 2003.

[23] T. Larsen, A. Bjarklev, A. Peterson, J. Folkenberg, and P. Pehrson. "Second-order polarization-mode dispersion in photonic crystal fibers", in *Technical Digest Optical Fiber Communication Conference, OFC'03,* Atlanta, Georgia, U.S.A., vol. 86, pp. 372–373, March 2003, paper WJ6.

[24] A. H. Gnauck and P. J. Winzer. "Optical phase-shift-keyed transmission", *Journal of Lightwave Technology*, vol. 23, no. 1, pp. 115–130, January 2005.

[25] A. Gnauck. "40-Gb/s RZ-differential phase shift keyed transmission", in *Technical Digest Optical Fiber Communication Conference, OFC'03,* Atlanta, Georgia, U.S.A., vol. 2, pp. 450–451, March 2003, paper ThE1.

[26] T. Tokle. *Optimised Dispersion Management and Modulation Formats for High Speed Optical Communication Systems.* Ph.D. thesis, Research Center COM, Technical University of Denmark, Kgs. Lyngby, Denmark, December 2004. ISBN 87-90974-60-3.

[27] J. Wang and J. M. Kahn. "Impact of chromatic and polarization-mode dispersion on DPSK systems using interferometric demodulation and direct detection", *Journal of Lightwave Technology*, vol. 22, no. 2, pp. 362–371, February 2004.

[28] C. Xu, X. Liu, and X. Wei. "Differential phase-shift keying for high spectral efficiency optical transmissions", *IEEE Journal of Selected Topics in Quantum Electronics*, vol. 10, pp. 281–293, March 2004.

[29] B. Zsigri, T. Tokle, C. Peucheret, M. D. Nielsen, and P. Jeppesen. "80 Gbit/s polarization multiplexed DPSK signal transmission over photonic crystal fiber", in *Proceedings OptoElectronics and Communications Conference, OECC'05,* Seoul, Korea, pp. 402–403, July 2005, paper 7B3-3.

[30] M. Nissov. *Long-Haul Optical Transmission Using Distributed Raman Amplification.* Ph.D. thesis, Department of Electromagnetic Systems, Technical University of Denmark, December 1997.

[31] N. S. Bergano. *Undersea Communications Systems*, In I. Kaminow and T. Li, editors, *Optical Fiber Telecommunications IVB Components,* Chapter 4, Academic Press, March 2002. ISBN 0-12-395173-9.

[32] A. H. Gnauck, P. J. Winzer, and S. Chandrasekhar. "Hybrid 10/40-G transmission on 50-GHz grid through 2800 km of SSMF and seven optical add-drops", *IEEE Photonics Technology Letters*, vol. 17, no. 10, pp. 2203–2205, October 2005.

[33] A. Chowdhury, G. Raybon, R.-J. Essiambre, and C. R. Doerr. "WDM CSRZ 40 Gbit/s pseudo-linear transmission over 4800 km using optical phase conjugation", *Electronics Letters*, vol. 41, no. 3, pp. 151–152, February 2005.

[34] F. Liu, J. Bennike, S. Dey, C. Rasmussen, B. Mikkelsen, P. Mamyshev, D. Gapontsev, and V. Ivshin. "1.6 Tbit/s (40×42.7 Gbit/s) transmission over 3600 km UltraWave^{TM} fiber with all-raman amplified 100 km terrestrial spans using ETDM transmitter and receiver", in *Technical Digest Optical Fiber Communication Conference, OFC'02,* Anaheim, California, U.S.A., March 2002, paper FC7-1.

[35] K. Kurokawa, K. Tajima, J. Zhou, K. Nakajima, T. Matsui, and I. Sankawa. "Penalty-free dispersion-managed soliton transmission over 100 km low loss PCF", in *Technical Digest Optical Fiber Communication Conference, OFC'05,* Anaheim, California, U.S.A., March 2005, post-deadline paper PDP21.

[36] J. A. West, N. Venkataramam, C. M. Smith, and M. T. Gallagher. "Photonic crystal fibers", in *Proceedings European Conference on Optical Communication, ECOC'01,* Amsterdam, The Netherlands, pp. 582–585, September 2001, paper Th.A.2.

[37] N. Venkataramam, M. T. Gallagher, C. M. Smith, D. Müller, J. A. West, K. W. Koch, and J. C. Fajardo. "Low loss (13 dB/km)

air core photonic band-gap fibre", in *Proceedings European Conference on Optical Communication, ECOC'02,* September 2002, post-deadline paper PD1.1.

[38] B. J. Mangan, L. Farr, A. Langford, P. J. Roberts, D. P. Williams, F. Couny, M. Lawman, M. W. Mason, S. Coupland, R. Flea, H. Sabert, T. A. Birks, J. C. Knight, and P. St. J. Russell. "Low loss (1.7 dB/km) hollow core photonic bandgap fiber", in *Technical Digest Optical Fiber Communication Conference, OFC'04,* Los Angeles, California, U.S.A., February 2004, post-deadline paper PDP24.

[39] P. J. Roberts, F. Couny, H. Sabert, B. J. Mangan, D. P. Williams, L. Farr, M. W. Mason, A. Tomlinson, T. A. Birks, J. C. Knight, and P. St. J. Russell. "Ultimate low loss of hollow-core photonic crystal fibres", *Optics Express*, vol. 13, no. 1, pp. 236–244, January 2005.

[40] R. S. Windeler, J. L. Wagener, and D. J. DiGiovanni. "Silica-air microstructured fibers: Properties and applications", in *Technical Digest Optical Fiber Communication Conference, OFC'99,* San Diego, California, U.S.A., pp. 106–107, February 1999, paper FG1.

[41] K. Tajima, J. Zhou, K. Nakajima, and K. Sato. "Ultra low loss and long length photonic crystal fiber", in *Technical Digest Optical Fiber Communication Conference, OFC'03,* Atlanta, Georgia, U.S.A., March 2003, post-deadline paper PD1.

[42] K. Tajima, J. Zhou, K. Kurokawa, and K. Nakajima. "Low water peak photonic crystal fibres", in *Proceedings European Conference on Optical Communication, ECOC'03,* Rimini, Italy, pp. 42–43, September 2003, post-deadline paper Th4.1.6.

[43] C. Peucheret, B. Zsigri, P. A. Andersen, K. S. Berg, A. Tersigni, P. Jeppesen, K. P. Hansen, and M. D. Nielsen. "Transmission over photonic crystal fiber at 40 Gbit/s using mid-span spectral inversion in a highly nonlinear photonic crystal fiber", in *Technical Digest Conference on Lasers and Electro-Optics, CLEO'03,* Baltimore, Maryland, U.S.A., June 2003, post-deadline paper CThPDB4.

[44] C. Peucheret, B. Zsigri, P. A. Andersen, K. S. Berg, A. Tersigni, P. Jeppesen, K. P. Hansen, and M. D. Nielsen. "40 Gbit/s transmission over photonic crystal fibre using mid-span spectral inversion in highly nonlinear photonic crystal fibre", *Electronics Letters*, vol. 39, no. 12, pp. 919–921, June 2003.

[45] C. Peucheret, B. Zsigri, K. P. Hansen, M. D. Nielsen, and P. Jeppesen. "Photonic crystal fibers for transmission and optical signal processing", *IEEE LEOS, Lasers & Electro-Optics Society Newsletter*, vol. 18, no. 4, pp. 7–8, August 2004.

[46] K. Nakajima, J. Zhou, K. Tajima, K. Kurokawa, C. Fukai, and I. Sankawa. "Ultra wide band 190 Gbit/s WDM transmission over a long length and low loss PCF", in *Technical Digest Optical Fiber Communication Conference, OFC'04,* Los Angeles, California, U.S.A., February 2004, post-deadline paper PDP23.

[47] K. Nakajima, J. Zhou, K. Tajima, K. Kurokawa, C. Fukai, and I. Sankawa. "Ultrawide-band single-mode transmission performance in a low-loss PCF", *Journal of Lightwave Technology*, vol. 23, no. 1, pp. 7–11, January 2005.

[48] P. A. Andersen, B. Zsigri, C. Peucheret, P. Jeppesen, K. P. Hansen, and M. D. Nielsen. "Photonic crystal fibers used in a multi-wavelength source and as transmission fiber in a WDM system", in *Technical Digest Conference on Lasers and Electro-Optics, CLEO'04,* San Francisco, California, U.S.A., May 2004, paper CThG4.

[49] B. Zsigri, C. Peucheret, M. D. Nielsen, and P. Jeppesen. "Recirculating loop transmission experiment over 57.6-km photonic crystal fiber", *Optics Engineering*, vol. 44, no. 7, pp. 070504–1–2, July 2005.

[50] B. Zsigri, C. Peucheret, M. D. Nielsen, and P. Jeppesen. "Transmission over 57.6 km of photonic crystal fiber", in *Proceedings OptoElectronics and Communications Conference, OECC'04,* Yokohama, Japan, pp. 482–483, July 2004, paper 14D1-2.

[51] C. Fukai, K. Nakajima, J. Zhou, K. Tajima, K. Kurokawa, and I. Sankawa. "Distributed Raman amplification based DWDM transmission in a low loss photonic crystal fibre", in *Proceedings European Conference on Optical Communication, ECOC'04,* Stockholm, Sweden, vol. 3, pp. 304–305, September 2004, paper We1.3.6.

[52] B. Zsigri, C. Peucheret, M. D. Nielsen, and P. Jeppesen. "Implementation of broadcast, transmission and wavelength conversion functionalities using photonic crystal fibers", in *Proceedings OptoElectronics and Communications Conference, OECC'05,* Seoul, Korea, pp. 790–791, July 2005, paper 8B3-1.

[53] K. Tsujikawa, K. Kurokawa, K. Tajima, K. Nakajima, T. Matsui, and I. Sankawa. "Penalty-free 10 Gb/s transmission in 1.0 μm band over 24 km low loss PCF", in *Proceedings European Conference on Optical Communication, ECOC'05,* Glasgow, Scotland, vol. 2, pp. 283–284, September 2005, paper Tu4.4.2.

[54] K. Nakajima, C. Fukai, K. Kurokawa, K. Tajima, T. Matsui, and I. Sankawa. "Distributed Raman amplification at 850 nm in a low loss photonic crystal fibre", in *Proceedings European Conference on Optical Communication, ECOC'05,* Glasgow, Scotland, vol. 2, pp. 285–286, September 2005, paper Tu4.4.3.

[55] M. D. Nielsen, N. A. Mortensen, J. R. Folkenberg, and A. Bjarklev. "Modal cutoff and the V parameter in photonic crystal fibers", *Optics Letters*, vol. 28, no. 23, pp. 2309–2311, December 2003.

Chapter 4

Signal processing using index guiding highly nonlinear photonic crystal fibre

In telecommunication applications, highly nonlinear photonic crystal fibres (HNL-PCFs) were the first to demonstrate the potential of photonic crystal fibres (PCFs). Numerous signal processing applications have been performed, benefitting from the widely tailorable dispersion profile and the large nonlinearity of HNL-PCFs.

The most intensively investigated phenomenon is supercontinuum generation in HNL-PCFs [1–7]. Supercontinuum is generated by launching high power, short pulses into a highly nonlinear medium, e.g. a nonlinear fibre, thereby stimulating various nonlinear processes. The interaction of nonlinear processes generate a broad continuous spectra, called supercontinuum. As the properties, such as bandwidth and stability, of the generated supercontinuum are highly dependent on the dispersion profile of the fibre, HNL-PCFs are a very attractive choice as a medium for supercontinuum generation. Supercontinuum finds its use in many different applications such as spectroscopy, optical coherence tomography, sensors and also in telecommunications as multi-wavelength sources [8, 9].

Several other telecommunication signal processing applications using HNL-PCFs have been also investigated. Wavelength conversion exploiting four-wave mixing (FWM), cross phase modulation (XPM), self phase modulation (SPM) and soliton self frequency shifting have been demonstrated [10–18]. Switching was implemented by a XPM scheme while 2-R regeneration was presented using SPM induced spectral broadening with offset bandlimiting optical filtering [19–21]. Parametric amplification [22] and Raman amplifications have been also demonstrated [23–27]. Optical time domain demultiplexing making use of a nonlinear optical loop mirror (NOLM) with a HNL-PCF as the nonlinear element has been presented. Signals with bit rates of 40 and 80 Gbit/s were demultiplexed to 10 Gbit/s [28–30].

The high effective nonlinearities obtainable in HNL-PCFs result in significantly reduced fibre lengths, compared to standard highly nonlinear fibres (HNLFs) based devices [16, 31]. Additionally, the flat nearly zero dispersion over a broad wavelength range can mitigate signal walk-off and pulse broadening [29]. In line with the research on signal processing applications of HNL-PCF, the improvements of transmission PCFs opened up the possibility to implement entirely PCF-based all optical systems, relying on PCFs for both signal processing and transmission.

This chapter presents transmission systems entirely made of index guiding PCFs, including both signal processing and transmission. In Section 4.2 the first 40 Gbit/s dispersion compensated transmission link built entirely from PCFs is described. Transmission over 5.6 km of large mode area photonic crystal fibre (LMA-PCF) and dispersion compensation by optical phase conjugation exploiting FWM in 50 m HNL-PCF with zero dispersion wavelength at 1552 nm is demonstrated [32, 33]. Section 4.3 describes a prototype optical network with broadcasting, transmission and wavelength conversion functionalities [17]. For the first time, broadcasting has been realised by XPM in a NOLM with 100 m HNL-PCF. One out of the four broadcasted channels has been transmitted over 10.4 km LMA-PCF and wavelength converted by exploiting FWM in 50 m of HNL-PCF. Finally, the chapter is summarised.

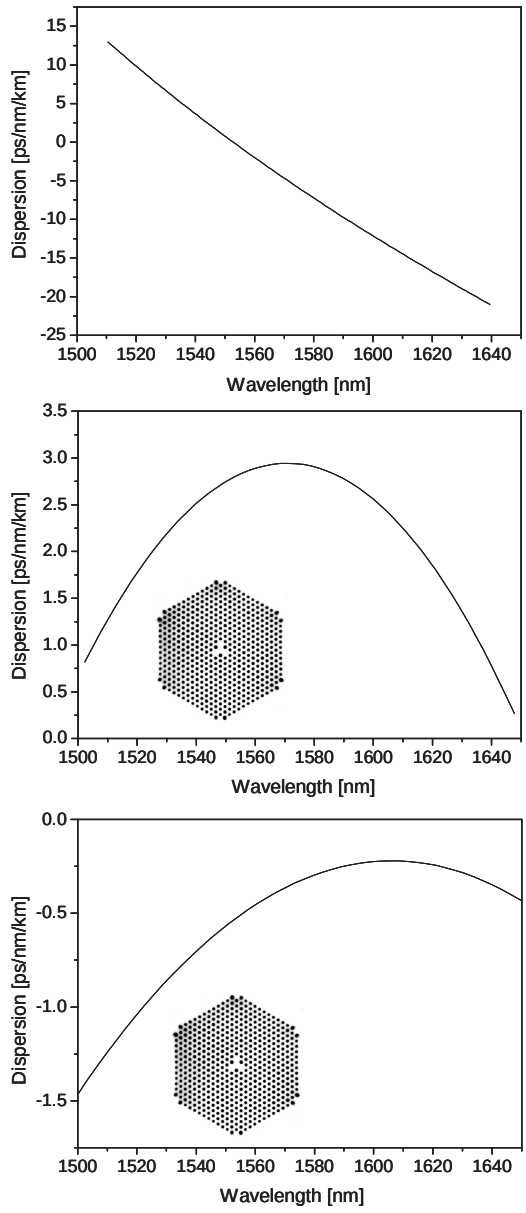

Figure 4.1: Dispersion as a function of wavelength for three highly nonlinear photonic crystal fibres used in the experiments: HNL-PCF1 (top), HNL-PCF2 (middle) and HNL-PCF3 (bottom). Fibre cross sections are shown as insets. The data was kindly provided by Crystal Fibre A/S.

Fibre spool	L [m]	α [dB]	A_{eff} [μm^2]	Dispersion	γ [$W^{-1} \cdot km^{-1}$]
HNL-PCF1	50	4.7	7	$\lambda_0 = 1552$ nm High dispersion slope	18
HNL-PCF2	100	3.3	8	Broad, flat, slightly positive dispersion	11
HNL-PCF3	50	2.3	8	Broad, flat, slightly negative dispersion	11

Table 4.1: Properties of the HNL-PCFs used in the system experiments. The stated α value gives the span loss including the SSMF pigtails as well. The parameters α, A_{eff} (effective area) and γ (nonlinear coefficient) are given at a wavelength of 1550 nm. The zero dispersion wavelength is noted by λ_0.

4.1 Fibre characteristics

In the experiments described in this chapter, three HNL-PCFs were used[1]. The fibres have a cladding diameter of 125 μm and were spliced to FC/PC connectorised standard single mode fibre (SSMF) pigtails.

The nonlinear photonic crystal fibres have closely packed cladding structures. The core of one of the fibres (HNL-PCF1) is formed by replacing one of the central air holes by a Ge doped rod [34]. The core of the other two fibres has a three-fold symmetric hybrid core region in order to obtain flat slightly positive (HNL-PCF2) or negative (HNL-PCF3) dispersion profiles [35]. The dispersion slope of HNL-PCF2 and HNL-PCF3 are 0.01 and 0.02 ps/(nm^2·km) around 1550 nm, respectively. The dispersion profile of all three fibres is shown in Figure 4.1 and their parameters are summarised in Table 4.1.

4.2 Mid-span spectral inversion dispersion compensation

In this section, 40 Gbit/s signal transmission over 5.6 km LMA-PCF is described. The transmission experiments described in the previous chapter show that, for 40 Gbit/s signals, this transmission length is beyond

[1] All three HNL-PCF have been kindly provided by Crystal Fibre A/S

the dispersion limit, therefore dispersion compensation is required.

Mid-span spectral inversion is an efficient dispersion compensation technique [36]. This technique relies on optical phase conjugation of the signal in a nonlinear medium. The optical phase conjugator (OPC) transposes the frequency components of the signal. The OPC is inserted in the fibre link between two fibre sections. In case OPC is implemented, frequency components that traveled slower in the first half of the link (before the OPC) will travel faster in the second half (after OPC). Therefore, by designing the link such that the accumulated dispersion before and after the OPC is equal, the dispersion can be compensated. Dispersion compensation of a single channel or wavelength division multiplexing (WDM) systems have already been demonstrated using optical phase conjugation realised in conventional HNLFs [37–39].

Here, four-wave mixing generation in a 50 m long HNL-PCF is exploited to realise dispersion compensation by optical phase conjugation. Error free transmission of a 40 Gbit/s non return-to-zero (NRZ) modulated signal over the 5.6 km PCF has been achieved. Thus the first entirely PCFs based optical link (including both transmission and dispersion compensation) has been demonstrated.

4.2.1 Experimental setup

The experimental setup is shown in Figure 4.2. A continuous wave (CW) light is modulated by an external Mach-Zehnder (MZ) modulator at 40 Gbit/s into the NRZ format. The length of the pseudo random bit sequence (PRBS) is 2^{31}-1 bits. The extinction ratio of the modulated signal is 13 dB. The transmission link consists of two spools of transmission PCFs with lengths of 2.6 and 3.0 km and an optical phase conjugator separating the two spools. The dispersion of both spools is 32 ps/(nm·km) at 1550 nm (see PCF1 and PCF2 in Table 3.1). The 2.6 km PCF is inserted before while the 3.0 km spool is inserted after the OPC. Optical phase conjugation is achieved by FWM in 50 m HNL-PCF with zero dispersion at 1552 nm and nonlinear coefficient of about 18 $W^{-1}{\cdot}km^{-1}$ (see HNL-PCF1 in Table 4.1). A CW laser tuned to the zero dispersion wavelength of the HNL-PCF, serves as the pump. The pump is amplified by a high power erbium doped fibre amplifier (HP-EDFA) and filtered by an optical bandpass filter (OBPF) for noise reduction before it is cou-

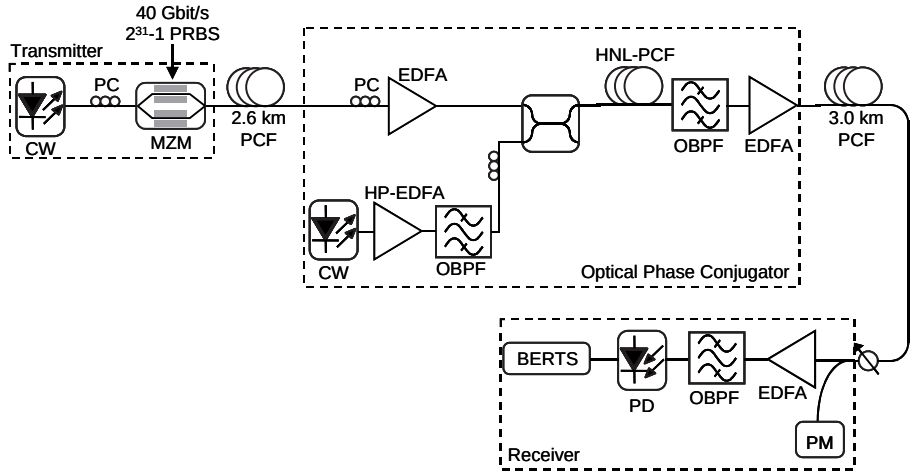

Figure 4.2: Experimental setup for 40 Gbit/s transmission over 5.6 km PCF using optical phase conjugation realised in 50 m of HNL-PCF as dispersion compensation. PM - power meter.

pled into the HNL-PCF together with the signal via a 3 dB coupler. The pump power level at the fibre input is 25 dBm. The polarisation states of the signal and pump are aligned to maximise the conversion efficiency. At the output of the HNL-PCF, the converted signal is selected using a combination of fibre grating and arrayed waveguide grating filters both having a full width at half maximum (FWHM) bandwidth of 1 nm. After transmission, the signal is detected using a pre-amplified receiver consisting of an erbium doped fibre amplifier (EDFA) with 4 dB noise figure followed by an OBPF and a photodiode with 50 GHz bandwidth.

4.2.2 Conversion efficiency of the optical phase conjugator

The conversion bandwidth of the OPC is characterised by inserting a tunable CW light probe as the signal into the OPC. The probe is tuned over a given wavelength range while the conversion efficiency (defined as the ratio of the power of the converted signal at the HNL-PCF output to the power of the signal at the input) is measured. The conversion efficiency is plotted in Figure 4.3 as a function of the wavelength separation between the probe and pump. A maximum conversion efficiency of

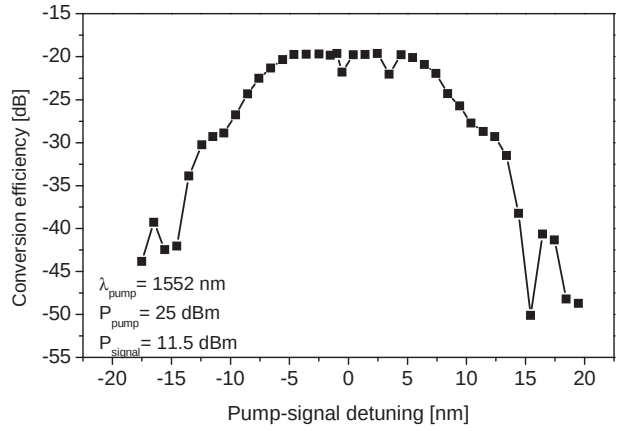

Figure 4.3: Four wave mixing conversion efficiency of the 50 m long HNL-PCF.

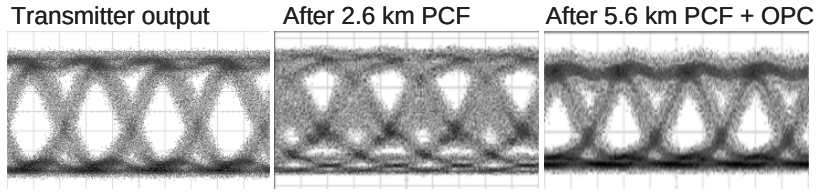

Figure 4.4: Eye-diagrams in the back-to-back case, after propagation through 2.6 km PCF and after the entire transmission link including 5.6 km transmission PCF and the OPC. Horizontal scale: 10 ps/div.

−20 dB for 25 dBm pump power is obtained. The 3 dB conversion bandwidth is measured to be 15 nm. The conversion bandwidth is mainly limited by the dispersion slope of the HNL-PCF. In the transmission experiment a signal wavelength of 1548.86 nm is chosen.

4.2.3 Results of the 40 Gbit/s transmission experiment

The eye diagrams recorded in the back-to-back case, after transmission over 2.6 km PCF, and after the entire transmission link including the 5.6 km PCF and the OPC are shown in Figure 4.4 (the vertical scale is different for the three eyes due to different average power in the photodetector). The eye diagram after propagation in the first 2.6 km PCF

is severely distorted due to dispersion. The eye diagram recorded at the output of the entire fibre link, including both the OPC and the remaining 3 km of the transmission fibre, is clear and wide open. Moreover some reshaping of the eye diagram is observable which is attributed to the bandpass filtering at the output of the HNL-PCF. The spectrum recorded at the output of the OPC indicating the wavelength allocation of the signal, pump and optical phase conjugated signals is shown in Figure 4.5. Due to the small average power of the converted signal (-11 dBm), amplification was necessary before it was launched into the second transmission fibre.

The bit error rate (BER) curves measured at the transmitter output and after transmission through the entire link are shown in Figure 4.6. A back-to-back sensitivity of -26.6 dBm is measured. The penalty induced by the complete dispersion compensated transmission link is 0.7 dB. The penalty is attributed to the difference between the accumulated dispersion before and after the OPC, and additionally to the noise induced by the amplification of the converted signal at the output of the HNL-PCF. The 14 ps/nm accumulated dispersion difference is caused mostly by the length difference of the two transmission spools. The signal and the converted signal are spaced 6.4 nm apart from each other and the dispersion slope of the transmission PCF is relatively small (S$\sim$0.067 ps/nm^{2}km), thus does not contribute much to the difference in accumulated dispersion. Therefore, by tailoring the lengths of the two transmission fibre spools, an even lower penalty is expected.

4.3 Implementation of broadcast, transmission and wavelength conversion functionalities using PCFs

Most of the communications occur through point-to-point connections, thus one user (transmitter) directly sends the information to the other user (receiver). However, for some applications, such as video conferencing or update of distributed databases, it is particulary useful to be able to send the information to a large number of users (multicasting) or alternatively to all users (broadcasting) simultaneously [40]. A large optical network typically consists of several sub-networks, operating on

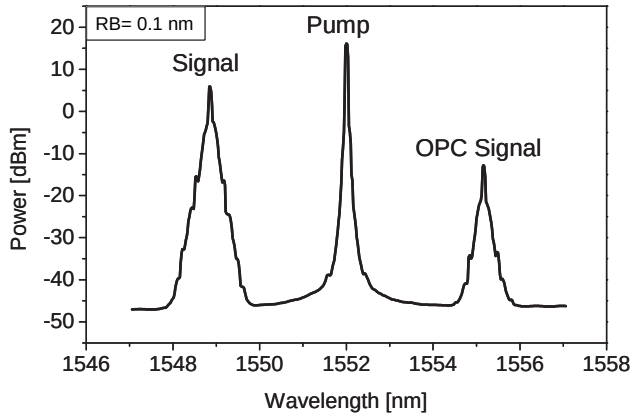

Figure 4.5: Optical spectrum recorded at the output of the HNL-PCF. The original signal, the pump and the wavelength converted (OPC signal) are shown. Resolution bandwidth is 0.1 nm.

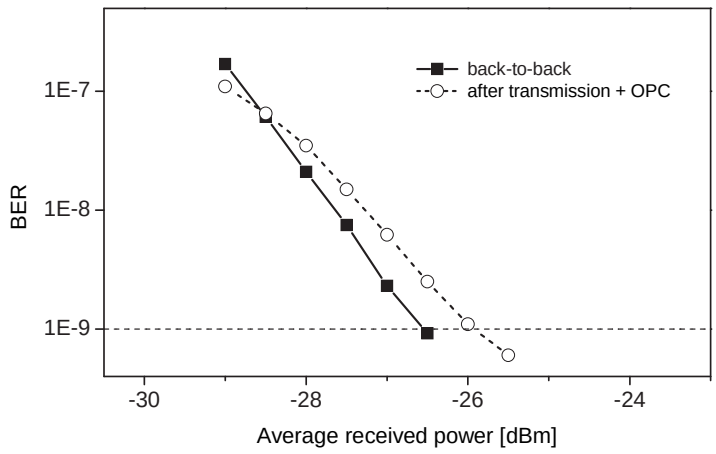

Figure 4.6: BER curves measured in the back-to-back case and after transmission over 5.6 km transmission PCF including the OPC.

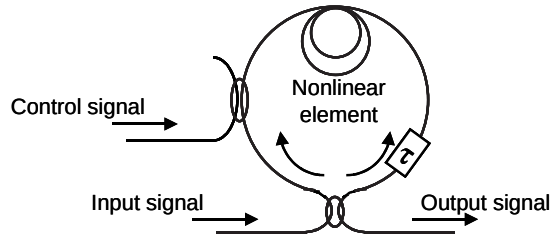

Figure 4.7: Schematic of a nonlinear optical loop mirror.

different wavelength channels, each having a number of users, capable of receiving given wavelengths. In case of multicasting, when information has to be transmitted from a source user to several users located in different sub-networks, wavelength conversion might be necessary at the ingress of the sub-networks. Therefore, for future all-optical networks, all optical implementation of multicasting, broadcasting, transmission and wavelength conversion functionalities is essential.

An effective way to realise various all optical signal processing functionalities is to use a nonlinear optical loop mirror (NOLM). A NOLM is an all optical implementation of the Sagnac interferometer, composed of a fibre loop whose ends are connected via two input ports of a 3 dB coupler, a nonlinear element and an additional coupler, as it is illustrated in Figure 4.7. The input signal of the NOLM is split into two counter propagating parts with equal power. A control signal is launched in the NOLM via the other coupler. Due to XPM, the control signal induces a nonlinear phase shift on the signals propagating through the nonlinear element. The induced phase shift is different for the clockwise and counterclockwise propagating signals. At the output of the NOLM, constructive or destructive interference of the counter propagating signals occurs depending on the nonlinear phase shift difference between them. Applications of the NOLM already have been demonstrated for high speed optical time domain multiplexing (OTDM) signal demultiplexing [28, 41, 42], wavelength conversion [11, 43] and regeneration [44]. Simultaneous wavelength conversion in a conventional HNLF based NOLM to several wavelengths has been already realised [45]. Therefore NOLMs can provide an efficient way of realising the multicasting functionality, thus generating the replica of the control signal on

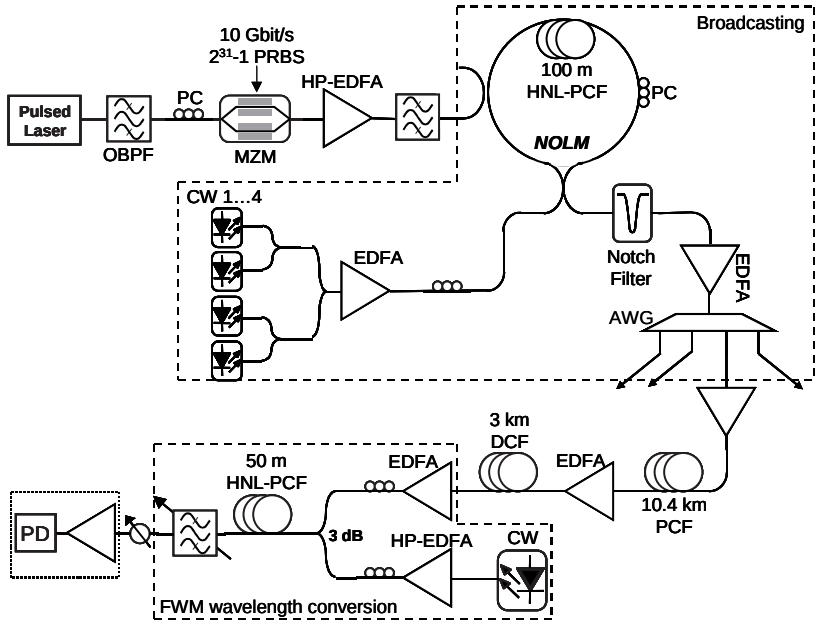

Figure 4.8: Experimental setup of the optical network demonstration with broadcast, transmission and wavelength conversion functionalities.

multiple wavelengths.

In the following, the demonstration of broadcast, transmission and wavelength conversion functionalities realised in PCFs are presented. For the first time to the author knowledge, broadcasting of four channels has been realised by exploiting XPM in a NOLM with 100 m HNL-PCF as nonlinear element. Transmission between subnetworks has been achieved by transmitting over 10.4 km LMA-PCF. Wavelength conversion at the subnetwork interface is demonstrated by generating FWM in 50 m of HNL-PCF. The combination of all these functionalities demonstrates the feasibility of realising complex and fully functional optical networks completely relying on PCFs.

4.3.1 Experimental setup

The experimental setup is shown in Figure 4.8. The broadcasting functionality was realised using cross phase modulation in a NOLM. The

control signal of the NOLM was the optical information signal at a wavelength of 1558.4 nm. This signal was to be replicated in a number of channels, thereby effectively achieving broadcasting. A pulse train from a mode-locked fiber ring laser (MLFRL) with 10 GHz repetition rate was modulated by a $LiNbO_3$ MZ modulator driven by a 10 Gbit/s, 2^{31}-1 bits long PRBS, generating a return-to-zero (RZ) modulated information signal. A high power erbium doped fibre amplifier (HP-EDFA) amplified the control signal to an average output power of 25.2 dBm before it was launched into the NOLM. The inputs of the NOLM were four CW laser sources tuned to the wavelengths of 1546.8, 1548.25, 1550.05 and 1551.8 nm with an average power of 0 dBm per channel. In the NOLM, a 100 m long HNL-PCF (see HNL-PCF2 in Table 4.1) with nonlinear coefficient equal to 11 $W^{-1}{\cdot}km^{-1}$ served as the nonlinear medium. The dispersion of the HNL-PCF is $\sim$3 ps/(nm·km) at 1550 nm with variations less than 1 ps/(nm·km) over 94 nm. At the output of the NOLM a notch filter eliminated part of the control signal before the four channels were amplified and demultiplexed by an arrayed waveguide grating (AWG). This corresponds to the situation where the four multicasted channels would be routed to different subnetworks. One selected channel (at 1548.25 nm) has been further transmitted over a partially dispersion compensated transmission span. The span consisted of 10.4 km LMA-PCF (D=31.5 ps/(nm·km) at 1550 nm) (see PCF4 in Table 3.1) and 3 km of conventional dispersion compensating fibre (DCF) (D=$-$109 ps/(nm·km) at 1550 nm). At the output of the transmission span, the signal was wavelength converted (to match the wavelength allocation of the destination subnetwork) using FWM in a 50 m long HNL-PCF with a nonlinear coefficient of about 11 $W^{-1}{\cdot}km^{-1}$ (see HNL-PCF3 in Table 4.1). The signal was amplified and its state of polarisation optimised for maximum conversion efficiency before it was input to the HNL-PCF together with a CW light pump with 27.2 dBm average power at 1544.4 nm. At the output of the HNL-PCF, an optical bandpass filter with a 3 dB bandwidth of 0.9 nm filtered out the FWM product at 1540.34 nm before it was launched into the pre-amplified receiver consisting of an EDFA followed by a photodiode with 15 GHz bandwidth.

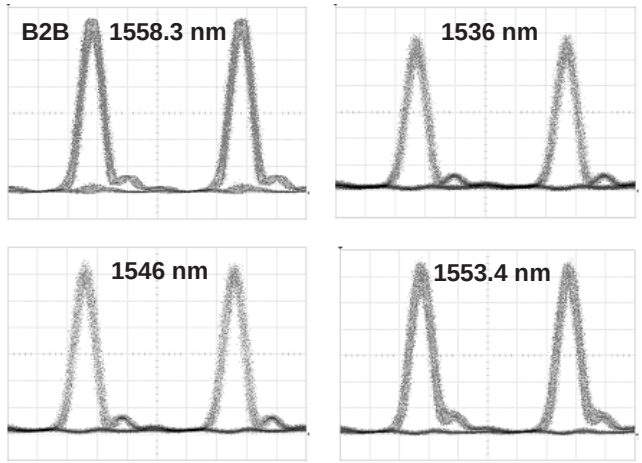

Figure 4.9: Eye diagrams of the original NOLM control signal (back-to-back) and the converted signals at wavelengths of 1536, 1546 and 1553.4 nm. Horizontal scale: 20 ps/div.

4.3.2 Characterisation of the XPM based NOLM wavelength conversion

The conversion bandwidth of the XPM based NOLM wavelength converter was first investigated. For this specific measurement, the four CW lasers in Figure 4.8 were replaced by an external cavity tunable laser source. The wavelength of the input signal was varied from 1536 nm up to 1556 nm with ∼2.5 nm steps. The choice of the exact wavelength was determined by the transfer function of the NOLM. It was ensured that the XPM based wavelength conversion was due to the interferometric operation of the NOLM by performing the selection of the converted signal by a tunable bandpass filter centred to the converted signal.

The eye diagrams of the original NOLM control signal (back-to-back) (recorded at the output of the MZ modulator) and the converted signals at wavelengths of 1536, 1546 and 1553.4 nm are shown in Figure 4.9. The eye diagrams show that the wavelength converted signals are very similar over the investigated wavelength band. The power penalty was used to quantify the quality of wavelength conversion. The power penalty as a function of the wavelength detuning (the wavelength difference between the control signal and the wavelength converted signal) is plotted

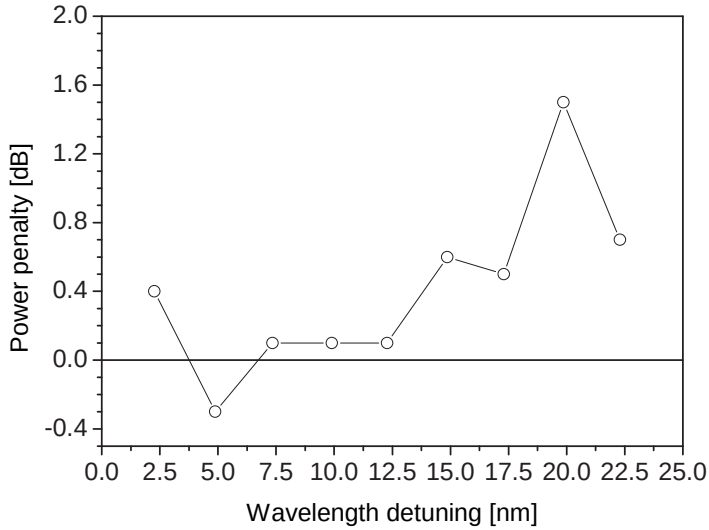

Figure 4.10: Power penalty as a function of wavelength detuning between the wavelength converted signal and the original NOLM control signal.

in Figure 4.10. Within the investigated 20 nm band, the power penalties of the converted signals were between −0.3 dB and 1.5 dB. Further increase of the detuning range was limited on the short wavelength side by the EDFA gain bandwidth, and by cross talk from the control signal on the long wavelength side. The obtained good performance over 20 nm bandwidth may permits the wavelength conversion to several wavelengths simultaneously, which in turn would allow the implementation of the broadcast functionality.

4.3.3 Results

Figure 4.11 shows the spectra recorded at the NOLM output, at the FWM stage input and at the FWM stage output. XPM induced broadening of the four input CW channels is clearly visible on the spectrum recorded at the NOLM output. The spectrum also shows FWM products between the control signal and the four input channels. Due to the requirements on the input signal wavelengths set by the NOLM transfer function and the fixed wavelength allocation of the AWG used to filter out the broadcast channels, the filtering of the channel that was

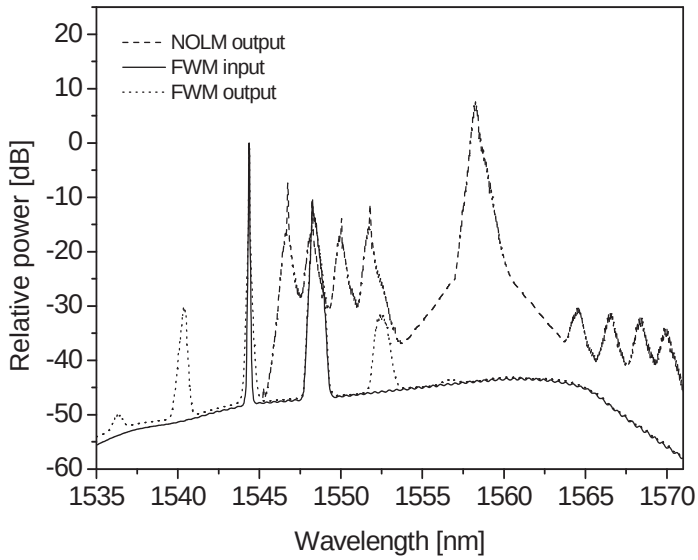

Figure 4.11: Spectra recorded at the NOLM output (dashed line), FWM stage input (solid line) and output (dotted line) (resolution bandwidth: 0.01 nm).

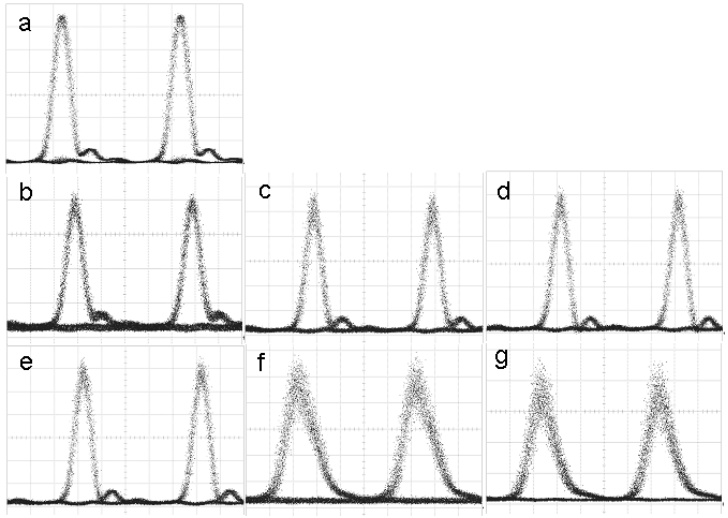

Figure 4.12: Eye diagrams of (a) the original NOLM control signal, (b-e) wavelength converted signals at the output of the AWG, (f) after transmission through 10.4 km PCF, (g) at the output of the FWM wavelength conversion stage. Horizontal scale: 20 ps/div.

transmitted further is slightly asymmetric.

In Figure 4.12 the eye diagrams of the original control signal of the NOLM (a), the four broadcast channels recorded at the output of the AWG (b-e), after transmission over 10.4 km PCF (f) and after wavelength conversion by FWM (g) are shown. The quality of the four broadcast channels is similar. After transmission, dispersion induced pulse broadening is observable on the pulse. On the FWM wavelength converted pulse optical signal to noise ratio (OSNR) degradation is visible, even though the eye diagram is still wide open.

The BER curves of the corresponding cases have been measured and are plotted in Figure 4.13. The back-to-back sensitivity was -29.2 dBm. The power penalties of the four broadcast channels were between 0.9 and 2.4 dB. These penalties are higher than the ones measured when the NOLM has been used to wavelength convert to only one wavelength. The signal degradation compared to the single channel wavelength conversion is attributed to FWM between the four channels while they are propagating in the NOLM. The degradation caused by the transmis-

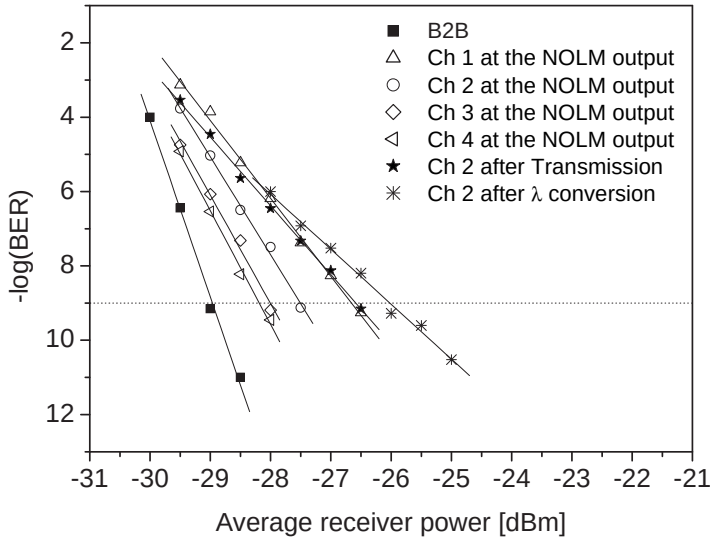

Figure 4.13: Bit error rate as a function of average receiver power measured for the original NOLM control signal, the four converted signals at the NOLM output, after transmission and after FWM wavelength conversion.

sion line is measured to be 0.9 dB. The penalty induced by the FWM wavelength conversion is 0.6 dB.

4.4 Summary

Signal processing applications of index guiding PCFs for telecommunications have been discussed in this chapter. Entirely PCF based transmission systems, realising both signal processing and transmission in index guiding PCFs, have been presented.

The first entirely index guiding photonic crystal fibre based dispersion compensated optical link has been presented. A 40 Gbit/s non return-to-zero signal has been transmitted over 5.6 km of large mode area photonic crystal fibre where dispersion compensation has been achieved by using optical phase conjugation utilising four-wave mixing in a 50 m long highly nonlinear photonic crystal fibre. The total penalty of the complete system, including both transmission and dispersion compensation, was 0.7 dB. It is expected that by optimising the lengths of the

transmission fibres before and after the optical phase conjugator, the penalty could be further reduced.

Furthermore, the first entirely photonic crystal fibre based prototype optical network with broadcast, transmission and wavelength conversion functionalities has been demonstrated. Broadcasting of four channels for the first time has been realised by cross phase modulation in a nonlinear optical loop mirror utilising 100 m highly nonlinear photonic crystal fibre as nonlinear element. Transmission of a selected channel over 10.4 km large mode area photonic crystal fibre and wavelength conversion of that channel exploiting four-wave mixing in a 50 m long highly nonlinear photonic crystal fibre have been also successfully demonstrated.

The presented experiments constitute the first demonstrations of optical systems completely made of photonic crystal fibres. These demonstrations clearly show the potential of photonic crystal fibres for both transmission and signal processing purposes.

References to Chapter 4

[1] K. M. Hilligsøe, T. V. Andersen, H. N. Paulsen, C. K. Nielsen, K. Mølmer, S. Keiding, R. Kristiansen, K. P. Hansen, and J. J. Larsen. "Supercontinuum generation in a photonic crystal fiber with two zero dispersion wavelengths", *Optics Express*, vol. 12, no. 6, pp. 1045–1954, March 2004.

[2] T. Hori, J. Takayanagi, N. Nishizawa, and T. Goto. "Flatly broadened, wideband and low noise supercontinuum generation in highly nonlinear hybrid fiber", *Optics Express*, vol. 12, no. 2, pp. 317–324, January 2004.

[3] K. Saitoh and M. Koshiba. "Highly nonlinear dispersion-flattened photonic crystal fibers for supercontinuum generation in a telecommunication window", *Optics Express*, vol. 12, no. 10, pp. 2027–2032, May 2004.

[4] K. Sakamaki, M. Nakao, M. Naganuma, and M. Izutsu. "Soliton induced supercontinuum generation in photonic crystal fiber", *IEEE Journal of Selected Topics in Quantum Electronics*, vol. 10, no. 5, pp. 876–884, September 2004.

[5] T. Yamamoto, H. Kubota, S. Kawanishi, M. Tanaka, and S. Yamaguchi. "Supercontinuum generation at 1.55 μm in a dispersion-flattened polarization-maintaining photonic crystal fiber", *Optics Express*, vol. 11, no. 13, pp. 1537–1540, June 2003.

[6] J. K. Ranka, R. S. Windeler, and A. J. Stentz. "Visible continuum generation in air-silica microstructure optical fibers with anomalous dispersion at 800 nm", *Optics Letters*, vol. 25, no. 1, pp. 25–27, January 2000.

[7] P. A. Andersen, C. Peucheret, K. M. Hilligsøe, K. S. Berg, K. P. Hansen, and P. Jeppesen. "Supercontinuum generation in a photonic crystal fibre using picosecond pulses at 1550 nm", in *Proceedings International Conference on Transparent Optical Networks / European Photonic Crystals Symposium, ICTON/ESPC'03,* Warsaw, Poland, vol. 1, pp. 66–69, July 2003, paper Mo.C1.6.

[8] P. A. Andersen, B. Zsigri, C. Peucheret, P. Jeppesen, K. P. Hansen, and M. D. Nielsen. "Photonic crystal fibers used in a multi-wavelength source and as transmission fiber in a WDM system", in *Technical Digest Conference on Lasers and Electro-Optics, CLEO'04,* San Francisco, California, U.S.A., May 2004, paper CThG4.

[9] Z. Yusoff, P. Teh, P. Petropoulos, K. Furusawa, W. Belardi, T. Monro, and D. Richardson. "24 channels $\times$ 10 GHz spectrally sliced pulse source based on spectral broadening in a highly nonlinear holey fiber", in *Technical Digest Optical Fiber Communication Conference, OFC'03,* Atlanta, Georgia, U.S.A., vol. 2, pp. 687–689, March 2003, paper FH3.

[10] K. K. Chow, C. Shu, C. Lin, and A. Bjarklev. "Polarization-insensitive widely tunable wavelength converter based on four-wave mixing in a dispersion-flattened nonlinear photonic crystal fiber", *IEEE Photonics Technology Letters*, vol. 17, no. 3, pp. 624–626, March 2005.

[11] C. H. Kwok, S. H. Lee, K. K. Chow, C. Shu, C. Lin, and A. Bjarklev. "Widely tunable wavelength conversion with extinction ratio en-

hancement using PCF-based NOLM", *IEEE Photonics Technology Letters*, vol. 17, no. 12, pp. 2655–2657, December 2005.

[12] G.-W. Lu, L.-K. Chen, C.-K. Chan, and C. Lin. "All-optical tunable wavelength conversion based on cross-polarisation modulation in nonlinear photonics crystal fibre", *Electronics Letters*, vol. 41, no. 4, pp. 55–56, February 2005.

[13] A. Zhang and M. S. Demokan. "Broadband wavelength converter based on four-wave mixing in a highly nonlinear photonic crystal fiber", *Optics Letters*, vol. 30, no. 18, pp. 2375–2377, September 2005.

[14] K. S. Abedin, T. Miyazaki, and F. Kubota. "Wavelength-conversion of pseudorandom pulses at 10 Gb/s by using soliton self-frequency shift in a photonic crystal fiber", *IEEE Photonics Technology Letters*, vol. 16, no. 4, pp. 1119–1121, April 2004.

[15] J. H. Lee, Z. Yusoff, W. Belardi, M. Ibsen, T. M. Monro, and D. J. Richardson. "A tunable WDM wavelength converter based on cross-phase modulation effects in normal dispersion holey fiber", *IEEE Photonics Technology Letters*, vol. 15, no. 3, pp. 437–439, March 2003.

[16] J. H. Lee, W. Belardi, K. Furusawa, P. Petropoulos, Z. Yusoff, T. M. Monro, and D. J. Richardson. "Four-wave mixing based 10-Gb/s tunable wavelength conversion using a holey fiber with a high SBS threshold", *IEEE Photonics Technology Letters*, vol. 15, no. 3, pp. 440–442, March 2003.

[17] B. Zsigri, C. Peucheret, M. D. Nielsen, and P. Jeppesen. "Implementation of broadcast, transmission and wavelength conversion functionalities using photonic crystal fibers", in *Proceedings OptoElectronics and Communications Conference, OECC'05,* Seoul, Korea, pp. 790–791, July 2005, paper 8B3-1.

[18] Y. Geng, P. A. Andersen, T. Tokle, C. Peucheret, and P. Jeppesen. "Wavelength conversion of a 6×40 Gb/s DPSK WDM signal using FWM in a highly non-linear photonic crystal fiber", in *Proceedings*

European Conference on Optical Communication, ECOC'05, Glasgow, Scotland, vol. 2, pp. 205–206, September 2005, paper Tu3.3.4.

[19] J. E. Sharping, M. Fiorentino, P. Kumar, and R. S. Windeler. "All-optical switching based on cross-phase modulation in microstructure fiber", *IEEE Photonics Technology Letters*, vol. 14, no. 1, pp. 77–79, January 2002.

[20] P. Petropoulos, T. M. Monro, W. Belardi, K. Furusawa, J. H. Lee, and D. J. Richardson. "A highly nonlinear holey fiber and its application in a regenerative optical switch", in *Technical Digest Optical Fiber Communication Conference, OFC'01,* Anaheim, California, U.S.A., March 2001, paper TuC3.

[21] P. Petropoulos, T. M. Monro, W. Belardi, K. Furusawa, J. H. Lee, and D. J. Richardson. "2R-regenerative all-optical switch based on a highly nonlinear holey fiber", *Optics Letters*, vol. 26, no. 16, pp. 1233–1235, August 2001.

[22] R. Tang, P. Devgan, J. Sharping, P. Voss, J. Lasri, and P. Kumar. "Microstructure-fiber based optical parametric amplifier in the 1550 nm telecom band", in *Technical Digest Optical Fiber Communication Conference, OFC'03,* Atlanta, Georgia, U.S.A., vol. 2, pp. 562–563, March 2003, paper ThT2.

[23] J. H. Lee. "All-optical signal processing devices based on holey fiber", *IEICE Transactions on Electronics*, vol. E88-C, no. 3, pp. 327–334, March 2005.

[24] Z. Yusoff, J. H. Lee, W. Belardi, T. M. Monro, P. C. Teh, and D. J. Richardson. "Raman effects in a highly nonlinear holey fiber: amplification and modulation", *Optics Letters*, vol. 27, no. 6, pp. 424–426, March 2002.

[25] C. Fukai, K. Nakajima, J. Zhou, K. Tajima, K. Kurokawa, and I. Sankawa. "Distributed Raman amplification based DWDM transmission in a low loss photonic crystal fibre", in *Proceedings European Conference on Optical Communication, ECOC'04,* Stockholm, Sweden, vol. 3, pp. 304–305, September 2004, paper We1.3.6.

[26] K. Nakajima, C. Fukai, K. Kurokawa, K. Tajima, T. Matsui, and I. Sankawa. "Distributed Raman amplification at 850 nm in a low loss photonic crystal fibre", in *Proceedings European Conference on Optical Communication, ECOC'05,* Glasgow, Scotland, vol. 2, pp. 285–286, September 2005, paper Tu4.4.3.

[27] J. H. Lee, Z. Yusoff, W. Belardi, T. M. Monro, P. C. Teh, and D. J. Richardson. "A holey fibre Raman amplifier and all-optical modulator", in *Proceedings European Conference on Optical Communication, ECOC'01,* Amsterdam, The Netherlands, September 2001, post-deadline paper PDA1.1.

[28] L. K. Oxenløwe, A. I. Siahlo, P. A. Andersen, K. S. Berg, A. T. Clausen, P. Jeppesen, K. P. Hansen, J. R. Folkenberg, K. Hoppe, and J. Hanberg. "Complete transmission system with a highly non-linear dispersion shifted photonic crystal fibre as the demultiplexer", in *Technical Digest Conference on Lasers and Electro-Optics, CLEO'03,* Baltimore, Maryland, U.S.A., June 2003, paper CFJ1.

[29] A. I. Siahlo, L. K. Oxenløwe, K. S. Berg, A. T. Clausen, P. A. Andersen, C. Peucheret, A. Tersigni, P. Jeppesen, K. P. Hansen, and J. R. Folkenberg. "A high-speed demultiplexer based on a nonlinear optical loop mirror with a photonic crystal fiber", *IEEE Photonics Technology Letters*, vol. 15, no. 8, pp. 1147–1149, August 2003.

[30] L. K. Oxenløwe, A. I. Siahlo, K. S. Berg, A. Tersigni, A. T. Clausen, C. Peucheret, P. Jeppesen, K. P. Hansen, and J. R. Jensen. "A photonic crystal fibre used as a 160 to 10 Gb/s demultiplexer", in *Proceedings OptoElectronics and Communications Conference, OECC'02,* Yokohama, Japan, July 2002, post-deadline paper PD1-4.

[31] W. Belardi, J. H. Lee, K. Furusawa, Z. Yusoff, P. Petropoulos, M. Ibsen, T. M. Monro, and D. J. Richardson. "A 10 Gbit/s tuneable wavelength converter based on four-wave mixing in highly nonlinear holey fibre", in *Proceedings European Conference on Optical Communication, ECOC'02,* Copenhagen, Denmark, September 2002, post-deadline paper PD1.2.

[32] C. Peucheret, B. Zsigri, P. A. Andersen, K. S. Berg, A. Tersigni, P. Jeppesen, K. P. Hansen, and M. D. Nielsen. "Transmission over photonic crystal fiber at 40 Gbit/s using mid-span spectral inversion in a highly nonlinear photonic crystal fiber", in *Technical Digest Conference on Lasers and Electro-Optics, CLEO'03,* Baltimore, Maryland, U.S.A., June 2003, post-deadline paper CThPDB4.

[33] C. Peucheret, B. Zsigri, P. A. Andersen, K. S. Berg, A. Tersigni, P. Jeppesen, K. P. Hansen, and M. D. Nielsen. "40 Gbit/s transmission over photonic crystal fibre using mid-span spectral inversion in highly nonlinear photonic crystal fibre", *Electronics Letters*, vol. 39, no. 12, pp. 919–921, June 2003.

[34] K. P. Hansen, J. R. Jensen, C. Jacobsen, H. R. Simonsen, J. Broeng, P. M. W. Skovgaard, A. Petersson, and A. Bjarklev. "Highly nonlinear photonic crystal fiber with zero-dispersion at 1.55 μm", in *Technical Digest Optical Fiber Communication Conference, OFC'02,* Anaheim, California, U.S.A., March 2002, post-deadline paper FA9.

[35] K. P. Hansen, J. R. Folkenberg, C. Peucheret, and A. Bjarklev. "Fully dispersion controlled triangular-core nonlinear photonic crystal fiber", in *Technical Digest Optical Fiber Communication Conference, OFC'03,* Atlanta, Georgia, U.S.A., pp. 806–808, March 2003, post-deadline paper PD02.

[36] A. E. Willner and B. Hoanca. *Fixed and tunable management of fiber chromatic disperison*, In I. Kaminow and T. Li, editors, *Optical Fiber Telecommunications IVB Components,* Chapter 14, Academic Press, March 2002. ISBN 0-12-395173-9.

[37] S. Watanabe, T. Chikama, G. Ishikawa, T. Terahara, and H. Kuwahara. "Compensation of pulse shape distortion due to chromatic dispersion and Kerr effect by optical phase conjugation", *IEEE Photonics Technology Letters*, vol. 5, no. 10, pp. 1241–1243, October 1993.

[38] S. Watanabe, S. Takeda, G. Ishikawa, H. Ooi, J. G. Nielsen, and C. Sonne. "Simultaneous wavelength conversion and optical phase

conjugation of 200 Gb/s (5×40 Gb/s) WDM signal using a highly nonlinear fiber four-wave mixer", in *Proceedings European Conference on Optical Communication, ECOC'97,* Edinburgh, Scotland, U.K., pp. 1–4, September 1997, paper TH3A.

[39] S. Watanabe and M. Shirasaki. "Exact compensation for both chromatic dispersion and Kerr effect in a transmission fiber using optical phase conjugation", *Journal of Lightwave Technology*, vol. 14, no. 3, pp. 243–248, March 1996.

[40] A. S. Tanenbaum. *Computer Networks.* Prentice Hall, Fourth edition, 2003. ISBN 0-13-066102-3.

[41] A. T. Clausen, A. I. Siahlo, J. Seoane, L. K. Oxenløwe, and P. Jeppesen. "320 to 10 Gbit/s demultiplexing using a NOLM based on commercially available components", *Electronics Letters*, vol. 41, no. 5, pp. 265–266, March 2005.

[42] A. I. Siahlo, A. T. Clausen, L. K. Oxenløwe, J. Seoane, and P. Jeppesen. "640 Gb/s OTDM transmission and demultiplexing using a NOLM with commercially available highly non-linear fiber", in *Technical Digest Conference on Lasers and Electro-Optics, CLEO'05,* Baltimore, Maryland, U.S.A., May 2005, paper CTuO1.

[43] J. Yu, X. Zheng, C. Peucheret, A. T. Clausen, H. N. Poulsen, and P. Jeppesen. "40-Gb/s all-optical wavelength conversion based on a nonlinear optical loop mirror", *Journal of Lightwave Technology*, vol. 18, no. 7, pp. 1001–1006, July 2000.

[44] M. Scaffardi, P. A. Andersen, L. K. Oxenløwe, M. Galili, D. Larsson, K. Yvind, P. Jeppesen, A. Bogoni, P. Ghelfi, and L. Poti. "Performance evaluation of a highly non-linear fibre based NOLM for regeneration up to 160 Gb/s", in *Technical Digest IEEE Lasers and Electro-Optics Society Annual Meeting, LEOS'04,* Rio Grande, Puerto Rico, November 2004, paper ThBB4.

[45] J. Yu, Y. Qian, P. Jeppesen, and S. N. Knudsen. "Construction of a single/multiple wavelength RZ optical pulse source at

40 GHz by use of wavelength conversion in a high-nonlinearity DSF-NOLM", in *Technical Digest Optical Fiber Communication Conference, OFC'01,* Anaheim, California, U.S.A., March 2001, paper WDD8.

Chapter 5

Dispersion compensating photonic crystal fibres

The previous chapters have described the properties and applications of large mode area photonic crystal fibres (LMA-PCFs) and highly nonlinear photonic crystal fibres (HNL-PCFs) in optical communication systems. In this chapter, photonic crystal fibres (PCFs) for dispersion compensation will be considered. First, basic figure-of-merits that are important to the evaluation of dispersion compensating fibres (DCFs) will be briefly introduced. This will be followed by an overview of the different dispersion compensating photonic crystal fibre (DC-PCF) designs reported until now. In section 5.3, a novel DC-PCF design, possessing a honeycomb cladding structure and an up-doped core region, will be proposed and the dispersion properties of this design will be numerically investigated [1]. The fibre is designed to match the relative dispersion slope of standard single mode fibre (SSMF). The designed fibre exhibits very large negative dispersion of -1353 ps/(nm·km) and effective area of 1.6 μm^2 at 1550 nm. A comparison between the proposed design and other reported DC-PCF designs is also presented. The advantages and the drawbacks of DC-PCFs are discussed. Finally, the chapter is summarised.

5.1 Figure of merits for dispersion compensation

Most of the transmission fibres used in telecommunications have non-zero dispersion at the transmission wavelength. SSMF [2] is commonly used as transmission fibre and it has ∼17 ps/(nm·km) dispersion at 1550 nm [3]. Transmission fibres with zero dispersion at the transmission wavelength are also available [3]. Nevertheless, in wavelength division multiplexing (WDM) systems, transmission fibres with non-zero dispersion are preferred in order to mitigate the undesirable effects of nonlinearities [4].

Dispersion causes time domain pulse broadening, thus limiting the maximum transmission distance of high speed systems [5]. In long haul systems with data rates of 10 Gbit/s and above, dispersion compensation is indispensable. Dispersion is a linear distortion thus, in the absence of nonlinear processes, it can be completely compensated. Several different optical dispersion compensating techniques have been proposed including the use of dispersion compensating fibres [6, 7], fibre Bragg gratings [8, 9], all-pass optical filters [10, 11] and optical phase conjugation [12, 13]. Dispersion can also be mitigated in the electrical domain [14, 15].

Dispersion compensation by DCFs is the most widely used compensation technique. It was first proposed in 1980 [16] and it is already a mature technique today. DCFs have opposite sign dispersion, most commonly normal dispersion, compared to the transmission fibre to be compensated. The dispersion of commercially available conventional DCFs is in the range of −85 to −100 ps/(nm·km) at 1550 nm [6]. By tailoring the length of the DCF, the absolute value of the accumulated dispersion of the transmission fibre (TF) and the DCF can be equalised, thus complete dispersion compensation can be achieved:

$$D_{\mathrm{TF}}(\lambda) \times L_{\mathrm{TF}} = -D_{\mathrm{DCF}}(\lambda) \times L_{\mathrm{DCF}} \tag{5.1}$$

where D is the dispersion coefficient, L is the length of the fibre and λ is the wavelength of the optical signal. In case of single wavelength dispersion compensation, this equation can be used to determine the length of the DCF needed. However in a WDM system, dispersion compensation over a broad wavelength range is required. In this case,

the wavelength dependence of the dispersion, the dispersion slope (S), has to be considered as well. As long as the dispersion can be assumed to have linear wavelength dependence over the wavelength range of interest, the wavelength dependence of the dispersion can be approximated by:

$$D(\lambda) = D(\lambda_0) + (\lambda - \lambda_0)S(\lambda_0) \tag{5.2}$$

where λ_0 is a wavelength within the wavelength window where D is assumed to be linear (e.g. the centre wavelength of the window) and $S(\lambda_0)$ is the dispersion slope at λ_0.

A commonly used measure to evaluate how well the wavelength dependence of the dispersion can be compensated for, is the relative dispersion slope (RDS) defined as the ratio of the dispersion slope and the dispersion of the fiber,

$$RDS = \frac{S}{D(\lambda_0)} \quad . \tag{5.3}$$

If the RDS of the transmission fiber and the DCF are equal, complete dispersion compensation over a broad wavelength range (where dispersion can be assumed to be linear) may be obtained. For most practical applications, it is difficult and even unnecessary to achieve complete dispersion and dispersion slope compensation over the entire wavelength range of interest. In case of approximate dispersion compensation, the compensation ratio (CR) expresses how much of the dispersion is compensated. The CR is defined as the absolute value of the ratio of the accumulated dispersion of the transmission fibre and the accumulated dispersion of the DCF.

$$CR(\lambda) = -\frac{D_{\mathrm{TR}}(\lambda) \times L_{\mathrm{TR}}}{D_{\mathrm{DCF}}(\lambda) \times L_{\mathrm{DCF}}} \tag{5.4}$$

Dependent of the specific application a few percent deviation from 100% of CR can be tolerated [17].

5.2 Dispersion compensating fibre designs

Typically DCFs are coiled up in a fibre spool and placed at the amplifier station, thus do not contribute to the transmission distance. DCFs

generally also have higher loss (∼0.5 dB/km) than transmission fibres. To avoid excessive losses, DCFs should be as short as possible, which requires the magnitude of the dispersion coefficient to be as large as possible. The chromatic dispersion of a fibre can be calculated as:

$$D(\lambda) = -\frac{\lambda}{c}\frac{d^2 n_{\text{eff}}(\lambda)}{d\lambda^2} \quad , \tag{5.5}$$

where λ is the wavelength of the guided light, c is the light velocity in vacuum and n_{eff} is the effective mode index of the guided mode. Thus from equation (5.5), large dispersion values can be obtained with fibre designs where the effective mode index changes rapidly with wavelength. However, the possible range of effective mode indices in an optical fibre is bounded by the refractive index of the core (n_{core}) and cladding (n_{clad}) as follows:

$$n_{\text{core}} \geq n_{\text{eff}} \geq n_{\text{clad}} \quad . \tag{5.6}$$

Therefore, the larger the refractive index difference between core and cladding, the larger dispersion values can be obtained at a single wavelength. When dispersion compensation over a wide wavelength range is needed, dispersion slope matching with the transmission fibre must also be ensured besides the large absolute values of dispersion. Consequently the magnitude of the dispersion coefficient of slope matched DCFs has to be compromised.

PCFs are attractive to be used for dispersion compensation due to the large index difference between air and silica and the fact that PCFs can be designed with large air holes such that their cladding is composed nearly entirely from air [18, 19]. Simple, small core triangular cladding structure PCFs with large air holes and a core formed by omitting one of the central air holes have been proposed for dispersion compensation [20]. The influence of hole size and pitch on the dispersion profile of this structure has been thoroughly investigated [21, 22]. Dispersion values as large as −1700 ps/(nm·km) at 1550 nm have been predicted for a fibre suitable for single channel compensation [21]. For fibres designed for broadband dispersion compensation, the absolute value of dispersion is reduced to −590 ps/(nm·km) at 1550 nm [21]. The broadband DC-PCF design, described in reference [21] provides partial dispersion compensation over 100 nm in concatenation with SSMF. A drawback of

the simple triangular cladding DC-PCFs design is that it possess very small effective areas, ∼1 to 1.6 μm^2 [20–22].

Another DC-PCF design is inspired by the W-refractive index profile of the dual-core conventional DCFs [23, 24]. The fibre cross section and the index profile of a conventional dual core fibre are shown in Figure 5.1. W-refractive index profile fibres have two concentrical cores. The inner core has raised index compared to the outer core and cladding. The fibre furthermore has an inner cladding with depressed index and a outermost cladding region, usually pure silica. The fibre supports two super-modes, one in the inner core and the other in the outer core. The two super-modes are phase matched at a wavelength λ_p, called the phase matching wavelength. For wavelengths below the phase matching wavelength, the fundamental mode is guided in the inner core. At the phase matching wavelength, strong mode coupling occurs between the modes guided in the inner and outer cores. For wavelength above the phase matching wavelength, the fundamental mode is guided in the outer core. Due to the large asymmetry of the two cores at the phase matching wavelength, the slope of the effective index of both the fundamental and the second-order modes are changing rapidly, which results in large absolute dispersion coefficient. The dispersion slope is negative for wavelengths below λ_p while it is positive for wavelengths above that. Therefore choosing the operation wavelength below λ_p both dispersion and dispersion slope of the transmission fibre can be compensated.

The W-refractive index profile in PCFs can be obtained by varying the hole size of the concentrical air hole rings [25–30]. The cross section of one possible dual-core DC-PCF design is shown in Figure 5.2. The central absent hole defect forms the inner core, the enlargened air hole ring closest to the core form the depressed index inner cladding, the air hole ring with smaller hole diameters forms the outer core. The remaining of the periodic structure is the outer cladding. The phase matching wavelength of the fibre can be changed by changing the air hole diameters and the pitch in the cladding [26, 27]. The number of air hole rings in the inner cladding changes the dispersion slope [26, 27]. An inner core with one air hole ring results in the largest obtainable dispersion coefficient for the given design, although the optimum fibre for broadband dispersion compensation (relative slope matched with transmission fibre) had three air hole rings in the inner cladding [26, 27]. A

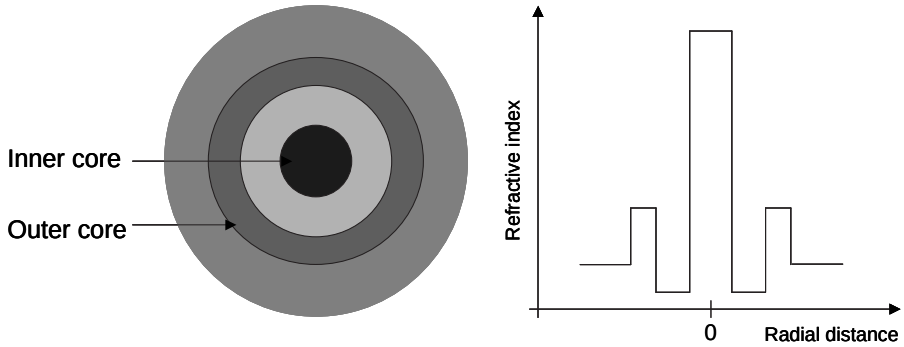

Figure 5.1: Cross section of conventional dual-core dispersion compensating fibre (left) and the corresponding refractive index profile (right). The fibre possesses two concentrical cores. The inner core has higher refractive index than the outer core. The fibre has two claddings as well. The inner cladding has a depressed index compared to the outer cladding.

dual-core DC-PCF with doped inner core has been also proposed [27].

Using the dual-core DC-PCF design, fibres suitable for single wavelength dispersion compensation with dispersion of −18000 ps/(nm·km) at 1550 nm and effective area of 12 μm^2 have been theoretically predicted [28]. Pure silica dual-core DC-PCFs for broadband dispersion compensation have been realised with a dispersion of −1211 ps/(nm·km) at 1550 nm and approximately dispersion slope matched with SSMF [25]. The mode field diameter (MFD) of this fibre is 3 μm. Another significance of this fibre is that this is currently the only fabricated DC-PCF. As a comparison, dispersion values of −5100 ps/(nm·km) have been predicted theoretically [23] and −1800 ps/(nm·km) has been realised in practice [24] for conventional dual-core DCF design. Dual-core fibres have also been proposed to increase the effective areas of DCFs. Fibres with effective area as large as 80 μm^2 and dispersion of −1600 ps/(nm·km) (no slope matching) have been predicted by simulations [30]. A dual-core design has also been proposed as DC-PCF Raman amplifier [29].

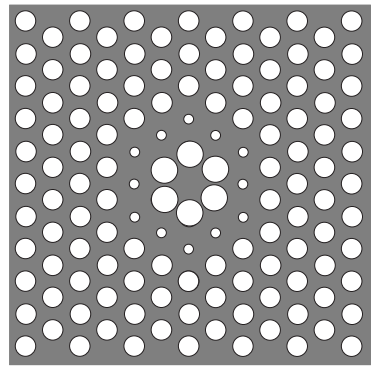

Figure 5.2: Cross section of one possible dual-core dispersion compensating photonic crystal fibre design. The central absent hole defect forms the inner core, the enlargened air hole ring closest to the core forms the depressed index inner cladding, the air hole ring with smaller hole diameters forms the outer core. The remaining of the periodic structure is the outer cladding.

5.3 Novel honeycomb structured dispersion compensating photonic crystal fibre

In this section, a novel DC-PCF design is proposed. The design presents a realisation of W-refractive index profile. The proposed DC-PCF design posses an up-doped core region and a honeycomb photonic crystal cladding structure. The fibre is designed to match the relative dispersion slope of SSMF. It is predicted by simulations that the designed fibre exhibits very large negative dispersion of -1353 ps/(nm·km) at 1550 nm and an effective area of 1.6 μm^2. A comparison of the proposed honeycomb DC-PCF design, the simple triangular cladding structure and the dual-core DC-PCFs is also performed. The section is structured as follows: first the proposed DC-PCF structure will be described. Then the simulation software, the MIT Photonic Bands package (MPB) [31], used to investigate the dispersion properties of the proposed structure and some of the critical parameters, will be briefly introduced. Finally the results will be presented.

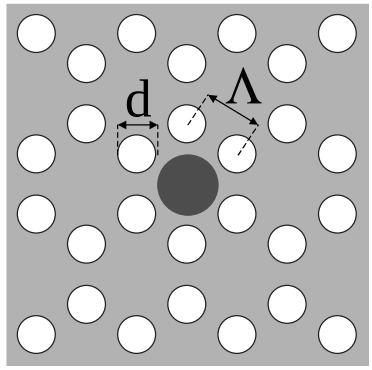

Figure 5.3: Cross section of the proposed dispersion compensating photonic crystal fibre. The fibre has a honeycomb cladding structure. The core defect is an up-doped circular region with diameter equal to the hole-to-hole spacing (Λ).

5.3.1 Fibre design

The structure of the proposed fibre design is shown in Figure 5.3. The cladding has a honeycomb lattice structure of circular air holes in silica. The diameter of the air holes is d, and the hole-to-hole spacing is equal to the pitch, Λ. The core is defined by an up-doped silica defect with a diameter of Λ. The size of the up-doped region is a trade-off. The doped region has to be small enough to keep it separated from the surrounding air holes. On the other hand the size of the doped region has to be large as a smaller diameter would require higher doping levels to reach the same dispersion value. Since the core is formed by raising the average refractive index, the fiber is index guiding [32].

5.3.2 Simulation parameters

This section briefly describes the simulation software and the artificially created periodic structure to be simulated.

To investigate the dispersion properties of the proposed structure, a freely available software package has been used, which expands the magnetic field and the dielectric function in plane waves [31]. Periodic dielectric structures can be efficiently modeled by plane waves due to the similar spatial extension of the modes of the structure and the plane waves. However guided localised modes are not periodic solutions,

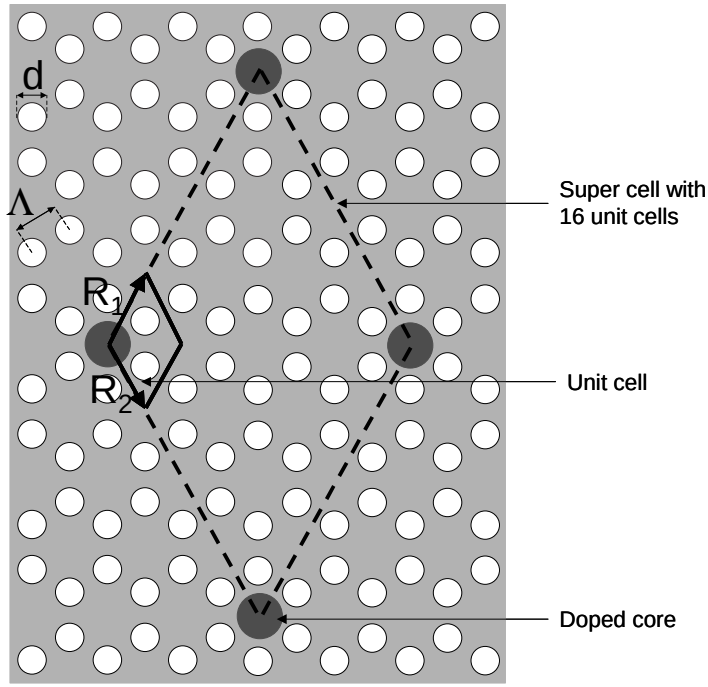

Figure 5.4: Unit cell (enclosed by the solid rhombus) and super cell (enclosed by the dashed rhombus) of the doped honeycomb cladding structured fibre. R_1 and R_2 are the unit vectors. The size of the drawn super cell is 16 unit cells.

therefore to analyse these modes, an artificial periodicity has to be created. This can be done by repeating the core region periodically in the infinite cladding structure as it is shown in Figure 5.4. The original periodic structure is described by the unit cell, defined by the two lattice vectors, R_1 and R_2. The artificial periodic structure is defined by the super cell. Both the unit and the super cells are illustrated in Figure 5.4. The size of the super cell is given by the number of unit cells, together making up the base of the simulated periodic structure. The choice of the super cell size is a trade off. The super cell size has to be large enough to well separate the simulated periodical cores (The size of the super cell should be significantly larger than the effective mode area of the guided modes [33]). On the other hand, with increasing super cell sizes the computation time increases. In all the presented simulations, the size of the super cell has been chosen to be either 8 or 16 unit cells. Super cell convergence is enhanced by using the transverse Bloch vector (3/8, 1/8) [34]. The resolution which gives the computational grid resolution, in pixels per lattice unit was 48. In the calculations, a perturbation theory has been used, which enabled to extract dispersion curves over a large range of Λ values from a single calculation of the waveguide dispersion and field energy distribution, at suitably chosen values of the material refractive indices [34] (in this case, the refractive index at 1550 nm is used). The refractive index of silica is calculated using a three-term Sellmeier polynomial with the coefficients given in reference [35] ($n \approx 1.444$ at 1550 nm). It is assumed that the high-index core region is obtained by Ge doping. The relevant doping levels were calculated by linear extrapolation, using the Sellmeier coefficients for Ge-doped silica reported in reference [35]. The presented chromatic dispersion values include both material and waveguide dispersion.

5.3.3 Dispersion properties of the DC-PCF

In this section, the dispersion properties of the proposed honeycomb DC-PCF will be presented. First, the influence of the structural parameters on the dispersion profile will be investigated. Subsequently, the DC-PCF is optimised for broadband dispersion compensation, thus optimised to match the RDS of the transmission fibre. Finally, the performance of the proposed DC-PCF for broadband dispersion compensation is evaluated

by calculating the compensation ratio of a transmission line consisting of 100 km SSMF fibre and matching length of the proposed DC-PCF.

In the following, the transmission fibre is assumed to be a SSMF. Therefore, for wide-band dispersion compensation the relative dispersion slope of DC-PCFs is matched with the dispersion slope of SSMF. The RDS of SSMF is 0.0035 nm^{-1}, assuming typical values of 17 ps/(nm·km) and 0.06 ps/(nm^2·km) as dispersion parameter at 1550 nm and dispersion slope, respectively [6].

The dispersion properties of the proposed DC-PCF design have been investigated with different doping levels (n_c) and systematically varied air hole diameters d/Λ and pitch Λ. First the effective index of the guided mode for fibre structures with different combinations of d/Λ and n_c have been calculated. The dispersion curves of each fibre structure have been calculated for a large range of pitches.

The relative hole size is varied between 0.6 and 0.9 in steps of 0.1. The refractive index of the up-doped region (n_c) is changed between 1.46 and 1.49 with steps of 0.01. The RDS-matching pitch has been calculated with an accuracy of 0.01 μm.

First, the individual effects of the parameters d/Λ, n_c and Λ on the dispersion curve have been investigated. Dispersion curves of fibres where two of the parameters have been kept constant and the third one was varied are compared in Figure 5.5. These fibres are not RDS matched. The presented results are obtained with a super cell size of 8. In Figure 5.5 (top), dispersion curves of fibres for different relative hole sizes are shown (pitch and doping level are the same). In Figure 5.5 (middle), the effect of scaling the structure is shown: the pitch is varied and the d/Λ and n_c parameters are kept constant. Figure 5.5 (bottom) shows the effect of doping, thus n_c is changed while d/Λ and Λ are kept unchanged. As one can see, the minimum dispersion point is shifting towards longer wavelengths with increasing d/Λ and Λ or n_c. Furthermore, the absolute value of the minimum point is increasing with increasing d/Λ, decreasing Λ or increasing n_c. This can be attributed to the smaller core area and tighter mode confinement as a result of the increasing d/Λ, decreasing Λ or increasing n_c. The dispersion slope of the fibre can also be set by adjusting these three parameters. Focusing on the dispersion curve between the maximum and minimum points of the curves, the dispersion slope is increasing with

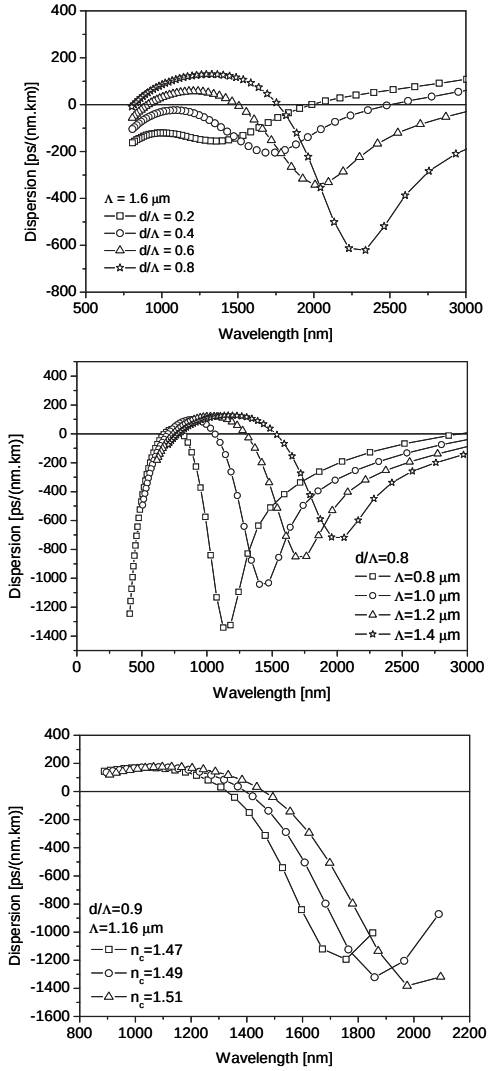

Figure 5.5: Dispersion versus relative hole size (top), the core doping level and the pitch being constant. Dispersion versus pitch (middle), the relative hole size and the core doping level being constant. Dispersion variation with core doping level (bottom), the pitch and relative hole size being constant. Super cell size is 8.

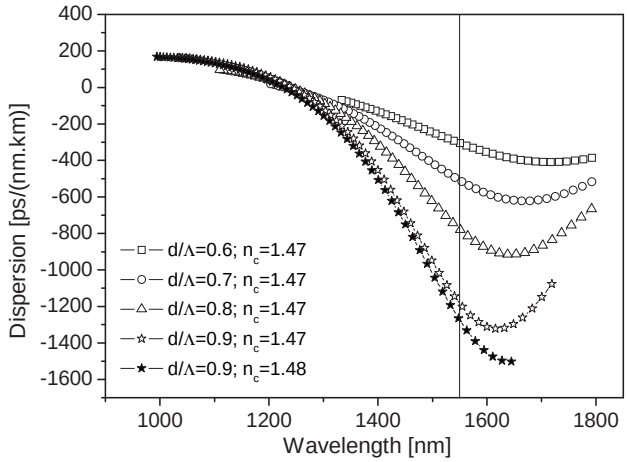

Figure 5.6: Dispersion as a function of wavelength for SSMF-RDS matched DC-PCF designs with n_c=1.47 for relative hole sizes of 0.6, 0.7, 0.8, 0.9 and n_c=1.48 for relative hole size of 0.9.

increasing d/Λ or decreasing Λ and n_c. Scaling the structure (increasing Λ) has also the effect of shifting the dispersion curves with wavelength, thus by choosing Λ the operation wavelength can be determined. As one can see, all three parameters affect the dispersion coefficient and dispersion slope. Therefore, in order to obtain RDS matched fiber with the largest negative dispersion coefficient at 1550 nm, all three parameters have been simultaneously varied in a systematic manner.

In the following results, only the fibre design with pitch providing 0.0035 nm^{-1} RDS at 1550 nm is shown for each structure. However, it should be mentioned that by optimising the hole diameter and the pitch of the DC-PCF, dispersion slope matching to any other commercially available transmission fibre can be easily obtained. The super cell size of the presented simulation is 16 unit cells.

The dispersion curves of the designs with d/Λ=0.6, 0.7, 0.8, 0.9 for n_c=1.47 are shown in Figure 5.6 together with the design with d/Λ=0.9 and n_c=1.48. The pitches for which RDS matching occurs are listed in Table 5.1 for all investigated structures. The RDS matched dispersion curves crosses 1550 nm close to the edge of the wavelength region where linear wavelength dependence can be assumed. Nevertheless, for

Structure d/Λ	n_c	Λ [μm]	D_{1550} ps/(nm·km)	S_{1550} ps/(nm^2·km)	A_{eff} [μm^2]
0.6	1.46	1.55	-220	-0.77	7.0
	1.47	1.39	-304	-1.07	4.9
	1.48	1.30	-349	-1.25	3.7
	1.49	1.23	-392	-1.40	3.1
0.7	1.46	1.40	-358	-1.25	5.4
	1.47	1.27	-481	-1.72	3.9
	1.48	1.19	-561	-1.99	3.1
	1.49	1.13	-628	-2.17	2.7
0.8	1.46	1.28	-585	-1.89	4.5
	1.47	1.18	-734	-2.70	3.2
	1.48	1.11	-852	-3.02	2.6
	1.49	1.06	-932	-3.25	2.3
0.9	1.46	1.20	-875	-2.90	3.6
	1.47	1.11	-1110	-3.88	2.6
	1.48	1.06	-1199	-4.69	2.2
	1.49	1.06	-1353	-4.72	1.6

Table 5.1: Properties of all investigated doped core honeycomb dispersion compensating photonic crystal fibres. The structural parameters d/Λ, core doping level and pitch are given. The dispersion parameter, dispersion slope and effective area are calculated at 1550 nm.

all presented fibre designs, the linear dependence is valid in at least the 1500-1600 nm wavelength range. For the designs with d/Λ=0.6 and n_c=1.48, 1.49, the region where linear approximation is reasonable extends to even further in the 1400-1700 nm range. The dispersion of SSMF can be considered to have linear wavelength dependence in the 1500-1600 nm wavelength range [2]. Therefore, the wavelength range where complete dispersion compensation can be obtained using the RDS matching condition is only valid in the 1500-1600 nm wavelength range.

The dispersion coefficients at 1550 nm of all the investigated RDS matched fibre designs and the corresponding effective areas are stated in Table 5.1 and plotted in Figure 5.7 (top) and (bottom), respectively. The effective areas have been calculated using equation (18) of reference [36], substituting the pure-silica refractive index value of 1.444 for n_1. As

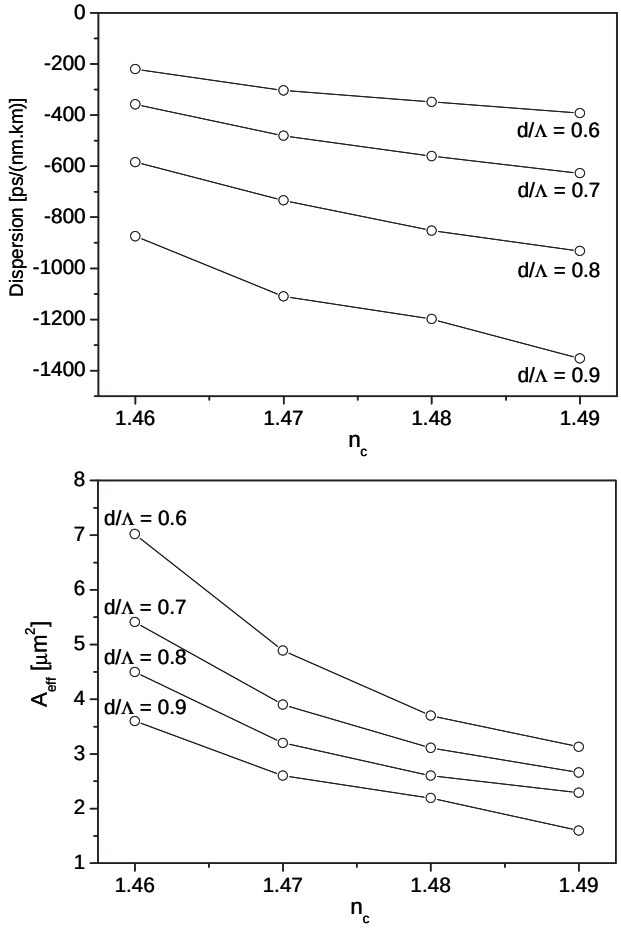

Figure 5.7: Dispersion coefficients at 1550 nm of all investigated RDS matched fibre designs (top) and the corresponding effective areas (bottom). The effective area is calculated based on reference [36].

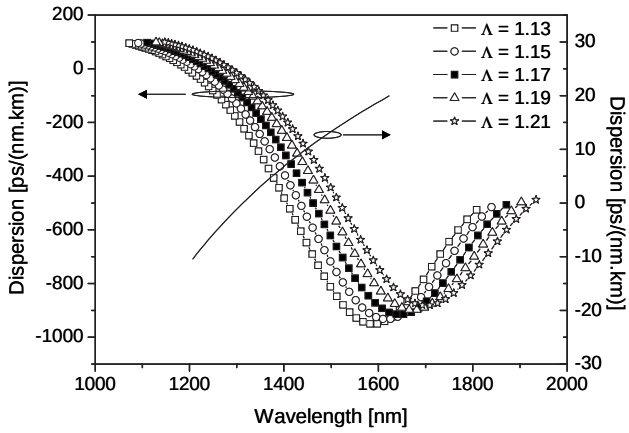

Figure 5.8: Dispersion as a function of wavelength for SSMF (solid line) and DC-PCF designs with d/Λ=0.9, n_c=1.47 and pitches of 1.13, 1.15, 1.17, 1.19 and 1.21. The fibre design with pitch of 1.17 is RDS matched.

discussed in reference [36], a more accurate treatment of the effects of Ge doping requires the introduction of several effective areas, complicating the comparison to other results in the literature.

The absolute value of dispersion coefficient at 1550 nm increases with increasing relative hole sizes and with increasing core doping levels. As it is expected, the effective area decreases simultaneously, which indicates tighter mode confinement.

In order to evaluate the performance of the proposed doped honeycomb DC-PCF design for broadband dispersion compensation, a transmission system consisting of 100 km of SSMF per span has been investigated. The RDS matched honeycomb design with d/Λ=0.9, doped region refractive index of 1.47 and Λ=1.17 μm has been used for dispersion compensation. The length of the DC-PCF has been chosen to obtain complete dispersion compensation at 1550 nm and is equal to 2.1 km. In order to account for the deviation of the fibre parameters due to production, the pitch of the RDS matched design has been varied to values of 1.13, 1.15, 1.19 and 1.21 μm, as well. The lengths needed to compensate 100 km of SSMF were 1.8, 1.9, 2.4 and 2.7 km, respectively. The dispersion curves of the considered DC-PCFs and the SSMF are plotted in Figure 5.8. The dispersion curve of the SSMF has been

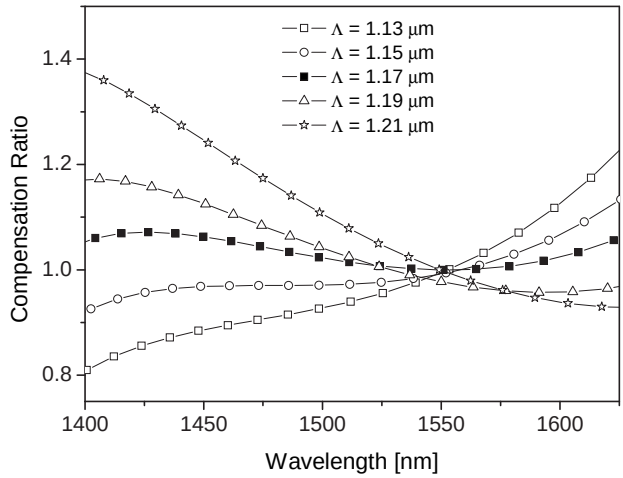

Figure 5.9: Compensation ration of a system with 100 km SSMF dispersion compensated by DC-PCF with d/Λ=0.9, n_c=1.47 and pitches of 1.13, 1.15, 1.17, 1.19 and 1.21. The lengths of the DC-PCFs were set to achieve complete dispersion compensation at 1550 nm.

calculated in the wavelength range of 1200 to 1625 nm using equation [2]:

$$D_{SSMF}(\lambda) \approx \frac{S_0}{4}\left[\lambda - \frac{\lambda_0^4}{\lambda^3}\right] \tag{5.7}$$

where the dispersion slope at the zero dispersion wavelength (S_0) and the zero dispersion wavelength (λ_0) are 0.086 ps/(nm^2·km) and 1313 nm, respectively. The compensation ratio of the system using all five DC-PCFs has been calculated and plotted in the 1400-1625 nm wavelength range in Figure 5.9. Using the RDS matched DC-PCF design (Λ=1.17 μm), the CR is nearly constant over the investigated wavelength range with less than 10 % deviation. It is also evident from the figure that structural variations result in larger fluctuations of the CR over a broader wavelength range. Nevertheless, assuming that 10 % variation of the CR from the complete dispersion compensation (CR=1) is tolerable in the system, the usable wavelength ranges for the DC-PCF with Λ values of 1.13, 1.15, 1.19, 1.17 and 1.21 μm are 1460-1590, 1400-1610, 1400-1625, 1460-1625 and 1500-1625 nm, respectively.

5.3.4 Comparison with existing DC-PCF designs

In this section, the dispersion and effective area of the doped core honeycomb DC-PCF will be compared to the simple triangular cladding structure and dual-core DC-PCF designs. The advantages and drawbacks of the DC-PCF designs will be outlined.

The effective area and dispersion of the reported RDS matched triangular cladding structured DC-PCF are $\sim$1 μm^2 and -590 ps/(nm·km) at 1550 nm, respectively [21]. A honeycomb fibre with comparable dispersion parameter of -585 ps/(nm·km) at 1550 nm (d/Λ=0.8 and n_c=1.46) has an effective area of 4.5 μm^2. A nearly RDS matched dual-core DC-PCF design has been reported with an effective area of $\sim$7 μm^2 and a dispersion parameter of -1211 ps/(nm·km) at 1550 nm [25]. This fibre can be compared to the honeycomb DC-PCF design with a dispersion coefficient of ~-1200 ps/(nm·km) at 1550 nm (d/Λ=0.9 and n_c=1.48) which has an effective area of 2.2 μm^2. Furthermore, it is interesting to note that conventional W-refractive index profile DCFs have effective areas of around 15 to 18 μm^2 [6].

For comparable dispersion parameters, the effective area of the doped honeycomb structure DC-PCF is roughly four times larger than that of the triangular cladding structure DC-PCF. However, the effective area of the proposed design is approximately three times smaller than that of a comparable dual-core design. Nevertheless, the simpler structure of the honeycomb structure DC-PCF makes fabrication easier and larger tolerances towards parameter fluctuations is expected compared to the dual-core design.

Due to the very small core areas of all three presented DC-PCF designs, their splicing to e.g. SSMF is difficult. As a result of large mode mismatch between the spliced fibres, large coupling losses are expected [37,38]. Nevertheless, the core of the honeycomb structured DC-PCF design is doped, thus it has a practical advantage over un-doped alternatives when it is spliced. If the holes partially collapse when it is spliced, light is still guided due to the doped core and additionally, the mode area will gradually increase, thus this tapering will reduce splicing losses.

Another drawback originating from the very small core area is that undesirable nonlinear effects are enhanced. Additionally, the heavy Ge doping of the core of the honeycomb design could raise the material

nonlinearity by as much as a factor of 2 [39]. However, due to the very high dispersion of the microstructured DCFs, lengths in the order of a few kilometres are necessary to compensate for the dispersion of 100 km SSMF. Therefore, it is expected that the considerably shorter lengths could mitigate the higher nonlinearities.

To the best of my knowledge, no investigations on the losses of DC-PCFs have been published until know, neither has the loss of the fabricated fibre been reported. Nevertheless, the loss of small core fibres is relatively high (∼9 dB/km at present), as it has been described in Chapter 2.

Furthermore, as a result of the small core and strong mode confinement, slight fluctuations of the structural parameters will shift the dispersion curve and change the relative dispersion slope. However, the fabrication tolerances of the fibre remains to be investigated. Another issue which has to be considered for small core DC-PCFs is their usually high unintentional birefringence, as it has been discussed for small core fibres in Chapter 2.

5.4 Summary

In this chapter, photonic crystal fibres have been considered for dispersion compensation. Large negative dispersion coefficients can be obtained for fibre designs where the effective index of the guided mode changes rapidly with wavelength. Therefore fibres with large refractive index differences between core and cladding may offer the possibility of large dispersion coefficients. Due to the large refractive index difference between air and silica, PCFs are potential applicants as dispersion compensating fibres.

An overview of the current status and different proposed dispersion compensating photonic crystal fibre designs were presented.

A novel dispersion compensating microstructured fibre design was proposed. The dispersion properties of this design were discussed in detail. The fibre has a honeycomb cladding structure with an up-doped core region whose diameter equals the centre-to-centre hole spacing. The fibre is designed to match the relative dispersion slope of standard single mode fibres. A dispersion coefficient as large as -1353 ps/(nm·km) for an effective area of 1.6 μm^2 at 1550 nm is achievable with this simple

cladding design. The performance of the honeycomb DC-PCF has been evaluated in a system consisting of 100 km of standard single mode fibre. Variation of the compensation ratio was below 10 % over 225 nm.

The results obtained for the honeycomb DC-PCF design have been compared to the other reported microstructured DCF designs, the triangular cladding structure and the dual-core DC-PCFs. The comparison shows that the honeycomb design exhibits larger negative dispersion values and more than 3 times larger mode area than the triangular DC-PCF design for comparable values of the dispersion coefficient. On the other, hand for the dual-core DC-PCF, larger dispersion coefficients have been reported and the effective area of this design is roughly 3 times larger than that for comparable honeycomb DC-PCF. A drawback of the proposed design is that its doped core is a source of increased nonlinearity and expectedly higher loss due to scattering. Nevertheless, due to its doped core, the honeycomb design offers the advantage that the mode field expands though remains still guided when the cladding holes partially collapse during splicing. This tapering will reduce mode mismatch when the proposed doped core honeycomb dispersion compensating photonic crystal fibre is spliced.

Generally DC-PCFs are a very promising technology as they can possess significantly larger negative dispersion than conventional fibre designs. Therefore, only a few kilometres of DC-PCF are sufficient to compensate for the dispersion of the usual 80 to 100 km SSMF spans. Furthermore, they can be designed to be relative dispersion slope matched with any choice of transmission fibre [21]. Additionally, single-material PCF designs avoid the problem of stress between core and cladding. In spite of the very attractive dispersion profile of DC-PCFs, there are several issues which have to be addressed before they can appear as a marketable product. The large negative dispersion values are associated with very small effective areas, which set some practical limitations. Small cores make it difficult to splice them to e.g. SSMF. Furthermore, due to the significant mode mismatch, large coupling losses are expected. In small core fibres, undesirable nonlinear effects are also enhanced. However the significantly reduced lengths needed could compensate for the increased nonlinearity of these fibres. Moreover, these fibres are also expected to have large unintentional birefringence, although their polarisation properties have not been investigated yet. Finally, fabrication

tolerances of DC-PCFs need to be addressed in the future, as small variation in the structural parameters can shift the dispersion profile of the fibre away from slope matching.

Although DC-PCFs have been presented only recently, already state-of-the-art results show a promising trend. Nevertheless, considerable research effort has to be allocated if DC-PCFs are to compete directly with standard DCFs. Only after further investigations of the current limitations may it be envisaged a commercially available dispersion compensation module based on DC-PCF.

References to Chapter 5

[1] B. Zsigri, J. Lægsgaard, and A. Bjarklev. "A novel photonic crystal fibre design for dispersion compensation", *Journal of Optics A: Pure and Applied Optics*, vol. 6, no. 7, pp. 717–720, July 2004.

[2] "Corning SMF-28 product information PI 1344". http://www.corning.com/, 2004.

[3] D. J. DiGiovanni, S. K. Das, L. L. Blyler, W. White, R. K. Boncek, and S. E. Golowich. *Design of Optical Fibers for Communications Systems*, In I. Kaminow and T. Li, editors, *Optical Fiber Telecommunications IVB Components,* Chapter 2, Academic Press, March 2002. ISBN 0-12-395173-9.

[4] P. Bayvel and R. Killey. *Nonlinear Optical Effects in WDM Transmission*, In I. Kaminow and T. Li, editors, *Optical Fiber Telecommunications IVB Components,* Chapter 13, Academic Press, March 2002. ISBN 0-12-395173-9.

[5] J. Zyskind, R. Barry, G. Pendock, M. Cahill, and J. Ranka. *High-Capacity, Ultra-Long-Haul Networks*, In I. Kaminow and T. Li, editors, *Optical Fiber Telecommunications IVB Components,* Chapter 5, Academic Press, March 2002. ISBN 0-12-395173-9.

[6] L. Grüner-Nielsen, S. N. Knudsen, B. Edvold, T. Veng, D. Magnussen, C. C. Larsen, and H. Damsgaard. "Dispersion compensating fibers", *Optical Fiber Technology*, vol. 6, no. 2, pp. 164–180, April 2000.

[7] T. Tokle. *Optimised Dispersion Management and Modulation Formats for High Speed Optical Communication Systems.* Ph.D. thesis, Research Center COM, Technical University of Denmark, Kgs. Lyngby, Denmark, December 2004. ISBN 87-90974-60-3.

[8] A. H. Gnauck, L. D. Garrett, F. Forghieri, V. Gusmeroli, and D. Scarano. "8×20 Gb/s 315 km, 8×10 Gb/s 480 km WDM transmission over conventional fiber using multiple broad-band fiber gratings", *IEEE Photonics Technology Letters*, vol. 10, no. 10, pp. 1495–1497, October 1998.

[9] L. Dong, M. J. Cole, A. D. Ellis, R. I. Laming, and T. Widdowson. "40 Gbit/s 1.55 μm RZ transmission over 109 km of non-dispersion shifted fiber with long continuously chirped fiber gratings", *Electronics Letters*, vol. 33, no. 18, pp. 1563–1565, August 1997.

[10] G. Lenz and C. K. Madsen. "General optical all-pass filter structures for dispersion control in WDM systems", *Journal of Lightwave Technology*, vol. 17, no. 7, pp. 1248–1254, July 1999.

[11] C. K. Madsen, J. A. Walker, J. E. Ford, K. W. Goossen, T. N. Nielsen, and G. Lenz. "A tunable dispersion compensating MEMS all-pass filter", *IEEE Photonics Technology Letters*, vol. 12, no. 6, pp. 651–653, June 2000.

[12] S. Watanabe, T. Chikama, G. Ishikawa, T. Terahara, and H. Kuwahara. "Compensation of pulse shape distortion due to chromatic dispersion and Kerr effect by optical phase conjugation", *IEEE Photonics Technology Letters*, vol. 5, no. 10, pp. 1241–1243, October 1993.

[13] S. Watanabe, S. Kaneko, and T. Chikama. "Long-haul fiber transmission using optical phase conjugation", *Optical Fiber Technology*, vol. 2, no. 2, pp. 169–178, April 1996.

[14] F. Buchali, H. Bülow, W. Baumert, R. Ballentin, and T. Wehren. "Reduction of the chromatic dispersion penalty at 10 Gbit/s by integrated electronic equalisers", in *Technical Digest Optical Fiber Communication Conference, OFC'00,* Baltimore, Maryland, U.S.A., pp. 268–270, March 2000, paper ThS1.

[15] S. Woodward, S.-Y. Huang, M. Feuer, and M. Boroditsky. "Demonstration of an electronic dispersion compensator in a 100 km 10 Gb/s ring network", *IEEE Photonics Technology Letters*, vol. 15, no. 6, pp. 867–869, June 2003.

[16] C. Lin, H. Kogelnik, and L. G. Cohen. "Optical-pulse equalization of low-dispersion transmission in single-mode fibers in the 1.3-1.7 μm spectral region", *Optics Letters*, vol. 5, no. 11, pp. 476–478, November 1980.

[17] C. Peucheret, N. Hanik, R. Freund, L. Molle, and P. Jeppesen. "Optimization of pre- and post-dispersion compensation schemes for 10-Gbit/s NRZ links using standard and dispersion compensating fibers", *IEEE Photonics Technology Letters*, vol. 12, no. 8, pp. 992–994, August 2000.

[18] W. Belardi, J. H. Lee, K. Furusawa, Z. Yusoff, P. Petropoulos, M. Ibsen, T. M. Monro, and D. J. Richardson. "A 10 Gbit/s tuneable wavelength converter based on four-wave mixing in highly nonlinear holey fibre", in *Proceedings European Conference on Optical Communication, ECOC'02,* Copenhagen, Denmark, September 2002, post-deadline paper PD1.2.

[19] A. Ortigosa-Blanch, A. Díez, M. Delgado-Pinar, J. L. Cruz, and M. V. Andrés. "Temperature independence of birefringence and group velocity dispersion in photonic crystal fibres", *Electronics Letters*, vol. 40, no. 21, pp. 1327–1328, October 2004.

[20] T. A. Birks, D. Mogilevtsev, J. C. Knight, and P. St. J. Russell. "Dispersion compensation using single-material fibers", *IEEE Photonics Technology Letters*, vol. 11, no. 6, pp. 674–676, June 1999.

[21] F. Poli, A. Cucinotta, M. Fuochi, S. Selleri, and L. Vincetti. "Characterization of microstructured optical fibers for wideband dispersion compensation", *Journal of the Optical Society of America A*, vol. 20, no. 10, pp. 1958–1962, October 2003.

[22] L. P. Shen, W.-P. Huang, G. X. Chen, and S. S. Jian. "Design and optimization of photonic crystal fibers for broad-band dispersion

compensation", *IEEE Photonics Technology Letters*, vol. 15, no. 4, pp. 540–542, April 2003.

[23] K. Thyagarajan, R. K. Varshney, P. Palai, A. K. Ghatak, and I. C. Goyal. "A novel design of a dispersion compensating fiber", *IEEE Photonics Technology Letters*, vol. 8, no. 11, pp. 1510–1512, November 1996.

[24] J.-L. Auguste, R. Jindal, J.-M. Blondy, M. Clapeau, J. Marcou, B. Dussardier, G. Monnom, D. B. Ostrowsky, B. P. Pal, and K. Thyagarajan. "−1800 ps/(nm.km) chromatic dispersion at 1.55 μm in dual concentric core fibre", *Electronics Letters*, vol. 36, no. 20, pp. 1689–1691, September 2000.

[25] B. J. Mangan, F. Couny, L. Farr, A. Langford, P. J. Roberts, D. P. Williams, M. Banham, M. W. Mason, D. F. Murphy, E. A. M. Brown, H. Sabert, T. A. Birks, J. C. Knight, and P. St. J. Russell. "Slope-matched dispersion-compensating photonic crystal fibre", in *Technical Digest Conference on Lasers and Electro-Optics, CLEO'04,* San Francisco, California, U.S.A., May 2004, post-deadline paper CPDD3.

[26] F. Gérôme, J.-L. Auguste, and J.-M. Blondy. "Design of dispersion-compensating fibers based on a dual-concentric-core photonic crystal fiber", *Optics Letters*, vol. 29, no. 23, pp. 2725–2727, December 2004.

[27] F. Gerome, J.-L. Auguste, and J.-M. Blondy. "Very high negative chromatic dispersion in dual concentric core photonic crystal fiber", in *Technical Digest Optical Fiber Communication Conference, OFC'04,* Los Angeles, California, U.S.A., vol. 2, pp. 575–577, February 2004, paper WA2.

[28] Y. Ni, L. Zhang, L. An, J. Peng, and C. Fan. "Dual-core photonic crystal fiber for dispersion compensation", *IEEE Photonics Technology Letters*, vol. 16, no. 6, pp. 1516–1518, June 2004.

[29] S. K. Varshney, K. Saitoh, and M. Koshiba. "A novel design for dispersion compensating photonic crystal fiber Raman amplifier",

IEEE Photonics Technology Letters, vol. 17, no. 10, pp. 2062–2064, October 2005.

[30] A. Huttunen and P. Törmä. "Optimization of dual-core and microstructure fiber geometries for dispersion compensation and large mode area", *Optics Express*, vol. 13, no. 2, pp. 627–635, January 2005.

[31] S. G. Johnson and J. D. Joannopoulos. "Block-iterative frequency-domain methods for Maxwell's equations in a planewave basis", *Optics Express*, vol. 8, no. 3, pp. 173–190, January 2001.

[32] J. C. Knight, T. A. Birks, P. St. J. Russell, and D. M. Atkin. "All-silica single-mode optical fiber with photonic crystal cladding", *Optics Letters*, vol. 21, no. 19, pp. 1547–1549, October 1996.

[33] S. E. B. Libori. *Photonic Crystal Fibers - From Theory to Practice.* Ph.D. thesis, Research Center COM, Technical University of Denmark, Kgs. Lyngby, Denmark, February 2002. ISBN 87-90974-29-8.

[34] J. Lægsgaard, A. Bjarklev, and S. E. B. Libori. "Chromatic dispersion in photonic crystal fibers: fast and accurate scheme for calculation", *Journal of the Optical Society of America A*, vol. 20, no. 3, pp. 443–448, March 2003.

[35] K. Okamoto. *Fundamentals of Optical Waveguides.* Academic Press, 2000. ISBN 0-12-525095-9.

[36] J. Lægsgaard, N. A. Mortensen, and A. Bjarklev. "Mode areas and field-energy distribution in honeycomb photonic bandgap fibers", *Journal of the Optical Society of America A*, vol. 20, no. 10, pp. 2037–2045, October 2003.

[37] J. Lægsgaard and A. Bjarklev. "Reduction of coupling loss to photonic crystal fibers by controlled hole collapse: a numerical study", *Optics Communications*, vol. 237, no. 4-6, pp. 431–435, July 2004.

[38] K. G. Hougaard, A. Bjarklev, E. Knudsen, S. B. Libori, and J. Riishede. "Coupling to photonic crystal fibers", in *Technical Digest Optical Fiber Communication Conference, OFC'02,* Anaheim, California, U.S.A., pp. 627–628, March 2002, paper ThGG11.

[39] T. Kato, Y. Suetsugu, and M. Nishimura. "Estimation of nonlinear refractive index in various silica-based glasses for optical fibers", *Optics Letters*, vol. 20, no. 22, pp. 2279–2281, November 1995.

Chapter 6

Photonic bandgap fibres

In this chapter, the potential of air-guiding photonic bandgap fibres (AG-PBGFs) for optical transmission system applications is investigated. The motivation for considering AG-PBGFs for optical communication is discussed, followed by the brief description of the basic properties of photonic bandgap fibres (PBGFs), which are of interest for transmission systems. Properties, such as design parameters, loss, dispersion and polarisation effects are addressed. Then, demonstrations of AG-PBGFs in telecommunication applications are presented. In Section 6.3.2, AG-PBGFs are considered as transmission fibres. Transmission of 10 Gbit/s signals over 150 and 400 m AG-PBGFs is presented and the deteriorating effect of the unusual polarisation properties of this fibre type is discussed. In Section 6.3.3, the demodulation of differential phase shift keying (DPSK) signals at different data rates using only 2.4 m of AG-PBGFs is demonstrated. In this experiment, the large birefringence of AG-PBGFs is exploited to realise a one bit delay polarisation interferometer. In Section 6.4 the chapter is summarised.

6.1 Introduction

PBGFs are a fundamentally new fibre type. Contrary to conventional fibres and even index guiding photonic crystal fibres (PCFs) whose guiding mechanism relies on total internal reflection (TIR), PBGFs guide light by the photonic bandgap (PBG) effect. PBG guidance results in radically new optical properties, which are considerably different from

those exhibited either by conventional fibres or by index guiding PCFs, and are very attractive for optical communication systems.

The possibility of guiding light in air is one of the most interesting unique features of PCF technology. In AG-PBGFs over 99% of the light field may be located in air [1]. Consequently, AG-PBGFs have attracted significant attention as they hold the promise of being the ultimate low loss transmission medium [2, 3] and they have the potential for negligible nonlinearity [4]. Furthermore, they are very bending insensitive [5]. Another consequence of guiding light in air, is that the material damage threshold associated with solid core fibres is eliminated, which is advantageous for high power applications [6]. An interesting feature of AG-PBGFs is that the position of the bandgaps, the wavelength region where light guidance occurs, is not bounded to the operational windows defined by the silica base material [5, 7, 8]. Therefore, this fibre opens up the possibility of using new transmission windows. On the other hand, these photonic bandgaps have limited bandwidth which may set limitations on the wavelength allocation of a wavelength division multiplexing (WDM) system.

In spite of the novelty of AG-PBGFs and the numerous appealing properties, AG-PBGFs are not as widespread and intensively investigated for telecommunication applications as index guiding PCFs. For AG-PBGFs, very large air filling fractions are required. Therefore the requirements on the fabrication tolerances are very strict. Due to the more relaxed fabrication tolerances of index guiding PCFs, their realisation has been achieved earlier (1996 [9]) than fibres guiding light by the PBG effect (1998 [10]). Furthermore, due to the analogy between conventional fibres and index guiding PCFs, many of the results (e.g dispersion, polarisation, splicing), found for conventional fibres can be applied with slight modification to index guiding PCFs [11]. Contrarily, it is not obvious to use these results in the case of AG-PBGFs. Moreover, new fundamental mechanisms (e.g. loss due to coupling to surface modes), not found in conventional fibres, can also appear in these fibres. Therefore, the research and development of PBGFs is slower than that of index guiding PCFs.

The initially large losses of AG-PBGFs (1 dB/m [12]) hindered their use for telecommunication applications. However the loss has been reduced significantly within the past five years (see figure 1.1) and getting

closer to the awaited "ultra low" loss. However, currently the loss of single mode AG-PBGFs is still considerably higher than that of index guiding PCFs and only couple of hundred metres are available [5, 13]. Nevertheless today, the loss of ∼13 dB/km for effectively single mode AG-PBGFs at 1550 nm [13] makes their investigations in different system applications possible.

6.2 Properties of photonic bandgap fibres

This section will briefly introduce the design parameters and optical properties like loss, dispersion and polarisation effects of AG-PBGFs. In this section, only some general guidelines that are characteristic for PBGFs are given. Parameter values are stated for a certain design to give an estimate of the order of magnitudes. However, most of the obtainable parameters vary on a large scale and are strongly dependent on the specific fibre design.

6.2.1 Design parameters

Light guidance by the PBG effect was first realised in low index core (LIC) fibres. The first demonstrations were performed by using honeycomb structure fibres (1998 [10,14]), and also the Kagomé structure was suggested [15]. These structures have the advantage that small relative air hole sizes are sufficient to achieve the PBG effect [16]. However, they guide light in the solid material surrounding the core defect, thereby exhibit ring shaped mode profiles. Therefore, honeycomb and Kagomé structured fibres are only used today if special dispersion or polarisation properties are needed [17, 18].

Today, most of the PBGFs are fabricated with a triangular cladding structure. Triangular cladding structures require large relative air hole sizes to exhibit PBG guidance. For fibres optimised for 1550 nm operation, pitch values of ∼2-5 μm and d/Λ values of ∼0.75-0.95 are typical [5,7,19–21]. The core of AG-PBGFs is air and is formed by omitting some of the central cells from the periodic structure. Typically, 7 or 19 cells are removed. These fibres are often referred as 7 or 19-cell PBGFs, respectively. For telecommunication applications, where single mode operation is important, the 7-cell design is preferred [22, 23] as the 19-cell

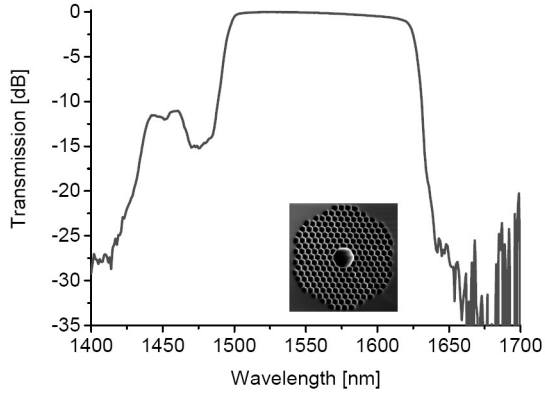

Figure 6.1: Transmission spectrum measured through a 2 m long air-guiding photonic bandgap fibre sample shown in the inset. The figure is kindly provided by T. P. Hansen [24, 29].

design supports higher order modes [5, 24, 25]. However, even the 7-cell design tends to support multiple modes. The fundamental mode can be well approximated by Gaussian distribution [8, 26, 27]. The cladding usually consists of a large number of air hole rings in order to reduce leakage loss [19]. Fibres are often produced with 7, up to 10 or even more air hole rings [1, 24, 28].

6.2.2 Loss

The transmission spectrum of a triangular cladding structure AG-PBGF presented in reference [24, 29] is shown in Figure 6.1. It is interesting to note that the attenuation spectrum of AG-PBGFs is not dominated by the physical mechanisms (such as fundamental scattering and absorption processes of silica) responsible for the loss in conventional silica fibres since the light is mainly guided in air.

The loss mechanisms found for index guiding PCFs are expected to contribute to the loss of AG-PBGFs as well. These loss mechanisms are Rayleigh scattering, scattering due to local imperfections and due to roughness at the air-silica interfaces, confinement or leakage loss, and bending loss. However, the magnitude and wavelength dependence of these loss contributions are different from those characteristics for index guiding PCFs. Additionally, AG-PBGFs have a significant loss

contribution, unique for this fibre type, that occurs due to coupling to surface modes. This loss mechanism has been shown to be dominating the 7-cell, effectively single mode design [24,25,30,31]. Furthermore, the cause of dominating loss in the currently lowest loss (1.2 dB/km [28]) 19-cell, multi-mode fibres is surface roughness due to frozen-in capillary waves [28].

In case of air guidance, Rayleigh scattering is expected to be significantly lower than the values measured for index guiding PCFs [8]. But so far, no measured values of Rayleigh scattering in AG-PBGFs have been reported. Similarly to index guiding PCFs, the surface roughness and structural imperfections such as variation in pitch or hole size, give rise to loss as well. The origin of confinement or leakage loss, is the same as for index guiding PCFs, i.e. the finite extent of the cladding. The leakage loss of AG-PBGFs has a minimum approximately at the centre of the bandgap and is increasing towards the band edges [19]. It has been shown that with increasing relative air hole sizes or with increasing number of air hole rings, the leakage loss can be significantly reduced. There is a minimum number of air hole rings for a given design necessary to reduce the leakage loss to an acceptable level, which is defined by the specific application. Depending on the relative air hole sizes, AG-PBGFs require at least 10 to 17 air hole rings to obtain leakage loss below 0.1 dB/km [19]. Macrobending losses of 7 cell AG-PBGF have been measured to bend radius down to 4 mm [5, 8]. No noticeable increase of the total fiber loss has been observed, except that the short wavelength band edge shifted towards longer wavelengths.

Currently, the dominating loss mechanism of 7-cell, effectively single mode, AG-PBGFs is due to mode coupling to surface modes [24, 25, 30, 31]. Surface modes are guided within the bandgap and are mainly located in the silica glass ring surrounding the core. They are very prone to scattering due to surface roughness and radiation mode coupling as they reside close to the air-silica boundary. As they extend into the cladding, they easily couple further to the continuum of the extended modes supported by the cladding, making surface modes very lossy. Even though more than 99% of the fundamental core mode is propagating in air, still some part is propagating in the silica ring surrounding the core. Therefore, the spatial overlap between the tail of the core mode and the lossy surface modes results in strong mode coupling. In

the wavelength region where surface modes occur with strong coupling between the core and the surface modes, they introduce high loss. It has been shown that surface modes are responsible for the high absorption peak within the bandgap of AG-PBGFs, which is visible in Figure 6.1 in the 1410-1480 nm wavelength region [25, 30, 31].

The effect of surface modes can be mitigated by increasing the core radius, thus reducing the overlap of core and surface modes. However this can result in multi-mode operation. At this point it should be also noted that the AG-PBGFs holding the current record losses of 1.2 dB/km [28] (not the earlier mentioned 13 dB/km of the few mode 7-cell fibre), have been obtained by increased core radius (19-cell AG-PBGF) [1, 28]. Thus, in these fibres, the effect of surface modes is mitigated. However they are multi-mode. Nonetheless, it has been shown that by carefully designing the core size, both surface modes can be significantly reduced and effectively single mode operation can be achieved [25, 30]. An other way to reduce the loss due to surface modes is to design the thickness of the silica ring in order to reduce the number of existing surface modes and to move their wavelength out of the bandgap [32].

It has been shown recently that the loss of AG-PBGFs is ultimately limited by scattering off the air-silica interfaces [28]. During fibre draw, surface capillary waves form on the inside of the capillaries and result in the roughness of the interface. This surface roughness due to frozen-in capillary waves cause light to be scattered out of the fibre. This mechanism is shown to be the limiting loss of the currently lowest loss (1.2 dB/km) 19-cell AG-PBGFs and predicted to set the fundamental limit for the loss of this fibre type. Nevertheless, in [28], several possibilities for the mitigation of surface capillary waves have been suggested. Furthermore they predict that, in spite of losses caused by surface roughness due to frozen-in capillary waves, the loss of AG-PBGFs can be reduced below the lowest loss possible for conventional fibres.

6.2.3 Dispersion

The bandgap guiding mechanism and periodic cladding structure also show their effect on the dispersion profile of AG-PBGFs. The dispersion profile of two 7-cell AG-PBGFs is plotted in Figure 6.2. The modeled

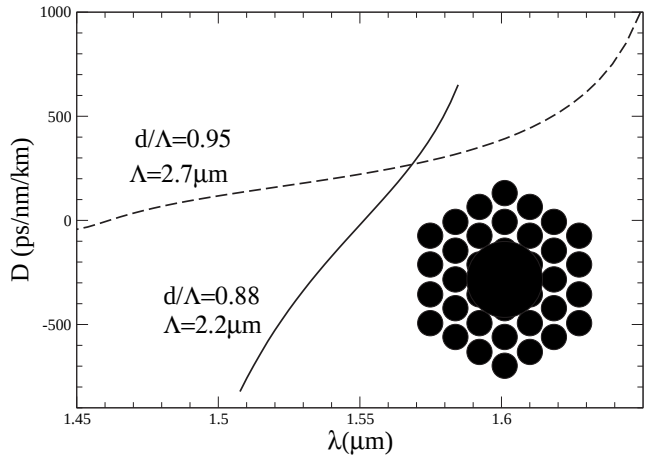

Figure 6.2: Dispersion as a function of wavelength for two 7-cell triangular structure air-guiding photonic bandgap fibres with d/Λ=0.88; Λ=2.2 μm (solid line) and d/Λ=0.95; Λ=2.7 μm (dashed line). Inset shows the schematic of the simulated fibre cross section. The figure is courtesy of J. Lægsgaard.

fibre cross section is shown for one of the fibres as an inset in Figure 6.2. The fibres have triangular cladding structure, and d/Λ=0.88 or 0.95 with pitch values of 2.2 or 2.7 μm, respectively.

Generally, PBGFs exhibit large negative dispersion at the short wavelength band edge and large positive dispersion at the long wavelength band edge and there is an inflection point in between. As an example, dispersion values of ∼1200 ps/(nm·km) has been measured at the long wavelength band edge [21]. The dispersion curve crosses the zero dispersion within the low-loss window [8, 19]. Typically, the dispersion curve is asymmetric with respect to the inflection point thus the dispersion slopes at the two band edges are different although both can be very large. The dispersion slope of the AG-PBGF reported in reference [21] has been measured to be ∼29 ps/(nm^2·km) at the long wavelength band edge. The fibre can be designed to possess significantly lower dispersion slope around the inflection point. Increased relative air hole sizes result in decreased dispersion slopes around the inflection point, as it is also visible in Figure 6.2 [19]. Fibres with low dispersion slope around the inflection point are attractive as transmission fibres in high speed transmission systems. The large negative dispersions at the short wavelength

band edge could be exploited for dispersion compensation, although the positive dispersion slope prevents them to be suitable for broadband dispersion compensation.

6.2.4 Polarisation

Until now, most of the research effort have been focusing on the understanding of the loss mechanisms in AG-PBGFs and very little has been done on the exploration of the polarisation properties. However, after AG-PBGF started to be used for different applications among others for transmission purposes [4], a better understanding of the polarisation properties of this new fibre type was needed. The polarisation properties of PBGFs are very unusual and at present not yet fully understood [8, 26, 27, 33].

AG-PBGF investigated until now, have large unintentional birefringence. Beat lengthes of 4 to 13 mm [8, 22, 26, 27] have been reported. Contrary to other highly birefringent fibres, AG-PBGFs are simultaneously subject to strong polarisation mode coupling. Furthermore, the polarisation mode dispersion (PMD) is strongly wavelength dependent with well defined minimum and maximum points that can not be related to any other features of the fibre, e.g. the structures of the loss spectrum. To obtain polarisation maintaining AG-PBGFs it is not sufficient to rely on the arbitrary asymmetries of the fibre structure resulting from fabrication. However, with intentionally introduced asymmetry, very high birefringence values (0.025 at 1550 nm) have been already published for a 4-cell core fibre [34, 35].

6.3 Demonstrations of telecommunication applications of photonic bandgap fibres

The potential of PBGFs has been already demonstrated for several different applications, such as high power delivery [6], chirped pulse amplification [36–38] and soliton pulse propagation [39, 40]. Until now, however, only two telecommunication applications of AG-PBGFs have been reported [22, 23]. In this section, these telecommunication applications are presented. First, the fibre characteristics of the AG-PBGFs used in the experiments are described. The experimental confirmation

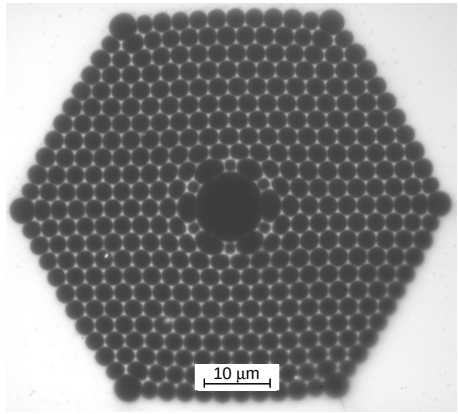

Figure 6.3: Microscope picture of the air-guiding photonic bandgap fibre used in the experiments. Kindly provided by Crystal Fibre A/S.

of the high birefringence and the negligible nonlinearity of the fibres is presented. In Section 6.3.2, a transmission experiment over a 150 m and a 400 m long AG-PBGFs is presented and the limiting effect of fibre polarisation is discussed [4, 22]. In Section 6.3.3, the high birefringence of the investigated AG-PBGF is exploited and a one bit delay polarisation interferometer, used as DPSK signal demodulator is demonstrated [23].

6.3.1 Fibre characteristics

In the experiments discussed below, 150 and 2.4 m long AG-PBGFs, specially designed for single mode operation around 1550 nm have been used. Both fibre samples are the same type. The fibres were kindly provided by Crystal Fibre A/S.

The cross-section of the air-guiding fibre is shown in Figure 6.3. The fibres have a triangular cladding structure with hole-to-hole spacing of 3 μm. The core is formed by omitting 7 of the central cells thus the fibres support a single mode in the core at 1550 nm. The core diameter, measured from corner to corner, is determined from the microscope pictures to be 10 μm. The cladding diameter of the fibres is 185 μm and they has a coated diameter of 240 μm, thus can be easily spliced to standard single mode fibre (SSMF) pigtails. The 150 m long fibre was spliced to 1 m long SSMF pigtails on both ends. The 2.4 m fibre was

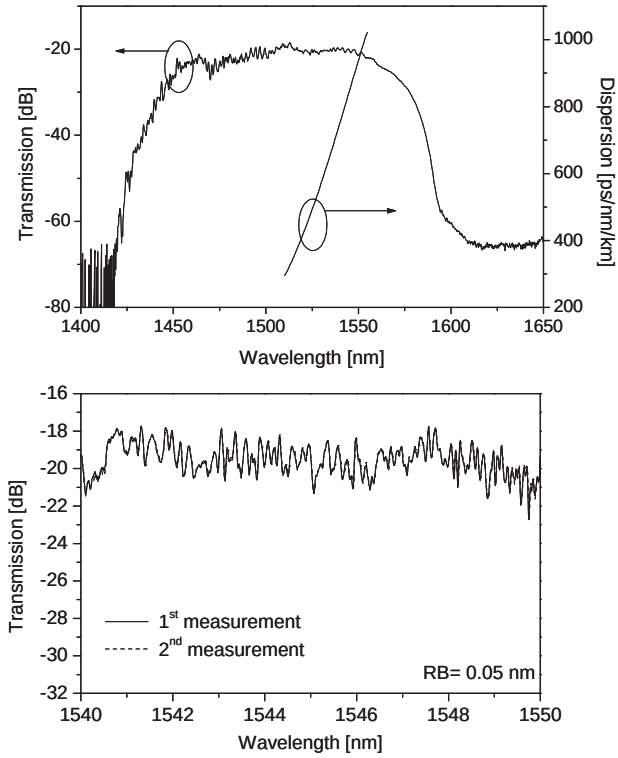

Figure 6.4: Transmission spectrum and dispersion as function of the wavelength measured for the 150 m air-guiding photonic bandgap fibre sample (top). Close up of the transmission spectrum in the 1540 to 1550 nm wavelength region (bottom). The dispersion curve was provided by Crystal Fibre A/S.

butt coupled in the experiments.

The measured transmission spectrum and the dispersion of the 150 m fibre sample is shown in Figure 6.4-top. The 150 m fibre has a bandgap extending from below 1450 nm up to beyond 1575 nm. Thus this $\sim$125 nm covers the entire third telecommunication window. Strong fluctuation is observable on the transmission spectrum in the low loss region. A close-up of the 1540 to 1550 nm wavelength region of the transmission spectrum is shown in Figure 6.4-bottom for two repeated measurements. The curves are indistinguishable, showing the same structure, thus confirm that the ripples are features of the bandgap. The total insertion

loss of the 150 m sample is 20 dB at 1545 nm, including the splices to SSMF. The measured dispersion curve shows a high anomalous value of 845 ps/(nm·km) at 1545 nm.

The 3 dB bandwidth of the 2.4 m long AG-PBGF extends up to 1600 nm and at the short wavelength side is below the measured range (measured between 1565 and 1600 nm). The two fibre samples have the same structure and only their lengths are different. Therefore the difference in the bandwidth of their bandgaps is attributed to the increased structural variations in the longer fibre. Variations of the fibre parameters, d and Λ, cause the closing of the bandgap [41]. The insertion loss of the 2.4 m fibre is very small and is mostly originating from the butt coupling to SSMF pigtails.

The fibre beat length was determined by transmitting an isolated pulse at 1545 nm over the 150 m AG-PBGF sample. The time shift of the pulse was measured while the input polarisation was changed systematically. A differential group delay of 69 ps was obtained and from it, a beat length of 1.1 cm has been determined. This value is in good agreement with the measurements done on a similar fibre by Wegmüller et al. [26]. The birefringence of the fibre was calculated to be 1.4×10^{-4} at 1545 nm by using the simple equation $B = \lambda/L_B$ (B - birefringence; λ - signal wavelength; L_B - beat length) [42].

The nonlinear coefficient of the AG-PBGFs has been measured by the continuous wave-self phase modulation (CW-SPM) method [43]. The four-wave mixing (FWM) spectra generated in the SSMF pigtailed 150 m long fibre sample and in the pigtails alone are compared in Figure 6.5. The average input power in both cases is 22 dBm. The two spectra are nearly indistinguishable confirming that the nonlinearity originating from the AG-PBGF itself is negligible.

6.3.2 Photonic bandgap fibre as transmission fibre

Numerous interesting properties of AG-PBGFs, most of all the potentially very low loss, negligible nonlinearity and the possibility to open up new wavelength windows make them very attractive to be used as transmission fibres. However, at present, the loss of single mode AG-PBGFs is almost two orders of magnitude higher than the loss of conventional fibres. Furthermore, due to the very strict requirements on the structural

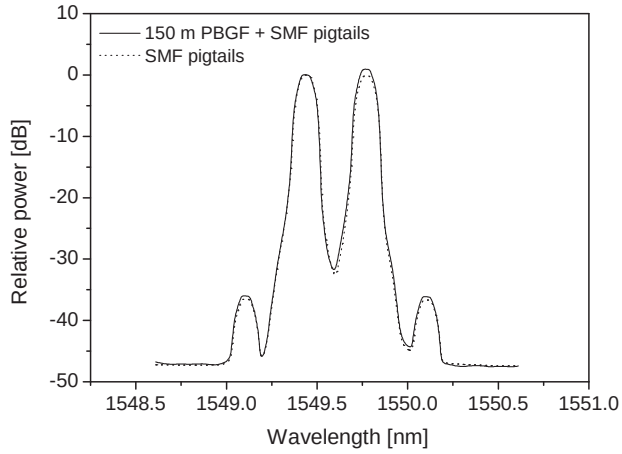

Figure 6.5: Normalised four-wave mixing spectrum recorded at the output of the SMF pigtailed 150 m air-guiding photonic bandgap fibre (solid line) and after the SMF pigtails only (dashed line). The total fibre input power is 22 dBm. Resolution bandwidth: 0.1 nm.

uniformity, only relatively short fibre pieces are available. The longest fibre length reported until now is 800 m [1]. Despite the high losses and short lengths, it is very interesting to investigate how the PBG guidance and the unique properties of PBGFs influence data transmission. Until now, to the author's knowledge, only one experimental demonstration on the potential of air-guiding fibers as transmission fibre has been published [4, 22].

In this section, this first and currently only data transmission over air-guiding photonic bandgap fibre is described. A 10 Gbit/s non return-to-zero (NRZ) signal at 1550 nm has been successfully transmitted over 150 m of single-mode AG-PBGF. Although error free transmission could be measured, potential problems for applications as transmission fibre have been identified.

Experimental setup

The experimental setup is shown in Figure 6.6. A continuous wave (CW) laser emitting at 1545 nm is modulated by an external chirp-free Mach-Zehnder (MZ) modulator generating a 10 Gbit/s NRZ modulated signal.

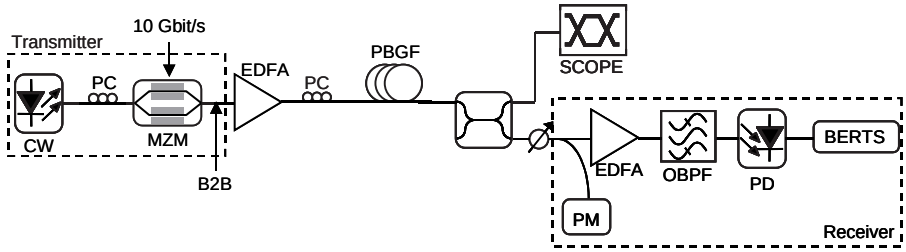

Figure 6.6: Experimental setup for the 10 Gbit/s photonic bandgap fibre transmission. PM - power meter.

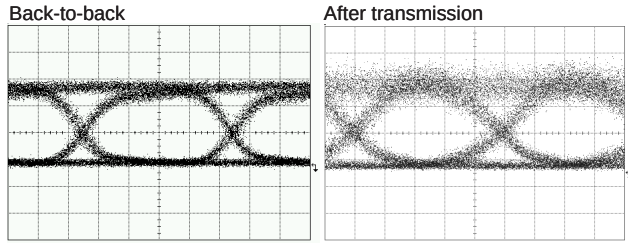

Figure 6.7: Eye diagrams in the back-to-back case and after transmission over 150 m photonic bandgap fibre. The PRBS length is 2^7-1 bits. (recorded in a 26.6 GHz bandwidth). Horizontal scale: 20 ps/div.

The modulating signal is a 2^7-1 bits long pseudo random bit sequence (PRBS). At the transmitter output, the signal had an extinction ratio of 14 dB. The signal was amplified up to an average power of 15 dBm before it was inserted into the transmission fibre. The transmission fibre was a 150 or 400 m long AG-PBGF. At the input of the fibre a polarisation controller (PC) was used to rotate the input state of polarisation of the signal. A pre-amplified receiver, consisting of an erbium doped fibre amplifier (EDFA), optical bandpass filter (OBPF) and a photodiode with a 3 dB bandwidth of 15 GHz, detected the signal.

Results

The eye diagrams recorded in the back-to-back case and after transmission over 150 m of AG-PBGF are shown in Figure 6.7. The eye diagram of the signal after transmission is open, however the one level is thick. The shape of the eye diagram changes with time and is strongly depen-

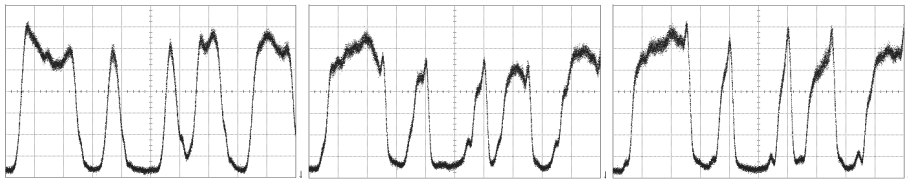

Figure 6.8: Eye pattern recorded after 150 m photonic bandgap fibre for three different launched input state of polarisation for the waveform of 01111001000101100111. Horizontal scale: 200 ps/div.

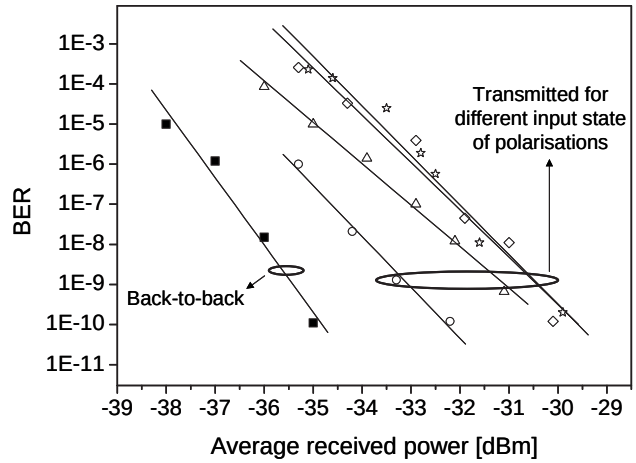

Figure 6.9: BER curves as a function of averaged received power in the back-to-back case and after transmission over 150 m photonic bandgap fibre. The BER curves measured after transmission correspond to several input state of polarisations.

dent on the state of polarisation of the light coupled into the fibre. In order to identify the source of distortion, the eye pattern for a waveform of 01111001000101100111 is recorded at the output of the fibre for different states of polarisation of the light at the fibre input. In Figure 6.8, the patterns for three different input states of polarisation are shown. The shape of the bit pattern is changing significantly with the input state of polarisation.

The bit error rate (BER) curves measured in the back-to-back case and at the output of the AG-PBGF for several different states of light polarisation at the fibre input are shown in Figure 6.9. A back-to-back

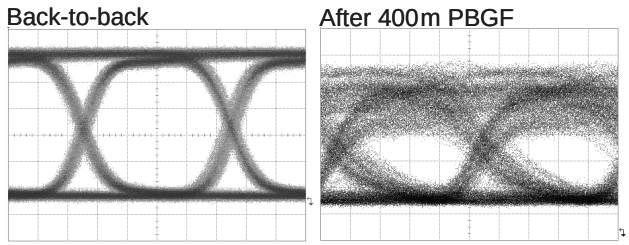

Figure 6.10: Eye diagrams in the back-to-back case and after transmission over 400 m of photonic bandgap fibre. The PRBS length is 2^7-1. (recorded in a 26.6 GHz bandwidth). Horizontal scale: 20 ps/div.

sensitivity of -35.4 dBm for a BER of 1.0×10^{-9} is obtained. Repeated measurements of the BER curve after transmission show strong fluctuation with time. Penalties in the range of 2-5 dB are measured. This fluctuation is attributed to polarisation effects due to environmental changes. Transmission over a 400 m AG-PBGF has also been attempted, but distortion due to polarisation effects prevented error-free detection of the signal after transmission. The eye diagrams recorded in the back-to-back and after transmission through 400 m AG-PBGF are shown in Figure 6.10. Severe distortion, splitting of the one level and the transition edges, is observable on the eye diagram recorded after transmission.

Currently, the high birefringence and simultaneous strong polarisation mode coupling of AG-PBGFs make them unsuitable for applications where long fibre lengths are needed. Therefore, it is essential that besides reducing the losses of air-guiding fibres the polarisation properties have to be significantly improved in order for AG-PBGFs to become marketable transmission fibres.

6.3.3 Photonic bandgap fibre based differential phase shift keying demodulator

In this section, phase-to-intensity conversion of DPSK signals in a one bit delay polarisation interferometer realised in an air-guiding fibre is presented. Exploiting the large birefringence values measured for AG-PBGFs, phase-to-intensity conversion is attainable in a very short AG-PBGF (only 2.4 m). Demodulation of 10 and 40 Gbit/s DPSK signals have been successfully performed using the short AG-PBGF one-bit de-

lay polarisation interferometer. The section starts with a brief introduction of DPSK signals and their demodulation. After the experimental setup, realising DPSK demodulation by means of a short AG-PBGF is presented. Finally, the results are discussed.

Differential phase shift keying

One of the promising modulation formats today is DPSK modulation. Its resilience towards transmission impairments and the ∼3 dB receiver sensitivity improvement of balanced detection compared to corresponding intensity modulated signals have been already exploited in several long-haul, large capacity systems [44–46]. DPSK signals carry the information encoded on the phase of the optical carrier. DPSK signals can not be directly detected, as photodiodes only detect the optical power and disregard the phase information. DPSK signals can be detected by coherent detection [42] or, alternatively, the phase information has to be converted to intensity modulation to allow for direct detection. Here, only the direct detection scheme is considered. Phase-to-intensity conversion can be realised by a one-bit delay MZ interferometer [44]. The interferometer compares the relative phase information of two consecutive bits. At the two outputs of the interferometer, intensity modulated signals corresponding to constructive and destructive interferences appear. Receiving the signals from the constructive and the destructive ports simultaneously, called balanced detection, may result in up to 3 dB improvement compared to detecting only one of the signals [44]. The NRZ-DPSK signal is converted to an amplitude modulated signal with return-to-zero (RZ) format whose pulse width is determined by the optical path difference between the two arms of the MZ interferometer [47]. The delay has to be smaller or equal to the bit duration. The smaller the relative delay, the smaller the duty cycle of the demodulated signal. One-bit delay MZ interferometer structures have also been proposed to be used at the transmitter to obtain RZ modulated signals of various duty cycles [47].

An equivalent MZ structure, exploiting the birefringence of a conventional polarisation maintaining fibre to induce the one bit delay between signals propagating along its two eigen-axes, has been recently realised [48].

Transmission of information over AG-PBGFs has been limited by

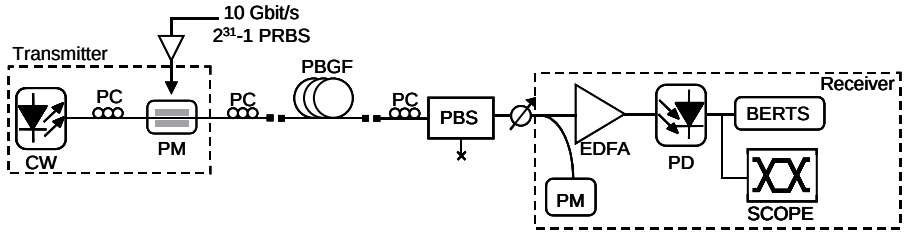

Figure 6.11: Experimental setup of the differential phase shift keying demodulation using air-guiding photonic bandgap fibre based polarisation delay interferometer.

the high unintentional birefringence of the fibre as it has been discussed in Section 6.3.2. Nonetheless this high birefringence can be exploited for realising short, compact devices relying on fibre birefringence. At short fibre lengths, the AG-PBGF act as polarisation maintaining fibre with very high birefringence. Birefringence values in the order of 10^{-3} have been reported for AG-PBGFs [26]. Typically, the birefringence of conventional polarisation maintaining fibres is approximately 2-5$\times 10^{-4}$, an order of magnitude lower than values measured for the investigated AG-PBGF. Therefore, the length of AG-PBGF necessary to realise the 25 ps delay needed to demodulate 40 Gbit/s DPSK signals is also an order of magnitude shorter than in case of using conventional polarisation maintaining fibres.

In the following sections a one bit delay polarisation MZ interferometer realised in a short AG-PBGF with high birefringence is described.

Experimental setup

The experimental setup is shown in Figure 6.11. A DPSK signal with constant intensity was generated by externally modulating a CW light from a tunable external cavity laser by a phase modulator (PM) inducing π phase shifts [44]. The phase modulator is capable of operation up to 40 Gbit/s. The wavelength of the CW source was varied during the measurements. The polarisation delay interferometer was realised in a 2.4 m long AG-PBGF (for details on the fibre see section 6.3.1). At the input of the AG-PBGF a PC was used to adjust the state of polarisation of the modulated light to couple it equally to the two eigenaxes of the fibre. The time delay between the two fields propagating in

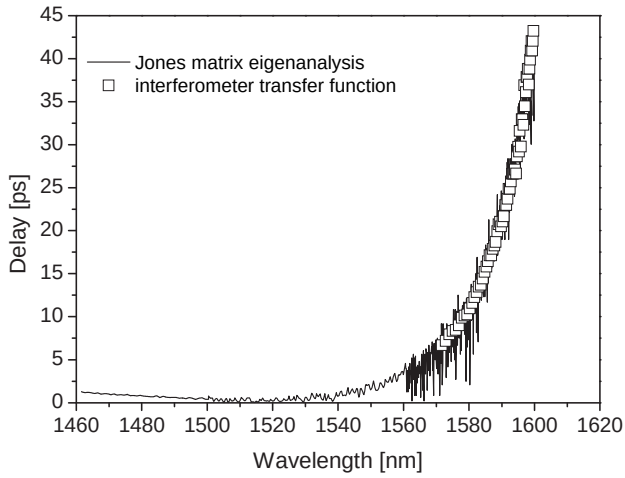

Figure 6.12: Delay between the two polarisation states of the 2.4 m long photonic bandgap fibre measured by the Jones matrix eigenanalysis (solid line)(measurement data provided by T. T. Alkeskjold) and calculated from the transfer function of the delay interferometer (squares) (measurement data provided by C. Peucheret and Y. Geng).

the two eigen-polarisations is induced by the birefringence of the fibre. After the fibre a polariser – aligned to 45° of the polarisation axes of the fibre – was used. The polariser caused the signals, propagating on the two orthogonal polarisation axes of the fibre, to interfere. In this experiment a polarisation beam splitter (PBS) was used as a polariser and a PC rotated the polarisation states of the signals to 45° of the PBS axes. At the two outputs of the polariser (PBS) the two complementary demodulated DPSK signals appear. One of the outputs is then input to a pre-amplified receiver consisting of an L-band EDFA, consisting of a C-band EDFA and 120 m of erbium-doped fibre [49] and a 50 GHz photodetector (PD).

Results

Figure 6.12 shows the wavelength dependence of the differential group delay of the 2.4 m AG-PBGF obtained by either using Jones matrix eigenanalysis [50, 51] or by calculating it from the periodicity of the measured transfer function of the delay interferometer. Measurements

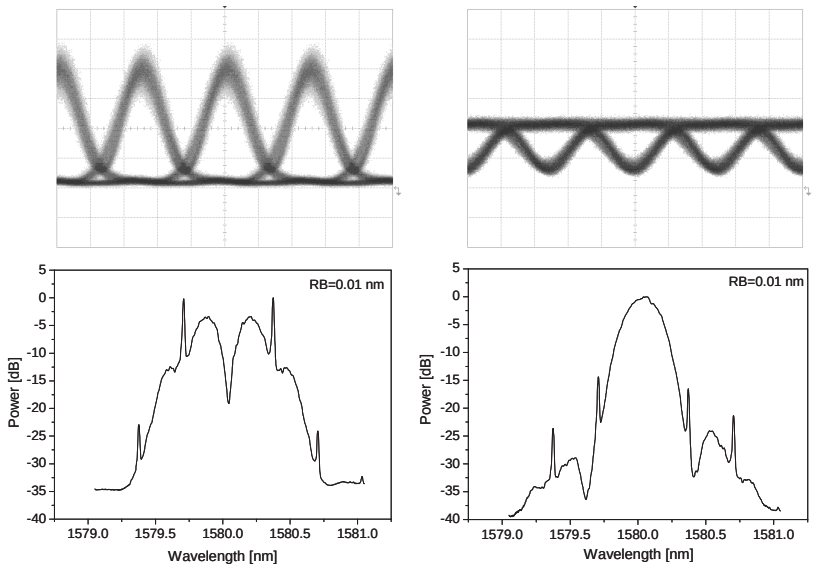

Figure 6.13: Demodulated differential phase shift keying eye diagrams (top) and spectra (bottom) of 39.8 Gbit/s signal at 1580 nm, corresponding to cases when one bit results from a relative phase difference of π (left) and 0 (right). Horizontal scale of the eye diagrams: 10 ps/div. Resolution bandwidth (RB)=0.01 nm.

obtained by the two methods are showing very good agreement. The delay is increasing rapidly with wavelength at the edge of the fibre bandgap. The delay of 25 ps, one bit duration of a 40 Gbit/s signal, is attained at a wavelength of 1592 nm. This delay corresponds to a birefringence of 3.1×10^{-3}.

The polarisation controller at the output of the AG-PBGF is rotated to obtain the demodulated signals corresponding to the constructive and destructive phase interferences. The detected eye diagrams and the spectra recorded at the output of the polarisation delay interferometer for the two cases are shown in Figure 6.13. The signal input to the AG-PBGF is a 39.8 Gbit/s DPSK modulated signal at 1580 nm. The left panel corresponds to the case when the relative phase difference of π results in a "1" bit, while the right panel shows the case when zero relative phase difference results in a "1" bit. The detected eye diagrams have the same waveform but inverted as a consequence of single ended detection. The spectra are as it is expected for the constructive and

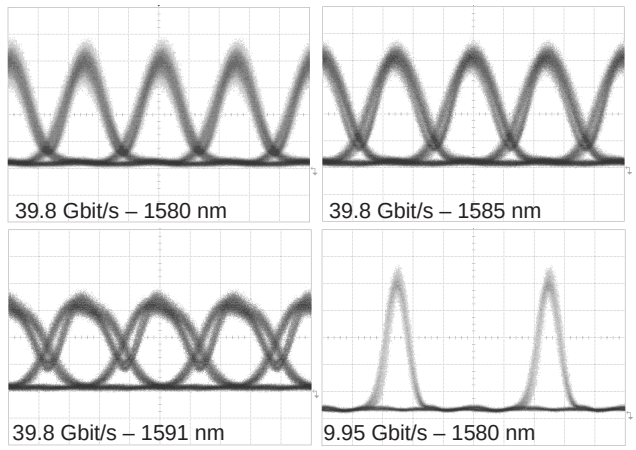

Figure 6.14: Eye diagrams recorded for 39.8 Gbit/s DPSK demodulated signals with wavelength of 1580, 1585 and 1591 nm, and 9.95 Gbit/s DPSK demodulated signal with wavelength of 1580 nm. Horizontal scale for the 39.8 Gbit/s signals: 10 ps/div and the vertical scale is the same in all three cases. Horizontal scale for the 9.95 Gbit/s signal: 20 ps/div and the vertical scale is different from the 39.8 Gbit/s cases.

destructive DPSK signals [44].

Furthermore, demodulation of 39.8 Gbit/s DPSK signals at wavelengths of 1580, 1585 and 1591 nm and a 9.95 Gbit/s DPSK signal at 1580 nm has been performed. The demodulated eye-diagrams are shown in Figure 6.14. The pulse width increases with increasing wavelength as a result of the larger delays obtained for longer wavelengths [47]. The pulse width of the demodulated 9.95 Gbit/s DPSK signal is very small as the delay of the interferometer is very small compared to the 100 ps bit duration.

BER curves measured for bit rates and wavelengths corresponding to the eye diagrams shown in Figure 6.14, presented in Figure 6.15. The receiver sensitivities (BER of 1.0×10^{-9}) measured for 39.8 Gbit/s operation at 1580, 1585 and 1591 nm were -23.3, -24.1 and -21.7 dBm, respectively. The sensitivity degradation observed for longer wavelengths can be explained by the broadened pulses due to longer delays (note that the average power into the photodiode is the same for all signals). The sensitivity improvement measured for the signal at 1580 nm is attributed to the local variations in the bandgap transmission and interferometer

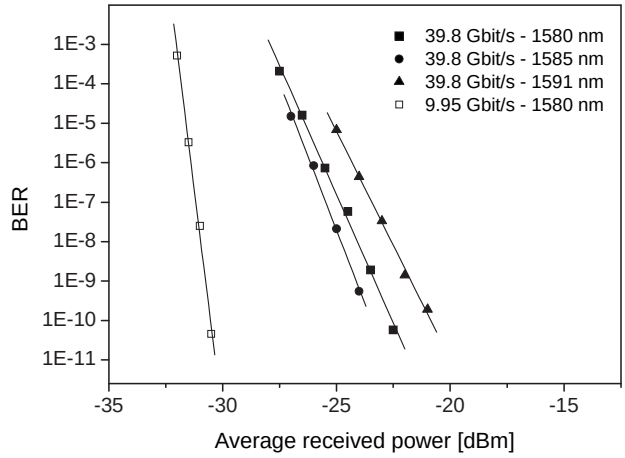

Figure 6.15: BER curves as a function of average received power for 39.8 Gbit/s DPSK demodulated signals with wavelengths of 1580, 1585 and 1591 nm and 9.95 Gbit/s DPSK demodulated signal with wavelength of 1580 nm.

extinction ratio. The sensitivity measured for the 9.95 Gbit/s signal at 1580 nm was −30.7 dBm. The improved sensitivity compared to the 39.8 Gbit/s operation is due to the reduced bit rate thus shorter pulse width. During the measurement the AG-PBGF based polarisation delay interferometer showed very stable operation. The short length of the device and the reported very high bending tolerance [5] of this fibre type allows the implementation of compact and stable polarisation delay interferometers.

6.4 Summary

This chapter has discussed the present role of air-guiding photonic bandgap fibres in telecommunication applications and their practical limitations. First, an overview of the unique properties of this fibre type has been presented, based on current literature. Properties such as structural parameters, loss, dispersion and polarisation were addressed. Photonic bandgap fibres guide light at wavelengths within bandgaps, defined by the cladding structure. These bandgaps have limited bandwidth but they may exist at wavelengths which are not practical for

solid core fibres. In air-guiding fibres, over 99 % of the light is guided in air, indicating the potential for ultra low loss and nonlinearity. These properties have made AG-PBGF very attractive for telecommunication applications. However, at present, the loss of effectively single mode air-guiding fibres is very high (13 dB/km) [13] and is limited mostly by a loss mechanism unique for this fibre type, caused by mode coupling to surface modes. By mitigating the effect of surface modes lower loss (1.2 dB/km [28]) AG-PBGFs have been demonstrated. The loss of this fibre is ultimately limited by the existence of surface capillary waves. However, this design supports multiple modes thereby is not suitable for transmission systems. The dispersion shows extreme high negative and positive values towards the short and long wavelength band edges respectively, and crosses zero within the bandgap. Current fibres have large unintentional birefringence and simultaneously exhibit strong polarisation mode coupling.

Two experimental demonstrations of AG-PBGFs in telecommunication applications have been described. The very low nonlinearity and large birefringence of the investigated air-guiding photonic bandgap fibre have been measured.

The first, and currently only, reported data transmission in AG-PBGF has been presented. A 10 Gbit/s NRZ modulated signal has been transmitted over 150 and 400 m AG-PBGFs. Error-free transmission has been measured after transmitting through 150 m of AG-PBGF, although the system performance was strongly dependent on the input state of polarisation into the fibre and fluctuated with time. The observed behaviour was attributed to polarisation effects in the fiber, caused by fiber birefringence due to changes in the environmental conditions. The eye diagram after transmission over 400 m air-guiding photonic bandgap fibre was open. However due to significant distortion caused by polarisation effects, error-free detection of the transmitted signal was not possible. These experiments demonstrate the potential of air-guiding photonic bandgap fibres as transmission media although they also reveal the current limitations of these fibres due to their unusual polarisation properties. In order to minimise those polarisation effects, the requirements on structural uniformity should be assessed. Therefore we conclude that at the present time, despite the very low nonlinearity and promisingly decreasing loss of AG-PBGFs, the severe

distortions due to polarisation prevents their use as transmission fibres.

The large birefringence of air-guiding photonic bandgap fibres has been exploited by realising a polarisation delay interferometer using only 2.4 m fibre for differential phase shift keying modulated signal demodulation. The phase-to-intensity conversion of 9.95 and 39.8 Gbit/s DPSK signals has been successfully demonstrated. The presented scheme can be used either as a DPSK demodulator at the receiver side, provided polarisation tracking is ensured, or alternatively can be used for the generation of various duty cycle RZ modulated signals at the transmitter side. Short PBGFs act as highly birefringent fibers as mode coupling is negligible. Their differential group delay is strongly wavelength dependent and it increases rapidly towards the band edge. Birefringence values as high as 10^{-3}, an order of magnitude higher than for conventional polarisation maintaining fibres, have been measured. Therefore, birefringence-based devices can be realised in an order of magnitude shorter fiber lengths using AG-PBGFs instead of conventional polarisation maintaining fibres. Additionally, the investigated AG-PBGFs are insensitive to bending to diameters down to 4 mm. Another expected advantage of AG-PBGFs is that, as they are single material fibre, the temperature induced polarisation changes associated with the different thermal expansion coefficients observed in conventional polarisation maintaining fibres should be negligible. Therefore, it is believed that AG-PBGFs enable the implementation of compact and stable, fibre birefringence based devices.

References to Chapter 6

[1] B. J. Mangan, L. Farr, A. Langford, P. J. Roberts, D. P. Williams, F. Couny, M. Lawman, M. W. Mason, S. Coupland, R. Flea, H. Sabert, T. A. Birks, J. C. Knight, and P. St. J. Russell. “Low loss (1.7 dB/km) hollow core photonic bandgap fiber”, in *Technical Digest Optical Fiber Communication Conference, OFC’04,* Los Angeles, California, U.S.A., February 2004, post-deadline paper PDP24.

[2] P. Russell. “Photonic crystal fibers”, *Science*, vol. 299, no. 5605, pp. 358–362, January 2003.

[3] C. M. Smith, N. Venkataraman, M. T. Gallagher, D. Müller, J. A. West, N. F. Borrelli, D. C. Allan, and K. W. Koch. "Low-loss hollow-core silica/air photonic bandgap fibre", *Nature*, vol. 424, pp. 657–659, August 2003.

[4] C. Peucheret, B. Zsigri, T. P. Hansen, and P. Jeppesen. "Transmission of information over air-guiding photonic bandgap fiber at 1550 nm", in *Proceedings OptoElectronics and Communications Conference, OECC'04,* Yokohama, Japan, pp. 480–481, July 2004, paper 14D1-1.

[5] T. P. Hansen, J. Broeng, C. Jakobsen, G. Vienne, H. R. Simonsen, M. D. Nielsen, P. M. W. Skovgaard, J. R. Folkenberg, and A. Bjarklev. "Air-guiding photonic bandgap fibers: spectral properties, macrobending loss, and practical handling", *Journal of Lightwave Technology*, vol. 22, no. 1, pp. 11–15, January 2004.

[6] J. D. Shephard, J. D. C. Jones, D. P. Hand, G. Bouwmans, J. C. Knight, P. St. J. Russell, and B. J. Mangan. "High energy nanosecond laser pulses delivered single-mode through hollow-core PBG fibers", *Optics Express*, vol. 12, no. 4, pp. 717–723, February 2004.

[7] J. A. West, J. C. Fajardo, M. T. Gallagher, K. W. Koch, N. F. Borrelli, and D. C. Allan. "Demonstration of an IR-optimized air-core photonic band-gap fiber", in *Proceedings European Conference on Optical Communication, ECOC'00,* Munich, Germany, pp. 41–42, September 2000, paper 10.2.3.

[8] G. Bouwmans, F. Luan, J. C. Knight, P. St. J. Russell, L. Farr, B. J. Mangan, and H. Sabert. "Properties of a hollow-core photonic bandgap fiber at 850 nm wavelength", *Optics Express*, vol. 11, no. 14, pp. 1613–1620, July 2003.

[9] J. C. Knight, T. A. Birks, P. St. J. Russell, and D. M. Atkin. "All-silica single-mode optical fiber with photonic crystal cladding", *Optics Letters*, vol. 21, no. 19, pp. 1547–1549, October 1996.

[10] J. C. Knight, J. Broeng, T. A. Birks, and P. St. J. Russell. "Photonic band gap guidance in optical fibers", *Science*, vol. 282, no. 5393, pp. 1476–1477, November 1998.

[11] J. C. Knight, T. A. Birks, P. St. J. Russell, and D. M. Atkin. "The analogy between photonic crystal fibres and step index fibres", in *Technical Digest Optical Fiber Communication Conference, OFC'99,* San Diego, California, U.S.A., pp. 114–116, February 1999, paper FG4-1.

[12] J. A. West, N. Venkataramam, C. M. Smith, and M. T. Gallagher. "Photonic crystal fibers", in *Proceedings European Conference on Optical Communication, ECOC'01,* Amsterdam, The Netherlands, pp. 582–585, September 2001, paper Th.A.2.

[13] N. Venkataramam, M. T. Gallagher, C. M. Smith, D. Müller, J. A. West, K. W. Koch, and J. C. Fajardo. "Low loss (13 dB/km) air core photonic band-gap fibre", in *Proceedings European Conference on Optical Communication, ECOC'02,* September 2002, postdeadline paper PD1.1.

[14] J. Broeng, S. E. Barkou, A. Bjarklev, J. C. Knight, T. A. Birks, and P. St. J. Russell. "Highly increased photonic band gaps in silica/air structures", *Optics Communications*, vol. 156, no. 4-6, pp. 240–244, November 1998.

[15] J. B. Nielsen, T. Søndergaard, S. E. Barkou, A. Bjarklev, J. Broeng, and M. B. Nielsen. "Two-dimensional Kagomé structure, fundamental hexagonal photonic crystal configuration", *Electronics Letters*, vol. 35, no. 20, pp. 1736–1737, September 1999.

[16] S. E. B. Libori. *Photonic Crystal Fibers - From Theory to Practice.* Ph.D. thesis, Research Center COM, Technical University of Denmark, Kgs. Lyngby, Denmark, February 2002. ISBN 87-90974-29-8.

[17] J. Broeng, T. Søndergaard, S. E. Barkou, P. M. Barbeito, and A. Bjarklev. "Waveguidance by the photonic bandgap effect in optical fibres", *Journal of Optics A: Pure and Applied Optics*, vol. 1, no. 4, pp. 477–482, July 1999.

[18] T. P. Hansen, J. Broeng, and A. Bjarklev. "Solid-core photonic bandgap fiber with large anormalous dispersion", in *Technical Digest Optical Fiber Communication Conference, OFC'03,* Atlanta, Georgia, U.S.A., pp. 700–701, March 2003, paper FI6.

[19] K. Saitoh and M. Koshiba. "Leakage loss and group velocity dispersion in air-core photonic bandgap fibers", *Optics Express*, vol. 11, no. 17, pp. 3100–3109, November 2003.

[20] J. A. West, N. Venkataramam, M. T. Gallagher, C. M. Smith, D. Müller, D. C. Allan, N. F. Borrelli, and K. W. Koch. "Photonic band-gap fiber − fiber of the future?", in *Technical Digest IEEE Lasers and Electro-Optics Society Summer Topical Meetings, LEOS Summer Topical Meetings '03,* Vancouver, Canada, pp. 9–10, July 2003, paper MA2.2.

[21] C. J. S. de Matos, J. R. Taylor, T. P. Hansen, K. P. Hansen, and J. Broeng. "Study of the dispersion of an air-core photonic bandgap fiber and its application as a linear chirped pulse compressor", in *Technical Digest Conference on Lasers and Electro-Optics, CLEO'04,* San Francisco, California, U.S.A., pp. 1357–1358, May 2004, paper CWK2.

[22] C. Peucheret, B. Zsigri, T. P. Hansen, and P. Jeppesen. "10 Gbit/s transmission over air-guiding photonic bandgap fibre at 1550 nm", *Electronics Letters*, vol. 41, no. 1, pp. 27–29, January 2005.

[23] C. Peucheret, Y. Geng, B. Zsigri, T. T. Alkeskjold, T. P. Hansen, and P. Jeppesen. "Demodulation of DPSK signals up to 40 Gb/s using a highly birefringent photonic bandgap fibre", in *Proceedings OptoElectronics and Communications Conference, OECC'05,* Seoul, Korea, pp. 50–51, July 2005, paper 5D1-2.

[24] T. P. Hansen, C. Jakobsen, H. R. Simonsen, J. Broeng, J. R. Folkenberg, P. M. W. Skovgaard, and A. Bjarklev. "Air-guiding photonic bandgap fibers", in *Technical Digest Optical Fiber Communication Conference, OFC'05,* Anaheim, California, U.S.A., March 2005, paper OTuI5.

[25] J. A. West, C. M. Smith, N. F. Borrelli, D. C. Allan, and K. W. Koch. "Surface modes in air-core photonic band-gap fibers", *Optics Express*, vol. 12, no. 8, pp. 1485–1496, April 2004.

[26] M. Wegmüller, N. Gisin, T. P. Hansen, C. Jakobsen, and J. Broeng. "Polarization properties of an air-guiding photonic bandgap fibre

for 1550 nm transmission", in *Proceedings European Conference on Optical Communication, ECOC'04,* Stockholm, Sweden, September 2004, paper Mo4.3.7.

[27] M. Wegmüller, M. Legré, N. Gisin, T. P. Hansen, C. Jakobsen, and J. Broeng. "Experimental investigation of the polarization properties of a hollow core photonic bandgap fiber for 1550 nm", *Optics Express*, vol. 13, no. 5, pp. 1457–1467, March 2005.

[28] P. J. Roberts, F. Couny, H. Sabert, B. J. Mangan, D. P. Williams, L. Farr, M. W. Mason, A. Tomlinson, T. A. Birks, J. C. Knight, and P. St. J. Russell. "Ultimate low loss of hollow-core photonic crystal fibres", *Optics Express*, vol. 13, no. 1, pp. 236–244, January 2005.

[29] T. P. Hansen. *Air-guiding photonic bandgap fibers.* Ph.D. thesis, Research Center COM, Technical University of Denmark, Kgs. Lyngby, Denmark, April 2005.

[30] J. A. West, C. M. Smith, N. F. Borrelli, D. C. Allan, and K. W. Koch. "Loss mechanisms in photonic band-gap fibres", in *Proceedings European Conference on Optical Communication, ECOC'04,* Stockholm, Sweden, pp. 10–13, September 2004, paper Mo.3.3.1.

[31] K. Saitoh, N. A. Mortensen, and M. Koshiba. "Air-core photonic band-gap fibers: the impact of surface modes", *Optics Express*, vol. 12, no. 3, pp. 394–400, February 2004.

[32] H. K. Kim, M. J. F. Digonnet, G. S. Kino, J. Shin, and S. Fan. "Simulations of the effect of the core ring on surface and air-core modes in photonic bandgap fibers", *Optics Express*, vol. 12, no. 15, pp. 3436–3442, July 2004.

[33] M. Wegmüller, M. Legré, N. Gisin, K. P. Hansen, T. P. Hansen, and C. Jakobsen. "Detailed polarization properties comparison for three completely different species of highly birefringent fibers", in *Proceedings Symposium on Optical Fiber Measurements, SOFM'04,* Boulder, Colorado, U.S.A., September 2004, 119-122.

[34] X. Chen, M.-J. Li, N. Venkataraman, M. T. Gallagher, W. A. Wood, A. M. Crowley, J. P. Carberry, L. A. Zenteno, and K. W. Koch.

"Highly birefringent hollow-core photonic bandgap fiber", in *Technical Digest Optical Fiber Communication Conference, OFC'05,* Anaheim, California, U.S.A., March 2005, paper OTuI1.

[35] X. Chen, M.-J. Li, N. Venkataraman, M. T. Gallagher, W. A. Wood, A. M. Crowley, J. P. Carberry, L. A. Zenteno, and K. W. Koch. "Highly birefringent hollow-core photonic bandgap fiber", *Optics Express*, vol. 12, no. 16, pp. 3888–3893, August 2004.

[36] C. J. S. de Matos and J. R. Taylor. "Multi-kilowatt, all-fiber integrated chirped-pulse amplification system yielding 40× pulse compression using air-core fiber and conventional erbium-doped amplifier", *Optics Express*, vol. 12, no. 3, pp. 405–409, February 2004.

[37] J. Limpert, T. Schreiber, S. Nolte, H. Zellmer, and A. Tünnermann. "All fiber chirped-pulse amplification system based on compression in air-guiding photonic bandgap fiber", *Optics Express*, vol. 11, no. 24, pp. 3332–3337, December 2003.

[38] C. J. S. de Matos, J. R. Taylor, T. P. Hansen, K. P. Hansen, and J. Broeng. "All-fiber chirped pulse amplification using highly-dispersive air-core photonic bandgap fiber", *Optics Express*, vol. 11, no. 22, pp. 2832–2837, September 2003.

[39] F. Luan, J. C. Knight, P. St. J. Russell, S. Campbell, D. Xiao, D. T. Reid, B. J. Mangan, D. P. Williams, and P. J. Roberts. "Femtosecond soliton pulse delivery at 800 nm wavelength in hollow-core photonic bandgap fibers", *Optics Express*, vol. 12, no. 5, pp. 835–840, March 2004.

[40] D. G. Ouzounov, F. R. Ahmad, D. Müller, N. Venkataraman, M. T. Gallagher, M. G. Thomas, J. Silcox, K. W. Koch, and A. L. Gaeta. "Generation of Megawatt optical solitons in hollow-core photonic band-gap fibers", *Science*, vol. 301, pp. 1702–1704, September 2003.

[41] J. A. West and D. C. Allan. "Effect of disorder on photonic bandgap fibers", in *Proceedings European Conference on Optical Communication, ECOC'02,* Copenhagen, Denmark, pp. 1–2, September 2002, paper S1.4.

[42] G. P. Agrawal. *Fiber-Optic Communication Systems*. John Wiley & Sons, Inc., Second edition, 1997. ISBN 0-471-17540-4.

[43] A. Boskovic, S. V. Chernikov, J. R. Taylor, L. Grüner-Nielsen, and O. A. Levring. "Direct continuous-wave measurement of n_2 in various types of telecommunication fiber at 1.55 μm", *Optics Letters*, vol. 21, no. 24, pp. 1966–1968, December 1996.

[44] A. H. Gnauck and P. J. Winzer. "Optical phase-shift-keyed transmission", *Journal of Lightwave Technology*, vol. 23, no. 1, pp. 115–130, January 2005.

[45] L. Becouarn, G. Vareille, P. Pecci, and J. F. Marcerou. "3 Tbit/s transmission (301 DPSK channels at 10.709 Gb/s) over 10270 km with a record efficiency of 0.65 (bit/s)/Hz", in *Proceedings European Conference on Optical Communication, ECOC'03,* Rimini, Italy, Paper PD45, September 2003.

[46] C. Rasmussen, T. Fjelde, J. Bennike, F. Liu, S. Dey, B. Mikkelsen, P. Mamyshev, P. Serbe, P. van der Wagt, Y. Akasaka, D. Harris, D. Gapontsev, V. Ivshin, and P. Reeves-Hall. "DWDM 40G transmission over trans-pacific distance (10000 km) using CSRZ-DPSK, enhanced FEC, and all-Raman-amplified 100 km UltraWave fiber spans", *Journal of Lightwave Technology*, vol. 22, no. 1, pp. 203–207, January 2004.

[47] P. J. Winzer and J. Leuthold. "Return-to-zero modulator using a single NRZ drive signal and an optical delay interferometer", *IEEE Photonics Technology Letters*, vol. 13, no. 12, pp. 1298–1300, December 2001.

[48] E. Ciaramella, G. Contestabile, and A. DErrico. "A novel scheme to detect optical DPSK signals", *IEEE Photonics Technology Letters*, vol. 16, no. 9, pp. 2138–2200, September 2004.

[49] A. Buxens, H. N. Poulsen, A. T. Claused, and P. Jeppesen. "Gain flattened L-band EDFA based on upgraded C-band EDFA using forward ASE pumping inan EDF section", *Electronics Letters*, vol. 36, no. 9, pp. 821–823, April 2000.

[50] B. L. Heffner. "Accurate, automated measurement of differential group delay dispersion and principal state variation using Jones matrix eigenanalysis", *IEEE Photonics Technology Letters*, vol. 5, no. 7, pp. 814–817, July 1993.

[51] B. L. Heffner. "Automated measurement of polarization mode dispersion using Jones matrix eigenanalysis", *IEEE Photonics Technology Letters*, vol. 4, no. 9, pp. 1066–1069, September 1992.

Chapter 7

Conclusion

This thesis has addressed several telecommunication applications of air-silica photonic crystal fibres (PCFs).

Like conventional fibres, PCFs have a core and cladding region. However the cladding of these fibres is an artificially-engineered photonic crystal structure formed by an arrangement of air holes in the silica background material. This microstructured cladding results in some remarkable optical properties. These fibres are expected to eliminate the limitations set by the materials and designs of conventional fibres. Due to the large index difference between air and silica, the properties of these fibres can theoretically be engineered to the extremes. By changing the structural parameters of the fibre, either extremely low or high values of effective area, dispersion or nonlinearity can be obtained. Moreover, large birefringence, endlessly single mode operation and resilience to bending loss can also be achieved. These unique possibilities make PCFs very attractive for several applications, including optical communication systems. Commonly PCFs are classified into two major groups: index guiding PCFs and photonic bandgap fibres (PBGFs), based on their guiding mechanism. In this thesis the two groups were investigated separately.

Index guiding photonic crystal fibres

Even though PCFs are widely used already in many different applications, they are still considered as new technology in optical communica-

tion systems. Investigations on the application of index guiding PCFs as transmission fibres began approximately three years ago, simultaneously with this Ph.D. project. Therefore, this work follows from the start the evolution of index guiding PCFs as transmission fibres and includes up-to-date state-of-the-art results. Initial experiments demonstrated the feasibility of large mode area photonic crystal fibres (LMA-PCFs) to be used as transmission media. Initially, the lengths of PCF, drawn in a single piece, and so the transmission distances over PCFs, were limited to 1.5 and 3 km. Improvements in the manufacturing techniques increased this value to approximately 12 km. Making use of a recirculating loop, the total transmission distance over PCF was increased to 57.6 km (10 Gbit/s), more than four times longer than any other PCF transmission over index guiding PCF reported at the time. The presented experiments have shown the potential of index guiding PCFs as transmission fibres. Polarisation multiplexing two 40 Gbit/s differential phase shift keying (DPSK) signals and transmitting over 19.2 km PCF increased the total capacity transmitted on a single wavelength over PCF to 80 Gbit/s. Thereby demonstrating the highest capacity per wavelength transmitted over PCF up to date. It has been found that the very low polarisation mode dispersion (PMD) of the tested PCF, which is a result of its very high symmetry, may make these fibres suitable for high speed, polarisation multiplexed systems.

The application of index guiding highly nonlinear photonic crystal fibres (HNL-PCFs) for signal processing in optical communications dates back to somewhat earlier date than transmission applications. Nevertheless it is only recently that HNL-PCFs optimised for telecommunication applications (having either zero dispersion wavelength at 1550 nm or broad, flat either positive or negative nearly zero dispersion) have been developed. The combination of signal processing using HNL-PCFs and transmission using LMA-PCFs made possible the realisation of the first completely PCFs based systems. During the course of this Ph.D. project, the first entirely index guiding photonic crystal fibre based optical link, comprising both transmission medium and dispersion compensation, has been presented. A 40 Gbit/s non return-to-zero signal has been transmitted over 5.6 km of large mode area photonic crystal fibre with dispersion compensation realised by optical phase conjugation utilising four-wave mixing in a 50 m long highly nonlinear photonic crystal fibre with

zero dispersion at 1552 nm. Furthermore, an entirely photonic crystal fibre based prototype optical network with broadcast, transmission and wavelength conversion functionalities has also been demonstrated. For the first time, broadcasting of four channels has been realised by cross phase modulation in a nonlinear optical loop mirror with 100 m highly nonlinear photonic crystal fibre as nonlinear medium. A selected channel has been transmitted over 10.4 km large mode area photonic crystal fibre and wavelength converted by four-wave mixing in a 50 m long highly nonlinear photonic crystal fibre. The presented experiments constitute the first demonstrations of entirely photonic crystal fibres based optical systems, and clearly show the potential of photonic crystal fibres for both transmission and signal processing purposes.

In addition, PCFs are very attractive as dispersion compensating fibre as they can exhibit very large and tailorable dispersion, due to the large refractive index difference between air and silica. Here, a novel up-doped core, honeycomb structure PCF design has been proposed for dispersion compensation. Calculations show that this design exhibits a dispersion coefficient as large as -1353 ps/(nm·km) and 1.6 μm^2 effective area at 1550 nm. As the fibre was designed to match the relative dispersion slope of standard single mode fibre, broadband dispersion compensation of 100 km standard single mode fibre over as much as 225 nm with compensation ratio variation less than 10 % can be achieved using the proposed design. However dispersion compensating photonic crystal fibre (DC-PCF) designs have been mostly numerically investigated until now, a number of practical problems are expected. Generally all DC-PCF fibres with large dispersion coefficient possess very small effective areas (in the order of a few μm^2). The technical challenges that may have to be faced include difficult splicing, large coupling loss and enhanced undesirable nonlinear effects. Moreover, slight fluctuations of the structural parameters may considerably change the properties of the fibre and result in high birefringence. The proposed doped core honeycomb DC-PCF design is expected to provide advantages over other existing DC-PCF designs, despite the doped core being a source of increased nonlinearity and expectedly higher loss due to scattering. Nevertheless, it has a very simple design, thus allows easy fabrication, and is expected to have larger tolerances towards parameter fluctuations. Moreover, when doped core microstructured fibres are spliced the cladding holes partially

collapse, but due to their doped core the mode field still remains guided. This forms a tapering and will reduce mode mismatch when these fibres are spliced.

Photonic bandgap fibres

PBGFs are a fundamentally different fibre type than conventional fibres or even index guiding PCFs. Air-guiding photonic bandgap fibres (AG-PBGFs) were expected to bring a major breakthrough in optical communication systems. Guiding light in air may result in ultimate low loss and nonlinearity. Furthermore this fibre type has the potential of opening up new transmission windows, which are not practical in silica based fibres. The fabrication of AG-PBGFs is cumbersome due to the large relative air hole sizes required. Therefore the development of AG-PBGFs is considerably slower than that of index guiding PCFs. It is only recently that PBGFs were considered for telecommunication applications and these first demonstrations have been presented in this thesis.

The first data transmission using AG-PBGF as transmission media is presented in the form of a 10 Gbit/s non return-to-zero (NRZ) modulated signal transmission over 150 and 400 m AG-PBGFs. The system performance was found to be very dependent on polarisation effects in the fiber, caused by fiber birefringence due to changes in the environmental conditions. However these experiments demonstrate the potential of air-guiding photonic bandgap fibres as transmission media. They also point out current limitations of these fibres due to their unusual polarisation properties. Therefore, before AG-PBGFs may be considered for transmission, thorough investigations are necessary on the requirements on their structural uniformity in order to minimise those polarisation effects.

The differential group delay of AG-PBGFs showed strong wavelength dependence, and birefringence values of an order of magnitude higher (10^{-3}) than for conventional polarisation maintaining fibres have been measured. The high birefringence of air-guiding photonic bandgap fibres has been exploited by realising the first polarisation delay interferometer using only 2.4 m AG-PBGF for the demodulation of differential phase shift keying modulated signals up to 39.8 Gbit/s. The combination of very stable operation and the short fibre length needed to realise such a

device and the remarkable bending properties of AG-PBGFs enables the implementation of compact and stable fibre birefringence based devices in AG-PBGF.

Outlook

At the early development photonic crystal fibres were expected to show great potentials, that may make them outperform standard fibre technology in specific optical transmission systems. The awaited breakthrough of PCFs, however, has not yet come due to practical limitations. So far, the relatively high loss and short lengths available for large mode area photonic crystal fibres set a limitation on their practical use as transmission fibre. Highly nonlinear photonic crystal fibres suffer from considerably higher loss than conventional highly nonlinear fibres (HNLFs), limiting their effective length. Furthermore only slight deviation of the structure may result in significant unintentional birefringence and considerable change of their other optical properties. Air-guiding photonic bandgap fibres exhibit large unintentional birefringence, as well, and their loss might be ultimately limited by the existence of frozen-in surface capillary waves. Most of the listed limitations are attributed to the immature manufacturing process of PCFs. Considerable work is allocated to address the problem of fabricating long PCFs with high symmetry and structural uniformity. Once these problems can be overcome, PCF may become a competitive technology to conventional fibres.

At present, PCFs may be strong candidates for applications where the currently high loss values can be tolerated and the unique properties of PCFs play a crucial role. As a transmission fibre, high numerical aperture fibres (HNAFs), a special subgroup of index guiding PCFs, found an application in the fiber to the home market as a consequence of their remarkable bending loss property [1–3].

PCFs may have a potential for realising small compact fibre based devices. Filling the cladding air holes of index guiding PCFs by various liquid crystals results in a PBGF whose optical properties can be changed by thermo-optical, electro-optical or all-optical methods [4, 5]. Liquid crystal filled fibres may be exploited to realise tunable devices for telecommunication. However this have to be addressed in future works.

References to Chapter 7

[1] H. Shinohara. "Broadband access in Japan: Rapidly growing FTTH market", *IEEE Communication Magazine*, vol. 43, no. 9, pp. 72–78, September 2005.

[2] N. Guan, K. Izoe, K. Takenaga, R. Suzuki, and K. Himeno. "Hole-assisted single-mode fibers for low bending loss", in *Proceedings European Conference on Optical Communication, ECOC'04,* Stockholm, Sweden, September 2004, paper Mo3.3.5.

[3] N. Guan, K. Izoe, K. Takenaga, R. Suzuki, K. Aikawa, and K. Himeno. "Holey fibers for low bending loss", *IEICE Transactions on Electronics*, vol. E89-C, no. 2, pp. 191–196, February 2006.

[4] T. T. Alkeskjold. *Optical devices based on liquid crystal photonic bandgap fibers.* Ph.D. thesis, Research Center COM, Technical University of Denmark, Kgs. Lyngby, Denmark, May 2005. ISBN 87-90974-69-7.

[5] M. W. Haakestad, T. T. Alkeskjold, M. D. Nielsen, L. Scolari, J. Riishede, H. E. Engan, and A. Bjarklev. "Electrically tunable photonic bandgap guidance in a liquid-crystal-filled photonic crystal fiber", *IEEE Photonics Technology Letters*, vol. 17, no. 4, pp. 819–821, April 2005.

List of Acronyms

AG-PBGF	air-guiding photonic bandgap fibre
AOS	acousto-optic switches
AWG	arrayed waveguide grating
B2B	back-to-back
BER	bit error rate
CR	compensation ratio
CW	continuous wave
DCF	dispersion compensating fibre
DC-PCF	dispersion compensating photonic crystal fibre
DGD	differential group delay
DPSK	differential phase shift keying
EDFA	erbium doped fibre amplifier
ESM	endlessly single mode
ESM-PCF	endlessly single mode photonic crystal fibre
FBG	fibre Bragg gratings
FWHM	full width at half maximum
FWM	four-wave mixing

HNAF	high numerical aperture fibre
HNLF	highly nonlinear fibre
HNL-PCF	highly nonlinear photonic crystal fibre
HP-EDFA	high power erbium doped fibre amplifier
LIC	low index core
LMA-PCF	large mode area photonic crystal fibre
MFD	mode field diameter
MLFRL	mode-locked fiber ring laser
M-TIR	modified total internal reflection
MZ	Mach-Zehnder
NOLM	nonlinear optical loop mirror
NRZ	non return-to-zero
OBPF	optical bandpass filter
OPC	optical phase conjugator
OTDM	optical time domain multiplexing
OSNR	optical signal to noise ratio
PBG	photonic bandgap
PBGF	photonic bandgap fibre
PBS	polarisation beam splitter
PC	polarisation controller
PCF	photonic crystal fibre
PD	photodetector
PMD	polarisation mode dispersion

PRBS	pseudo random bit sequence
RDS	relative dispersion slope
RZ	return-to-zero
SMF	single mode fibre
SPM	self phase modulation
SSMF	standard single mode fibre
TIR	total internal reflection
WDM	wavelength division multiplexing
XPM	cross phase modulation